REPUBLIC of TÜRKİYE
SİVAS CUMHURİYET UNIVERSITY
GRADUATE SCHOOL of NATURAL and APPLIED SCIENCES

LONG-TERM PRODUCTION PLANNING of an OPEN-PIT IRON MINE

MASTER THESIS

Abdul Aziz MAHBOOB
(20229221022)

Mining Engineering Department

Supervisor: Prof. Dr. Bülent ERDEM

SİVAS
AUGUST 2025

This study by **Abdul Aziz MAHBOOB** entitled "**LONG-TERM PRODUCTION PLANNING of an OPEN-PIT IRON MINE**" was accepted by the following jury as a **MASTER THESIS** in the **MINING ENGINEERING DEPARTMENT.**

Supervisor:	**Prof. Dr. Bülent ERDEM** Sivas Cumhuriyet University	……
Member:	**Prof. Dr. Niyazi BİLİM** Konya Technical University	……
Member:	**Dr. Lecturer Zekeriya DURAN** Sivas Cumhuriyet University	……

This thesis has been approved as a **MASTER THESIS** by Sivas Cumhuriyet University, Graduate School of Natural and Applied Sciences.

Prof. Dr. Nail ALTUNAY

Director of the Graduate School of Natural and Applied Sciences

This dissertation was written in accordance with the rules of the Guidelines for Dissertation Writing of the Graduate School of Natural and Applied Sciences, which was adopted by the Sivas Cumhuriyet University Senate Resolution No. 7 dated 20.08.2014.

All rights reserved.
Quotations and references are possible, provided the source is acknowledged.

© Abdul Aziz MAHBOOB, 2025

ETHICS

In this thesis, which I have written in accordance with the Thesis Writing Guide (Guidelines) of Sivas Cumhuriyet University Graduate School of Natural and Applied Sciences, I declare that;

- ✓ I have obtained all information and documents within the framework of the academic rules,
- ✓ I have presented all visual, auditory and written information and results in accordance with the academic ethical rules,
- ✓ In the case of using the works of others, I have referred to the relevant works in accordance with academic standards and have cited all the works I have referred to as sources,
- ✓ All information is correct and complete, I have not made any changes to the data used,
- ✓ I have not submitted any part of the thesis as another thesis to Sivas Cumhuriyet University or any other university.

25.08.2025

Abdul Aziz MAHBOOB

ACKNOWLEDGEMENTS

I would like to thank my supervisor Prof. Dr. Bülent ERDEM, with whom I worked in all phases of the thesis.

I would like to thank the company Micromine® and its Turkish representative YSK Group Muhendislik Ltd. Şti. for allowing me to use the mine planning and design package program for educational purposes in my thesis.

I would like to thank my jury members Prof. Dr. Niyazi BİLİM and Dr. Lecturer Zekeriya DURAN for their understanding and support both in reading the thesis and in defending it.

ABSTRACT

LONG-TERM PRODUCTION PLANNING of an OPEN-PIT IRON MINE

Abdul Aziz MAHBOOB

Master of Science Thesis
Department of Mining Engineering
Supervisor: Prof. Dr. Bülent ERDEM
2025, 82+XI pages

This thesis presents an advanced framework for open-pit mine modeling and production optimization of iron ore deposits using mine planning software. Using data from 42 iron ore exploration drill holes, resource estimation was conducted separately for three types of ore bodies by applying both inverse distance weighting (IDW) and kriging methods. The aim was to estimate the spatial distribution of iron grades and to evaluate the accuracy of each interpolation technique.

The study not only focuses on optimizing the pit boundary, but also examines different pit development strategies that control the evolution of the pit over time. After evaluating the ultimate pit and the nested pits, the ultimate pit was selected due to its planning flexibility, operational continuity and better long-term financial resilience for continued operation, and was finally designed as a single-phase development.

The final open pit plan was divided into standard mining blocks, which formed the basis for mine planning and production scheduling. A practical scheduling strategy was then developed to spread the mining of the blocks over several production periods, ensuring a balance between profitability and operational constraints. Production planning was carried out over a 15-year period for 3,772 mining blocks with a maximum annual capacity of 25 million tons and a minimum and maximum ore grade of 25%-38% over the years.

Key words: Open-pit mine modeling, Pit limit optimization, Scheduling, Resource estimation, Inverse distance weighting, Production optimization.

ÖZET

BİR AÇIK DEMİR MADENİNİN UZUN DÖNEMLİ ÜRETİM PLANLAMASI

Abdul Aziz MAHBOOB

Yüksek Lisans Tezi
Maden Mühendisliği Anabilim Dalı
Danışman: Prof. Dr. Bülent ERDEM
2025, 82+XI sayfa

Bu tez, maden planlama yazılımı kullanılarak demir cevheri yataklarının açık ocak madenciliği modellemesi ve üretim optimizasyonu için gelişmiş bir çerçeve sunmaktadır. 42 adet demir cevheri arama sondajından elde edilen verilerle, üç farklı cevher tipi için ayrı ayrı kaynak tahmini yapılmış; bu süreçte ters mesafe ile ağırlıklandırma (IDW) ve krigleme yöntemleri uygulanmıştır. Amaç, demir tenörlerinin uzamsal dağılımını kestirmek ve her bir interpolasyon tekniğinin doğruluğunu değerlendirmektir.

Tez, nihai şev sınırı optimizasyonuna odaklanmanın yanı sıra, ocağın zaman içindeki gelişimini yönlendiren çeşitli ocak geliştirme stratejilerini de incelemektedir. Nihai ocak ve yuvalı ocaklar değerlendirildikten sonra, planlama esnekliği, operasyonel süreklilik ve uzun vadeli finansal dayanıklılık açısından en uygun olan nihai ocak daha fazla operasyon için seçilmiş ve tek fazlı bir gelişim şeklinde tasarlanmıştır.

Son açık ocak tasarımı, maden planlaması ve üretim programlamasının temelini oluşturan standart maden bloklarına bölünmüştür. Daha sonra, kârlılık ile operasyonel kısıtlamalar arasında denge sağlayan bir üretim planlaması stratejisi geliştirilmiş ve blokların çok yıllı üretim dönemleri boyunca sıralı olarak çıkarılması sağlanmıştır. Üretim planlaması, 15 yıllık bir süre boyunca toplam 3772 maden bloğu için yapılmış olup, yıllık en fazla 25 milyon tonluk bir üretim kapasitesi ile cevher tenör oranı, yıllar içinde %25 ile %38 arasında değişmiştir.

Anahtar kelimeler: Açık ocak modelleme, açık ocak sınırlarının optimizasyonu, çizelgeleme, kaynak kestirimi, ters mesafe ile ağırlıklandırma, üretim optimizasyonu

TABLE of CONTENTS

Page

ABSTRACT ..... **vii**
ÖZET ..... **viii**
TABLE of CONTENTS ..... **ix**
LIST of FIGURES ..... **x**
LIST of TABLES ..... **xi**
1. INTRODUCTION **1**
2. LITERATURE REVIEW **4**
2.1. General 4
2.2 Previous Studies on Mine Planning 4
2.3. Open Pit Mining Problems 7
3. MATERIALS AND METHODS **8**
3.1. Materials 8
3.2. Methods 8
3.2.1. Time value of money *9*
3.2.2. Lerchs-Grossmann algorithm *10*
3.2.3. Pit advancing *14*
4. STATISTICAL ANALYSIS of DRILLHOLE DATA and ORE GRADES **17**
4.1. Drillhole Data 17
4.2. Grade Distribution of Ore 18
4.3. Geostatistical Evaluation 21
4.3.1. Orebody modeling *21*
4.3.2. Blank and geologic block models *24*
5. RESOURCE ESTIMATION **25**
5.1. Compositing of Drillhole Data 25
5.2. Variogram Analyses 27
5.3. Cross Validation of the Models 35
5.4. Grade Assignment for the High Grade Orebody 39
5.5. Grade Assignment for the Medium Grade Orebody 43
5.6. Grade Assignment for the Low Grade Orebody 46
5.7. Combining the Orebodies 49
6. PIT OPTIMIZATION and DESIGN **52**
6.1. Ultimate Pit Optimization 52
6.2. Nested Pit Optimization 62
6.3. Pit Design 66
7. GRADE-TONNAGE OPERATIONS **70**
7.1. Creating Mining Blocks 70
7.2. Grade-Tonnage Processes 70
7.3. Production Scheduling 73
8. CONCLUSIONS and RECOMMENDATIONS for FURTHER RESEARCH **77**
8.1. Conclusions 77
8.2. Recommendations for Further Research 78
REFERENCES **79**

LIST of FIGURES

Page

Figure 1.1 Iron ore world trade by observatory of economic complexity (URL-2) 2
Figure 1.2 Top iron ore trading countries (URL-2) 3
Figure 3.1 Orebody geometry for Lerchs-Grossmann 2-D algorithm 10
Figure 3.2 Assigning grade values to ore (URL-3) 12
Figure 3.3 Block economic values (URL-3) 12
Figure 3.4 Cumulative totals of block economic values (URL-3) 12
Figure 3.5 Sum of block values with its maximum neighborhood on the left (URL-3) 13
Figure 3.6 Finding the most suitable pit limit (URL-3) 13
Figure 3.7 Final pit limit (URL-3) 13
Figure 3.8 Ultimate pit limits in the case of worst-case algorithm 14
Figure 3.9 Ultimate pit limits in the case of best-case algorithm 15
Figure 3.10 Pit limits in the case of multiple benching algorithm 16
Figure 4.1 Validation of drillholes 17
Figure 4.2 Drillholes on the topography 18
Figure 4.3 Grade distribution histogram of high grade iron ore analyses 19
Figure 4.4 Grade distribution histogram of medium grade iron ore analyses 20
Figure 4.5 Grade distribution histogram of low grade iron ore analyses 20
Figure 4.6 Ore and rock layers intersected by drillholes 21
Figure 4.7 The distribution of ore grades in drill holes 21
Figure 4.8 The designed search ellipsoid for solid body modeling 22
Figure 4.9 The solid body model of the ore body 23
Figure 4.10 Cross-sections from the solid body model of the ore body and host rock 23
Figure 4.11 Blank block model 24
Figure 4.12 Geologic block model 24
Figure 5.1 Sampling interval length distribution of high grade orebody 25
Figure 5.2 Sampling interval length distribution of medium grade orebody 26
Figure 5.3 Sampling interval length distribution of low grade orebody 27
Figure 5.4 Variogram maps of the high grade orebody 29
Figure 5.5 Semi variograms of the high-grade orebody 30
Figure 5.6 Variogram maps of the medium grade orebody 31
Figure 5.7 Semi variograms of the medium grade orebody 32
Figure 5.8 Variogram maps of the low grade orebody 33
Figure 5.9 Semi variograms of the low-grade orebody 34
Figure 5.10 Cross validation plots of the high grade orebody 36
Figure 5.11 Cross validation plots of the medium grade orebody 37
Figure 5.12 Cross validation plots of the low grade orebody 38
Figure 5.13 The high-grade orebody with grades assigned to blocks with kriging 40
Figure 5.14 The medium grade orebody with grades assigned to blocks with kriging 43
Figure 5.15 The low-grade orebody with grades assigned to blocks with kriging 46
Figure 5.16 The combined orebody 50
Figure 6.1 The ultimate pit (isometric view to the southeast) 60
Figure 6.2 The ultimate pit and the block model of the combined orebody (cross-section view) 61
Figure 6.3 The nested pits and the block model of the combined orebody (isometric view to the southeast) 64
Figure 6.4 The nested pits and the block model of the combined orebody (cross section view) 65
Figure 6.5 The optimization scenario of nested pits by stages (bench lagging) 66
Figure 6.6 The optimization scenario of nested pits by periods (bench lagging) 66
Figure 6.7 The up mode pit design by the package 67
Figure 6.8 The designed open-pit mine and the block model of the combined orebody (isometric view to the northeast) 68
Figure 6.9 The cross section view of the designed open-pit mine and the block model of the combined orebody 69
Figure 7.1 The mining blocks in the optimum pit (isometric view to the southwest) 71
Figure 7.2 The cross section view of the mining blocks in the optimum pit 72

LIST of TABLES

Page

Table 1.1 The top iron ore reserves by country (URL-1) 2
Table 1.2 Iron ore production in 2023 by country (URL-1) 3
Table 4.1 Descriptive statistics for the high grade iron ore 19
Table 4.2 Descriptive statistics for the medium grade iron ore 20
Table 4.3 Descriptive statistics for the low grade iron ore 20
Table 4.4 The geometry of the search ellipsoid formed in accordance with the data parameters 22
Table 4.5 The characteristics of the solid body model of the ore body 22
Table 5.1 Descriptive statistics for compositing of the high-grade ore body 26
Table 5.2 Descriptive statistics for compositing of the medium grade orebody 26
Table 5.3 Descriptive statistics for compositing of the low grade orebody 27
Table 5.4 Parameter values of the search ellipsoid used by the estimation algorithms for the high-grade orebody 40
Table 5.5 Estimated tonnage of resources by the IDW algorithm for the high grade orebody 41
Table 5.6 Estimated tonnage of resources by the ordinary kriging algorithm for the high grade orebody 42
Table 5.7 Parameter values of the search ellipsoid used by the estimation algorithms for the medium grade orebody 43
Table 5.8 Estimated tonnage of resources by the IDW algorithm for the medium grade orebody 44
Table 5.9 Estimated tonnage of resources by the kriging algorithm for the medium grade orebody 45
Table 5.10 Parameter values of the search ellipsoid used by the estimation algorithms for the low-grade orebody 46
Table 5.11 Estimated tonnage of resources by the IDW algorithm for the low-grade orebody 47
Table 5.12 Estimated tonnage of resources by the kriging algorithm for the low grade orebody 48
Table 5.13 Estimated tonnage of resources for the combined orebody 51
Table 6.1 Input parameter values used in ultimate pit optimization 52
Table 6.2 The results of ultimate pit optimization 59
Table 7.1 Ore and waste quantities of mining blocks in the ultimate pit 70
Table 7.2 Yearly production figures of the iron mine 73
Table 7.3 Monthly production figures of the iron mine 74

1. INTRODUCTION

Iron is the primary raw material for steel production, which was already being used before 3000 BC, albeit from meteorites or meteoritic iron. 1200 BC is known as the Iron Age because iron was smelted and used instead of bronze for weapons and other tools. This smelting spread from Anatolia or Türkiye to Europe, Asia and Africa. Over time, in the 18th and 19th centuries, iron became an important part of life. Iron became the backbone of the industrial revolution; all machines were made of iron. Even in today's modern age, iron is of crucial importance, as more than 85 or 90 percent of metals are made of iron.

Iron is found in iron-containing minerals such as hematite (Fe_2O_3) with a high iron content, magnetite (Fe_3O_4) with the highest iron content, goethite (FeO(OH)) with a medium iron content, limonite ($FeO(OH)\cdot nH_2O$) with a rather low iron content, siderite ($FeCO_3$) with a low iron content. The deposits of iron ore minerals are diverse, but we will discuss some important deposits here:

1) Hematite deposits are also iron oxide minerals that occur in a variety of geologic environments. It can be found in igneous, metamorphic and sedimentary rocks. It is usually associated with BIFs, but can also occur as residual deposits or enriched deposits formed by weathering and erosion of iron-bearing rocks.
2) Magnetite deposits are iron oxide minerals that can occur in igneous, metamorphic or sedimentary rocks. These types of deposits are often associated with mafic and ultramafic intrusions.
3) Goethite and limonite deposits are other types of iron oxide minerals that are formed during the weathering of iron-rich rocks. These deposits are characterized by high moisture content and low iron content and are generally considered to be lower quality iron ore deposits.
4) Carbonate iron deposits are also known as sedimentary-exhalative iron deposits, which are formed by precipitation of iron minerals from hydrothermal fluids in sedimentary basins. These deposits are characterized by their association with carbonate rock.
5) Skarn deposits: The contact between intrusion and carbonate-rich rock containing iron ore minerals and other valuable minerals forms skarn deposits. Skarn deposits are usually smaller than other types of iron ore deposits, but can still be economically viable sources of iron ore.

Hematite and magnetite are the two most important iron ore minerals and are commonly found in iron ore deposits all over the world.

Table 1.1 The top iron ore reserves by country (URL-1)

Country	Crude ore reserve 2024 (billions of tons)	Iron content reserve 2024 (billions of tons)
Australia	58	27
Brazil	34	15
Russia	29	14
China	20	6.9
India	5.5	3.4
Canada	6	2.3
Iran	3.3	1.5
United States of America	3.2	1.3
Kazakhstan	2.5	0.90
South Africa	0.99	0.62

As already mentioned, iron is an important mineral in today's world and its trade is of international importance. In 2023, global trade in iron ore reached US$ 162 billion, a decrease of 7.84% from 2022, when trade amounted to US$ 175 billion. Over the last five years, trade in this category has grown at an annualized rate of 8.49% and it ranked 18th out of 1217 world trade products.



Figure 1.1 Iron ore world trade by observatory of economic complexity (URL-2)

By 2023, Australia was the largest producer of iron ore with 900+ million tons but the majority of iron ore production was exported, followed by Brazil with 400+ million tons of iron ore production. China and India follow with 300- million tons. Russia, Iran and Canada with 90- million tons are the most important countries, which together with South Africa, Kazakhstan, the USA, Sweden and Türkiye produce most of the world's iron ore.

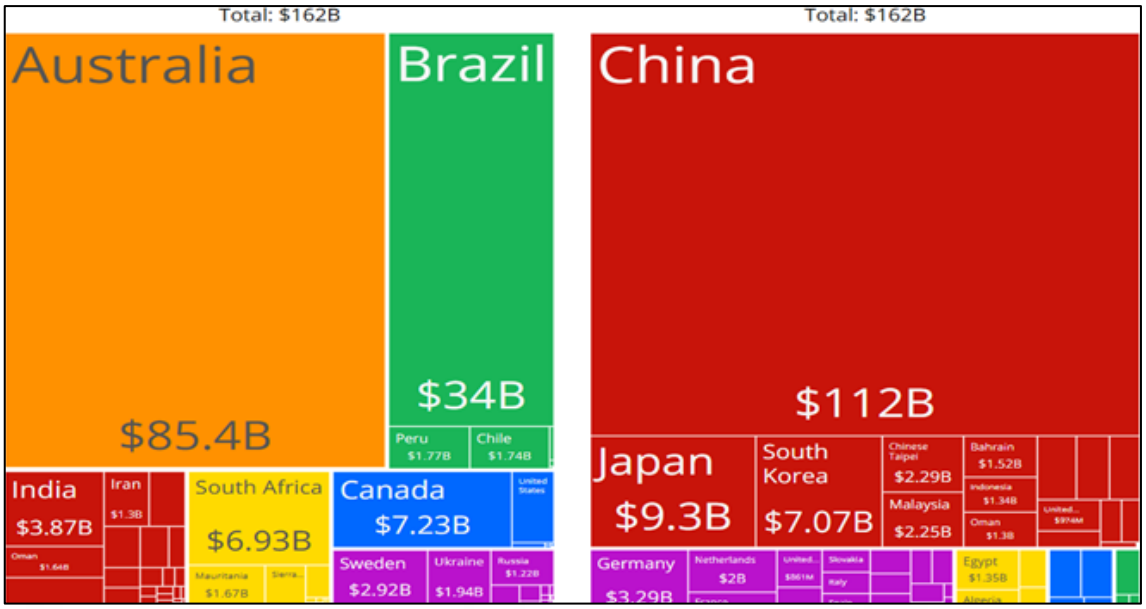

Figure 1.2 Top iron ore trading countries (URL-2)

Table 1.2 Iron ore production in 2023 by country (URL-1)

Country	Ore production (million tons)	Country	Ore production (million tons)
Australia	960	Kazakhstan	53
Brazil	440	United States of America	44
China	280	Sweden	38
India	270	Ukraine	36
Russia	88	Peru	19
Iran	77	Chile	18
Canada	70	Türkiye	17
South Africa	61		

In 2023, Australia was at the top of the export list with around 700 million tons of iron ore exports and a trade volume of US$85 billion, representing 52% of the global iron trade. Brazil is the second largest country exporting iron ore with 260 million tons, South Africa with 46 million tons, India with 27 million tons and Canada with 25 million tons are the top exporting countries in 2023, while other countries only export 92 million tons.

China tops the import list with around 1.2 billion tons and a trade volume of US$112 billion, which corresponds to 69% of global trade. Japan with 98 million tons, South Korea with 70 million tons, Germany with 37 million tons, Taiwan with 25 million tons and the Netherlands with 22 million tons are the most important importing countries. Italy, France, Türkiye and the USA import less than 20 million tons of iron ore.

2. LITERATURE REVIEW

2.1. General

A successful production system brings significant benefits for the company and society. One of the most important factors for the successful transformation of raw materials into products is the appropriate planning and management of production. Mining is one of the sectors that require long-term production planning, as it involves many uncertainties and is a capital-intensive business.

Surface mine production planning is usually carried out as short-term and long-term production planning. Short-term production planning is usually carried out at the operational level on a weekly and daily basis, while long-term planning sets production limits on an annual basis, which can be divided into half-yearly or quarterly periods. Long-term plans therefore set a limit for short-term plans and require the inclusion of several parameters that should be carefully evaluated. The main objective of production planning in open pit mining is to determine ore and waste mining sequences that satisfy geotechnical, process and other operational constraints so that the overall benefit of block selection should be maximized in the different periods. On this basis, production plans typically aim to maximize the total amount of end product or maximize net present value (NPV). Maximization of the end product is generally sought when market pressures or other commitments are present. The majority of long-term production planning is done to maximize NPV (Kaydım, 2022).

Long-term production planning (LTPP) is a large-scale optimization problem that aims to find the block mining sequence that generates the highest possible NPV while satisfying a variety of physical and economic constraints (Osanloo et al., 2008).

Successful production management, which is one of the main functions of the company, can create benefits at the level of the company, the market and the country's economy. An important part of production management is production planning and scheduling. Planning and scheduling provide the company with the ability to easily see the future and be prepared for uncertainties. As in many other sectors, the management of production is of great importance in the mining sector. For this reason, the quantitative decision-making techniques developed for production planning and scheduling have also been applied to mining (Karaöz, 2014).

2.2 Previous Studies on Mine Planning

There are dozens of research studies, which have been conducted by various Masters and PhD students and scientists on long and short-term production planning for open pit mines. This research has included geostatistical and classical methods for resource estimation, solid body and block modeling, nested and final pit determination and selection. Ultimately, the aim is to optimize the long-term planning of a mine.

The estimation of mineral resources is about exposing the quality of an ore body with its quantity in order to legitimize investments. The main problem with estimation is the uncertainty of samples from drill holes or prospecting samples, so powerful classical and geostatistical estimation methods are used. Accordingly, the estimation of mineral resources involves the evaluation of the quality, quantity, continuity, location and orientation of geological features to ensure reliable estimates (Lindi, 2004).

Geostatistical techniques such as kriging and conditional simulation are often used for resource estimation. Matheron (1971) introduced the concept of geostatistics, which was further refined by Journel and Huijbregts (1978) for the estimation of mineral resources.

Knudsen (1975) compared the geostatistical method for estimating ore reserves with the polygon method, the inverse square distance (IDS) method and the Ellipsoid method. Each method was evaluated for its ability to accurately predict the grades of individual blocks and total ore reserves for a bench at the Pima Mine. The study showed that the geostatistical method is neither better nor worse than the Ellipsoid or IDS method, but that the polygon method is inferior. Furthermore, it is emphasized that the geostatistical method is superior due to its ability to produce confidence limits for the estimates.

Ergin et al. (1998) used both the classical polygon method and the inverse distance weighting method in a computerized program SURPAC2000™ in a lignite basin of Edirköy-Saray, Thrace and found differences between the results.

Osanloo et al. (2008) explained production planning by using different types of algorithms to solve long-term production planning problems and mentioned that there are two approaches to solve LTPP problems: (1) deterministic and (2) uncertainty-based approaches. The deterministic approach assumes that all inputs have fixed, known real values; the uncertainty-based approach takes into account the variability of some data (e.g. ore grade, future product demand, future product price).

Topal and Ramazan (2012) have developed a linear network programming (LP) model to optimize strategic planning and production planning by maximizing NPV. The developed model was tested in many mines in Western Australia and it was found that the production program of a mine with a high production capacity was efficiently optimized.

Acan (2013) created an iron (hematite) field block model using the nearest neighbor method and the inverse distance weighting method. The results obtained by both methods were evaluated and differences in the estimated reserve quantity and grade distributions were found.

Dimitrakopoulos and Jewbali (2013) focused on the optimization of long-term production planning in open pit mining under geological uncertainty. They presented an approach that uses stochastic optimization and simulated geological scenarios to manage risk and improve decision making. This method helps to maximize the value of the mine while taking into account the uncertainty of ore grades and other geological factors.

Moharaj and Wangmo (2014) conducted a study on resource estimation from drilling data at a gold mine using SURPAC™ software. Three different methods were used for the estimation: the inverse distance weighting method, the nearest neighbor method and the ordinary kriging method. The parameters were not changed for all three methods and the calculation times were similar. Therefore, the efficiency of the nearest neighbor and inverse distance methods was compared with the ordinary kriging method, which is widely recognized as the best linear estimation method. According to the results, compared with the kriging method, the nearest neighbor method found that the distribution of iron content is higher than the actual value, and the reserve amount is lower than the required value. It was also found that the inverse distance weighting method overestimated the distribution of iron content and the reserve quantity of the study area.

Akisa et al. (2015) performed the mine planning and optimization of a gold field using the Surpac and Whittle packages. First, the block model of the field was created and the inverse distance weighting method was used to estimate the distribution of gold grade in the field. In addition, the pit optimization process selected the most suitable pit shell using the 3-dimensional Lerchs-Grossmann algorithm. The NPV was found to be particularly sensitive to the gold price and operating costs.

Shishvan and Sattavand (2015) presented a new technique for long-term planning of open pit production based on the concept of ant colony optimization (ACO). The application was tested on a real-size copper-gold deposit using two types of ant colony optimization: the max–min ant system (MMAS) and the ant colony system (ACS). Various mathematical techniques such as integer programming and relaxation methods have been tried to solve the problem of long-term production planning in open pit mining, but all suffered from not being able to solve examples of realistic size and detail.

When estimating resource models, the reliability of the estimated amount of ore depends on the accuracy of the prediction. The geological model is designed to reflect realistic values and incorporate the site's resource. It is based on the selection of a prediction method that is consistent with this data. To demonstrate that the resource model provides consistent results, the estimated ore quantity must also be tested using various estimation methods. Mines with well-classified geological features, variables and discontinuities that are estimated and approximated as accurately as possible enable the effective implementation of economic and strategic decisions in long-term and short-term production plans or during production (Fenerli and Güven, 2019).

Karakut (2019) used geostatistical analyzes (statistical and variogram analysis) to calculate the tonnage based on grade distribution and determined the distribution of the ore in the deposit using the kriging method. The expected costs for the mining and processing phases were determined. In addition, a series of nested pits were created by changing the selling price of the ore.

Luan Mai et al. (2019) have presented a risk-based optimization method for long-term production planning in open pit mines. It takes into account geological uncertainties, equipment constraints and the quality of the ore. Stochastic simulations are used to create production plans that improve reliability and economic performance compared to conventional methods.

2.3. Open Pit Mining Problems

When we talk about mining, especially surface mining, it is a process with advantages and problems. Nowadays, this type of mining is widely used throughout the mining industry because it is economically and technologically simple and facilitates the use of heavy equipment. However, the flexibility of the market is one of the biggest problems in this industry, especially for metals. We don't know what the characteristics of the market are, when and how? Because the market changes daily and hourly due to market demand, political issues, currency fluctuations, climate changes, pandemics and so on. If it is a long-term production plan, it must be flexible enough to adapt to these dynamic conditions.

Another problem with open pit mining is the uncertainty of the ore, as you only have limited drilling data or samples from the area to be estimated and it is very important to get a fair estimate of grades and tonnages for mining. Inaccurate resource models are a guide to risky decisions.

The dependence of mining blocks is also one of the main problems with open pit mining. You can’t just mine the valuable block before the non-valuable block. So the costs become high and the net value decreases. To solve the problem, Lerchs and Grossmann (1966) developed their own algorithm to optimize the open pit limit that maximizes the NPV. This algorithm forms the basis for many modern pit optimization software tools.

Pushbacks, or phases, are smaller pits within the ultimate pit limit designed to optimize cash flow and operational efficiency. Studies by Whittle (1988) and subsequent improvements by other researchers have focused on sequencing pushbacks to enhance NPV while managing operational constraints.

Determining optimal cutoff grades is crucial for maximizing NPV. Lane's theory (1988) on cutoff grade optimization provides a framework for balancing ore and waste extraction to achieve economic efficiency. Recent work by Asad and Topal (2011) extends these principles to dynamic cutoff grade policies.

Production planning involves scheduling the extraction of ore and waste over the life of the mine to maximize economic returns and ensure operational feasibility.

Long-term production schedules are developed to align with the strategic objectives of the mining project. Techniques such as linear programming and goal programming are used to optimize the extraction sequence. Newman et al. (2010) review various methods and their applications in mine production scheduling.

Limitations of the equipment in long-term production is a classic problem that must be solved for capacity control, maximum utilization, and hauling of ore and waste. It is possible to use conveyor belts for ore transportation in open mines and to increase the capacity of trucks and other transportation equipment.

3. MATERIALS AND METHODS

3.1. Materials

The primary dataset used in this study consists of exploration drilling data from 42 drill holes totaling 1321 samples of drilled material. This data was organized and converted into Excel spreadsheets and categorized into four main components: Collar, Geology, Survey and Assay.

The collar data contains information such as the hole ID, the coordinates of the longitude (east) and latitude (north), the reduced level (RL) and the maximum depth of the individual boreholes.

The geology file contains the hole ID, the depth from, the depth to, the interval and the lithologic code representing the geologic features encountered during drilling.

The survey data comprises the hole ID, azimuth, dip, and depth, which are essential for understanding the orientation and trajectory of each borehole.

The assay file contains details of the chemical analysis, including the depth from, depth to, interval and iron content (Fe%) of each sample.

In addition to the drilling data, the second key material utilized in this study is the topography of the explored area, which serves as a spatial reference for geological modeling, block modeling, and open-pit design.

3.2. Methods

This part of the study describes the methodology applied to the project, which combines both economic principles and mathematical algorithms to support long-term mine planning. In open pit mining, the definition of pit boundaries is of crucial importance as it has a direct impact on the efficiency and profitability of resource extraction. The aim is to minimize waste extraction and maximize ore recovery, as excessive waste extraction leads to increased operating costs and a loss of time and value. To solve this problem, the Lerchs-Grossmann algorithm, which was first introduced by Lerchs and Grossmann in the 1960s, was used to determine the optimum boundaries of the excavation pit.

In addition, the study discusses various pit development strategies that determine the development of the pit over time. These include the worst-pit method, the best-pit method, and multiple benching (or staggered pushbacks). Each method represents a different sequencing approach and has implications for cash flow, operational feasibility and project risk. By comparing these strategies, the study aims to find a balanced and economically viable approach to pit development.

3.2.1. Time value of money

The time value of money (TVM) is a historical financial concept based on the principle that a sum of money today is more valuable than the same sum in the future. Put simply, a Turkish lira (₺) today is worth more than a Turkish lira tomorrow.

Historically, this concept was mainly observed in the practice of lending money with interest. There is evidence in ancient historical records to suggest that forms of interest indebtedness existed during the time of the Pharaohs, including the period traditionally associated with the Prophet Moses (peace be upon him). Moreover, such practices were common in the pre-Islamic era before the advent of Islam. It is documented that some of the uncles of Prophet Mohammad (peace be upon him) and other wealthy individuals from the tribe of Quraish were involved in deals that consisted of lending money at interest for a year, if they did not have it, they were to double the interest a year later, it was a profit without losses. These practices were widely known and often criticized as exploitation of the poor, which eventually led to the prohibition of riba (usury or interest) in Islam.

In the modern era of banking, the same concept is used for both sides: The bank gives you the debt and in return receives the same money with interest, you give the bank the money and receive the interest.

In the 20th century, engineers used the concept of TVM in mining for capital budgeting and feasibility studies. It was very important for assessing the net present value of mining projects as the cash flow and total cost of the project was delayed.

One of the biggest challenges in mining projects is the uncertainty of future conditions. Investors and companies often do not have the necessary capital in the initial stages and still have to commit to significant expenditures, such as acquiring ore bodies, developing infrastructure and ensuring long-term operational readiness. However, several unpredictable factors can affect the financial success of the project over time. These include the future market value of the mined ore, currency fluctuations, changes in the political or regulatory environment and macroeconomic conditions such as inflation or interest rates. All these factors contribute to the risk that a project planned today will not yield the expected return tomorrow. Therefore, the time value of money is essential in mining economics as it helps to discount future cash flows and assess whether a project is still worthwhile under uncertain and potentially damaging future scenarios.

When planning a surface mine, an accurate estimate of revenues and costs is essential to determine the financial feasibility of a project. As outlined by Hustrulid et al. (2013), key economic considerations include ore grade, recovery rates, metal prices, and capital and operating costs. However, these estimates must be evaluated in the context of the time value of money. Since mining projects typically span many years from exploration to production, future revenues and costs must be discounted to their present value in order to accurately assess profitability. Financial tools such as net present value and internal rate of return (IRR), which are central to TVM, allow engineers and investors to account for inflation, market uncertainty and opportunity costs. Without the application of these principles, there is a significant risk that the value of a project will be

overestimated, particularly in volatile sectors such as mining where political, economic and environmental factors can change dramatically over time.

3.2.2. Lerchs-Grossmann algorithm

The pit that exists at the end of mining is called the 'final' or 'ultimate' pit. There are several intermediate pits between the birth and death of an open pit mine (Hustrulid et al., 2013).

The most common algorithm for determining the pit limit of a mine was first published in a paper entitled 'Optimum design of open-pit mines' by Lerchs and Grossmans (1965). This algorithm uses economic block values and slope constraints to define a pit shape that has the highest possible net profit. It remains one of the most fundamental tools for modern open-pit mine planning. In this algorithm, each block is assigned an economic value to determine and optimize the final pit limit. To identify the profitable blocks, this algorithm uses graphical theory. The chosen form in this algorithm is not only geotechnically stable, but also economically recognized, i.e. both the ore value and the mining costs are taken into account.

Figure 3.1 shows a 2D sectional view demonstrating the application of the Lerchs-Grossmann (1965) algorithm to calculate the economic value of a mine. In this method, the ore body and surrounding waste rock are discretized into a regular grid by dividing the section into rows and columns to create a matrix of blocks. Each block is assigned an economic value based on its content, usually a positive value for ore and a negative value for waste rock. This matrix serves as input to the optimal pit limit algorithm, which determines the most profitable configuration for mining by maximizing the overall economic value.



Figure 3.1 Orebody geometry for Lerchs-Grossmann 2-D algorithm

Lerchs and Grossmann (1965) first made calculations on 2D sections and then combined these sections to create a 3D pit. The basic steps used to find open pit boundaries with dynamic programming method are explained by Hustrulid et al. (2013).

$$M_{ij} = \sum_{k=1}^{i} M_{kj}$$

The process, which describes this equation is:
The block positions are designated with an i, j numbering system. Following the nomenclature used by Lerchs and Grossmann, i refers to the rows and j to the columns. The first step in this

procedure is to calculate the cumulative gains for each column of blocks, starting from top to bottom. Each vertical column of blocks is independent of the others.

In the second stage, grade values are assigned to the individual blocks within the ore body. Blocks that have no economic significance remain empty and are not considered further (Figure 3.2).

In the third stage, the economic value of each block is calculated taking into account various technical and economic parameters, such as the selling price of the ore at a certain grade, the operating, processing and selling costs as well as the block size, the density of the ore and overburden and the smelting recovery rate (Figure 3.3).

In the fourth stage, a column is added to the far left and a row to the top of the matrix to facilitate the cumulative economic analysis. From top to bottom, the cumulative economic value is plotted for each block (Figure 3.4).

The fifth stage comprises the dynamic block evaluation, in which a new value is assigned to each block in the matrix (starting at the beginning of the first column). This value is calculated by adding the block's own value to the minimum of the values of its neighboring blocks— - from the rows above and below the block and from the column to the left of it (Figure 3.5).

In the sixth and final step, the determination of the operational (pit) boundaries, the process begins with the determination of the highest cumulative value, starting with the top row on the far right of the matrix. From this point, the algorithm proceeds backwards and selects the neighboring block with the highest value among the three blocks in the left column, thereby determining the optimal extraction path (Figure 3.6).

In the final stage of the Lerchs and Grossmann (1965) algorithm, the total economic value of the pit is determined by summing the values of all blocks that lie within the optimal pit boundaries, as defined in Figure 3.7.

In this example, the calculated economic value of the pit amounts to 2099 units, representing the maximum recoverable value under the given constraints.

0	0	0	0	0	0	0	0	0	7	0	0	0	0	0	0	0	0	0	0	0	0
0	0	0	0	0	0	0	0	0	5	6	3	0	0	0	0	0	0	0	0	0	0
0	0	0	0	0	0	3	0	0	7	1	7	8	0	0	0	0	0	0	0	0	0
0	0	0	0	0	0	0	7	0	0	1	4	8	8	0	0	0	0	0	0	0	0
0	0	0	0	0	0	0	0	4	0	0	9	8	1	9	0	0	0	0	0	0	0
0	0	0	0	0	0	0	0	4	5	0	0	7	1	6	0	0	0	0	0	0	0
0	0	0	0	0	0	0	0	5	3	0	0	0	6	6	0	0	0	0	0	0	0
0	0	0	0	0	0	0	0	0	0	0	0	0	0	0	0	0	0	0	0	0	0

Figure 3.2 Assigning grade values to ore (URL-3)

-4	-4	-4	-4	-4	-4	-4	-4	-4	62	-4	-4	-4	-4	-4	-4	-4	-4	-4	-4	-4	-4
-4	-4	-4	-4	-4	-4	-4	-4	-4	40	51	-4	-4	-4	-4	-4	-4	-4	-4	-4	-4	-4
-4	-4	-4	-4	-4	-4	-4	-4	-4	62	-4	62	74	-4	-4	-4	-4	-4	-4	-4	-4	-4
-4	-4	-4	-4	-4	-4	-4	62	-4	-4	-4	28	74	74	-4	-4	-4	-4	-4	-4	-4	-4
-4	-4	-4	-4	-4	-4	-4	-4	28	-4	-4	86	74	-4	86	-4	-4	-4	-4	-4	-4	-4
-4	-4	-4	-4	-4	-4	-4	-4	28	40	-4	-4	62	-4	51	-4	-4	-4	-4	-4	-4	-4
-4	-4	-4	-4	-4	-4	-4	-4	40	-4	-4	-4	-4	51	51	-4	-4	-4	-4	-4	-4	-4
-4	-4	-4	-4	-4	-4	-4	-4	-4	-4	-4	-4	-4	-4	-4	-4	-4	-4	-4	-4	-4	-4

Figure 3.3 Block economic values (URL-3)

0	0	0	0	0	0	0	0	0	0	0	0	0	0	0	0	0	0	0	0	0	0
0	-4	-4	-4	-4	-4	-4	-4	-4	-4	62	-4	-4	-4	-4	-4	-4	-4	-4	-4	-4	-4
0	-8	-8	-8	-8	-8	-8	-8	-8	-8	102	47	-8	-8	-8	-8	-8	-8	-8	-8	-8	-8
0	-12	-12	-12	-12	-12	-12	-12	-12	-12	164	43	54	66	-12	-12	-12	-12	-12	-12	-12	-12
0	-16	-16	-16	-16	-16	-16	-16	50	-16	160	39	82	140	62	-16	-16	-16	-16	-16	-16	-16
0	-20	-20	-20	-20	-20	-20	-20	46	12	156	35	168	214	58	70	-20	-20	-20	-20	-20	-20
0	-24	-24	-24	-24	-24	-24	-24	42	40	196	31	164	276	54	121	-24	-24	-24	-24	-24	-24
0	-28	-28	-28	-28	-28	-28	-28	38	80	192	27	160	272	105	172	-28	-28	-28	-28	-28	-28
0	-32	-32	-32	-32	-32	-32	-32	34	76	188	23	156	268	101	168	-32	-32	-32	-32	-32	-32

Figure 3.4 Cumulative totals of block economic values (URL-3)

0	0	0	0	0	0	0	0	0	0	0	0	0	0	0	0	0	0	0	0	0	0
0	-4	-4	-4	-4	-4	-4	-4	-4	-4	62	112	221	229	283	429	577	713	755	825	903	930	926
0	-8	-12	-12	-12	-12	-12	-12	-12	-12	116	225	233	287	433	581	717	759	829	907	934	926	922
0	-12	-20	-24	-24	-24	-24	-24	-24	14	178	241	295	441	589	725	767	837	915	942	930	922	914
0	-16	-28	-36	-40	-40	-40	-40	26	10	198	241	375	601	737	779	849	927	954	938	926	914	906
0	-20	-36	-48	-56	-60	-60	-60	6	38	202	293	461	675	795	865	943	970	950	934	918	906	894
0	-24	-44	-60	-72	-80	-84	-84	-18	46	258	289	457	737	791	963	990	966	946	926	910	894	882
0	-28	-52	-72	-88	-100	-108	-112	-46	62	254	285	449	729	842	1014	986	962	938	918	898	882	866
0	-32	-60	-84	-104	-120	-132	-140	-78	30	250	277	441	717	830	1010	982	954	930	906	886	866	850

Figure 3.5 Sum of block values with its maximum neighborhood on the left (URL-3)

0	0	0	0	0	0	0	0	0	0	0	0	0	0	0	0	0	0	0	0	0	0
0	-4	-4	-4	-4	-4	-4	-4	-4	-4	62	112	221	229	283	429	577	713	755	825	903	930	926
0	-8	-12	-12	-12	-12	-12	-12	-12	-12	116	225	233	287	433	581	717	759	829	907	934	926	922
0	-12	-20	-24	-24	-24	-24	-24	-24	14	178	241	295	441	589	725	767	837	915	942	930	922	914
0	-16	-28	-36	-40	-40	-40	-40	26	10	198	241	375	601	737	779	849	927	954	938	926	914	906
0	-20	-36	-48	-56	-60	-60	-60	6	38	202	293	461	675	795	865	943	970	950	934	918	906	894
0	-24	-44	-60	-72	-80	-84	-84	-18	46	258	289	457	737	791	963	990	966	946	926	910	894	882
0	-28	-52	-72	-88	-100	-108	-112	-46	62	254	285	449	729	842	1014	986	962	938	918	898	882	866
0	-32	-60	-84	-104	-120	-132	-140	-78	30	250	277	441	717	830	1010	982	954	930	906	886	866	850

Figure 3.6 Finding the most suitable pit limit (URL-3)

		-4	-4	-4	-4	-4	-4	-4	62	-4	-4	-4	-4	-4	-4	-4	-4	-4	-4	-4	
			-4	-4	-4	-4	-4	-4	40	51	-4	-4	-4	-4	-4	-4	-4	-4	-4		
				-4	-4	-4	-4	-4	62	-4	62	74	-4	-4	-4	-4	-4	-4			
					-4	-4	62	-4	-4	-4	28	74	74	-4	-4	-4	-4				
						-4	-4	28	-4	-4	86	74	-4	86	-4	-4					
							-4	28	40			62	-4	51	-4						
								40					51	51							

Figure 3.7 Final pit limit (URL-3)

3.2.3. Pit advancing

It is important to answer the question of what kind of miner you are: an executive, a civil servant or a researcher. It all depends on whether you, as an engineer, are planning an open pit production for a long or short time, but for whom and what you are against. If you are a businessman, it means he/she wants the wealth as soon as possible, if it is the government then they are not in a hurry and the mine means wealth for them and they don't want to waste even a small part of the ore body, but if it is a researcher then it is about solving the problems of the past and they can explore any scenario.

Once the ultimate pit boundary has been determined using the Lerchs-Grossmann algorithm, this final pit must be subdivided into mineable sections. These sections are called 'pit advancement stages'. What is the operating strategy in terms of management, economic reliability and cash flow? Which set of equipment will you be using? What are the stages or methods; the worst-case, the best-case or multiple benching?

In the worst case, excavation begins at the surface, along the uppermost elevation. Blocks of low value, mostly waste, are removed. When the top layer is finished within the limits of the planned pit, mining continues with the benches of the lower layer. This method of extracting ore bodies usually takes an unnecessarily long time and is usually not economic, as it can take years to reach the ore body. The big problem with this scenario is therefore the delay in profit, which can jeopardize the project until the end, and the financial burden.

Its use in open pit mining is rare, governments or educational institutions may use the scenario. Governments may need the mineral for some long-term construction projects, but for educational purposes, evaluating sensitivity analysis is important to know how poorly the project may turn out if the sequencing is bad. A worst-case example of an iron mine is shown in Figure 3.8, where numerous waste blocks were to be mined first.

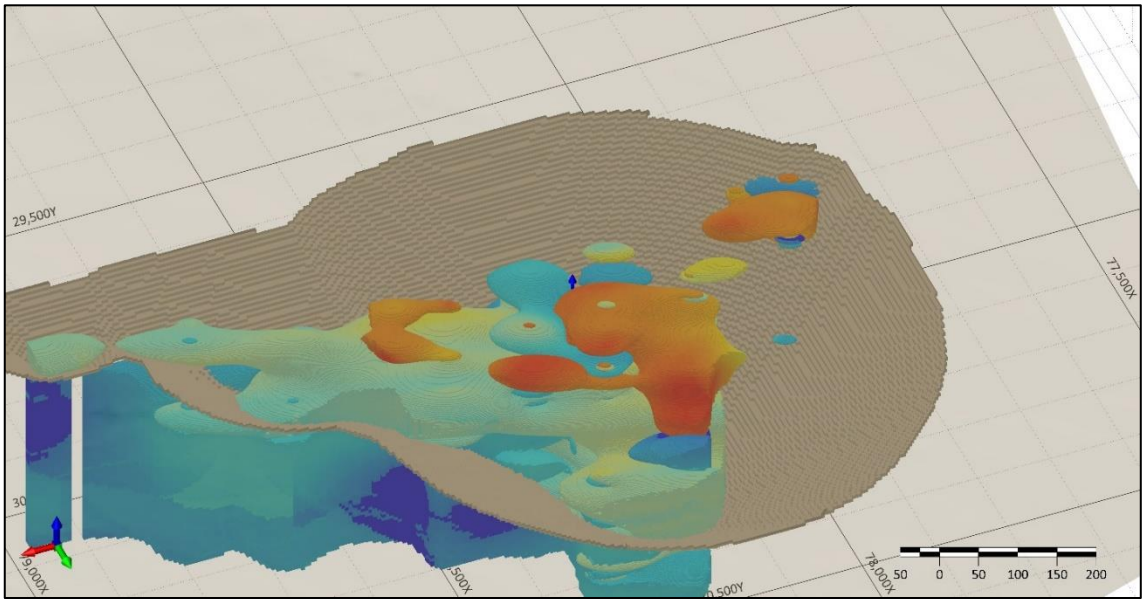

Figure 3.8 Ultimate pit limits in the case of worst-case algorithm

The basic idea of the best-case scenario is to start mining at the point where the high-grade ore is closest to the surface. This choice is preferred when management wants to realize its profit as quickly as possible. In most cases, mining companies do not want to take risks with their projects and want cash flow to start as soon as possible. Therefore, they use the best-case scenario, which allows them to make a profit in the first few years of the mine. In Figure 3.9, we can see that the initial pit, which includes the high-grade parts of the ore body closest to the surface, is colored dark red. We can see the huge ore body down to the source below the pit, as the company is aiming for a quick return on investment.

In multiple benching, the final pit is divided into several phases and a sensible plan is needed for each sector, especially for cash flow flexibility. We do not excavate the pit from top to bottom, but divide it into different parts. The first subdivision is to extract the part closest to the ore and make the profit so as not to delay the project, then go further down and extract another mass closest to the ore and continue this until the final stage, as shown in Figure 3.10. Mining with multiple benches may or may not reduce the NPV compared to the best-pit method, but it has the operational flexibility, longer operating time of mining, can respond to the fluctuation of market conditions and current resources, and is the most practical and realistic scenario. Therefore, it must be carefully planned.

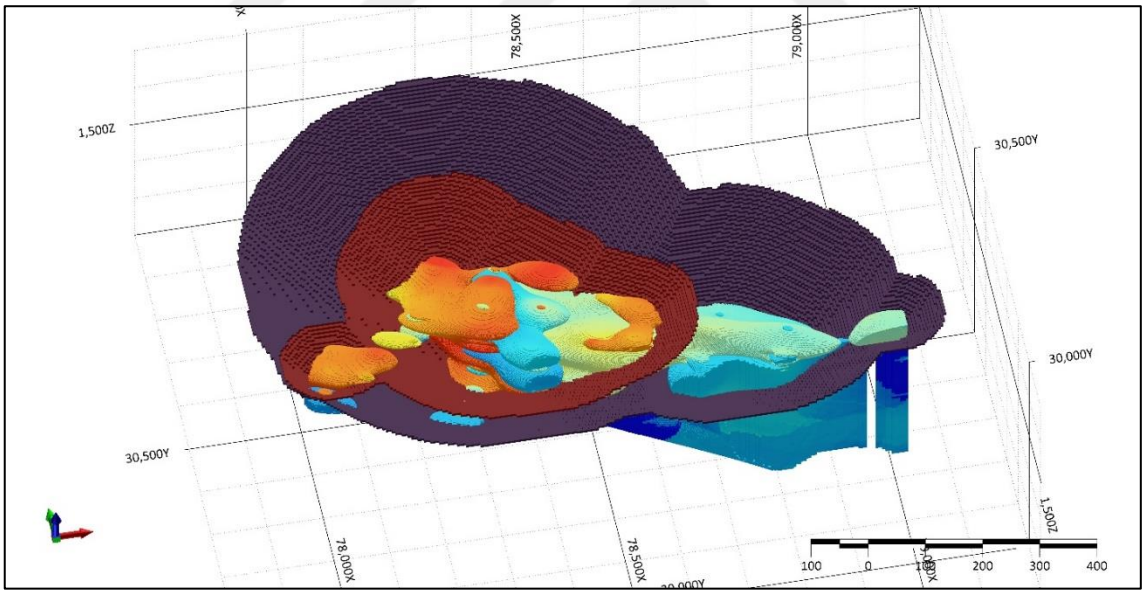

Figure 3.9 Ultimate pit limits in the case of best-case algorithm

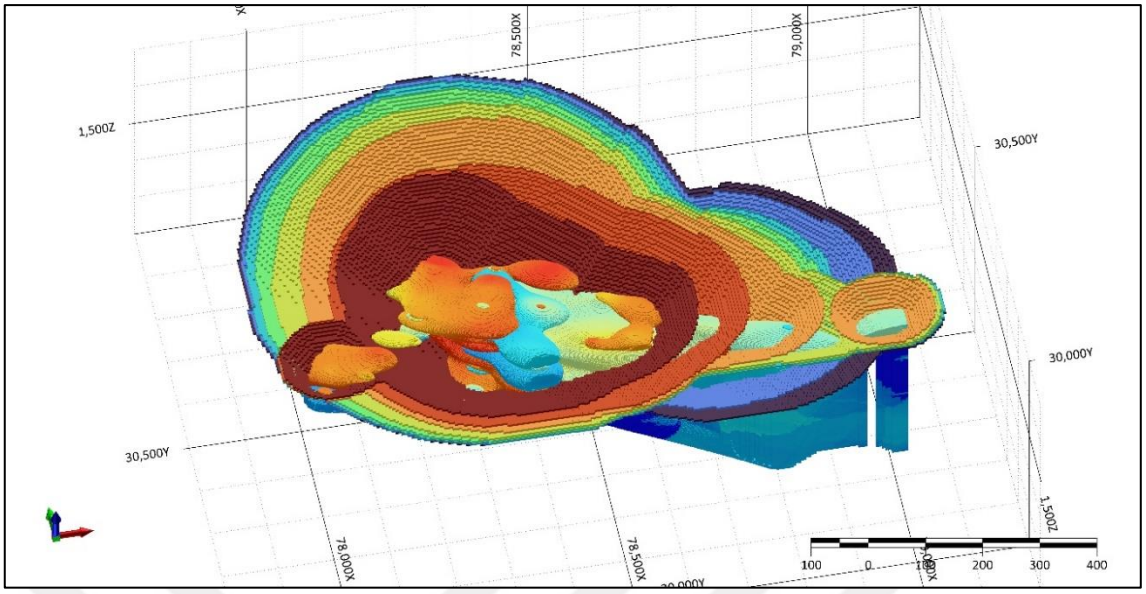

Figure 3.10 Pit limits in the case of multiple benching algorithm

4. STATISTICAL ANALYSIS of DRILLHOLE DATA and ORE GRADES

4.1. Drillhole Data

In the modern age of technological mining, the availability of drilling data is essential for planning production or open pit mining. Once the drill samples are analyzed, both long-term and short-term planning and schedules are easier to create. This section outlines the process from the collection, organization and analysis of drilling data in the study area to the long-term production planning of an open pit iron mine. Due to a verbal confidentiality agreement made during the collection of the drilling data, specific details about the location of the ore deposit and the exploration work remain undisclosed. Therefore, it is assumed that the mine is located in western Afghanistan.

A total of 42 exploration holes were drilled in a ferruginous zone that extends over a length of approximately 3800 meters and a width of 2000 meters. The shallowest borehole reached a depth of 62 meters, while the deepest borehole reached 345 meters. The data from our drilling has been categorized as follows:

a) Collar: - contains the hole ID by numbering, the path of the hole as vertical or horizontal, easting and northing of each hole, RL or reduced level (RL) and the maximum depth of each hole.
b) Survey: - contains the name of each hole, including azimuth, dip and depth.
c) Geology: - contains hole ID, depth from, depth to, interval and lithologic code.
d) Analysis: - contains the results of the chemical analysis, in particular the iron content (Fe%) for each sampled section.

The categorized data was stored in an Excel file in four sheets and all drill hole data was checked and validated in Micromine™ for errors and inconsistencies in samples, coordinates and missing holes (Figure 4.1). Figure 4.2 shows a perspective view of drillholes on the topography.

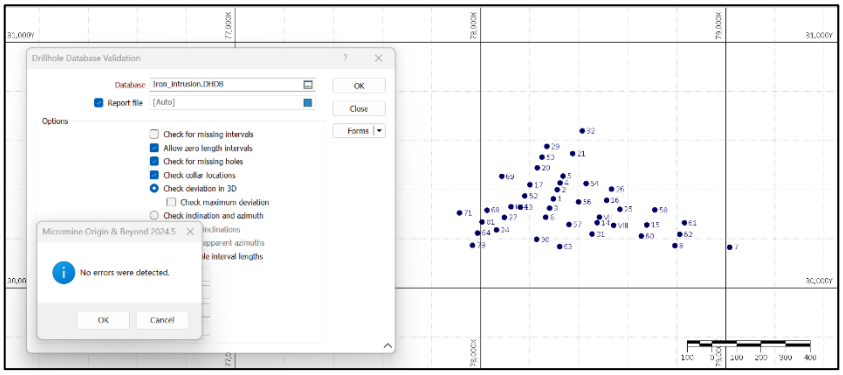

Figure 4.1 Validation of drillholes

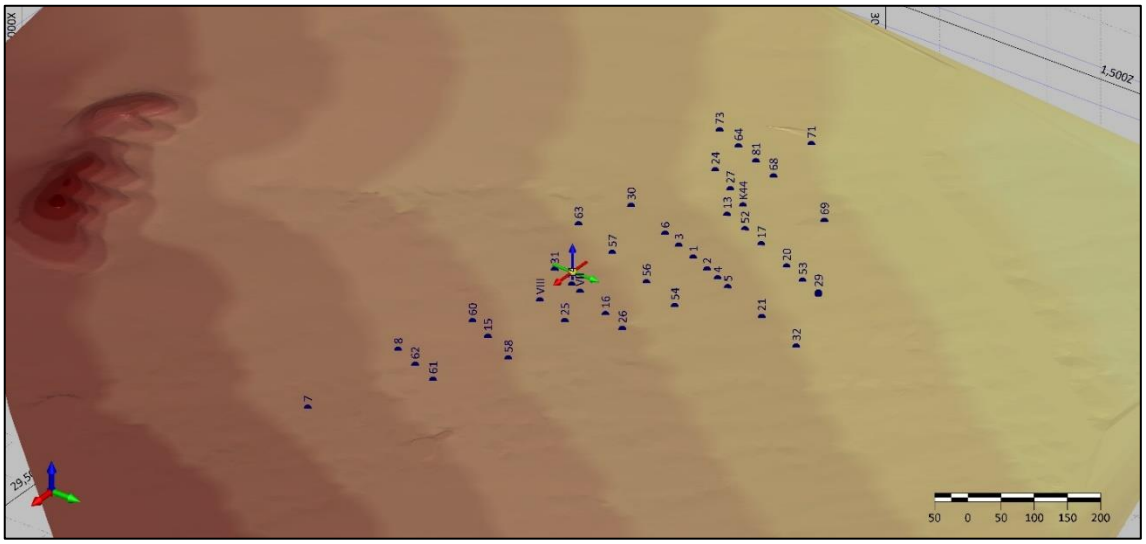

Figure 4.2 Drillholes on the topography

4.2. Grade Distribution of Ore

Estimating the grade is one of the most important steps in the technical and economic investigation of an ore body. This may be because mining projects are highly dependent on the exact level of grade and extensive mining knowledge is required to estimate the concentration and tonnage of ore deposits (Choudhury, 2015).

With the increasing use of earth materials, the average ore grade is decreasing due to extreme market demand and this demand also has a direct impact on prices. As prices rise, the lower grade ore becomes acceptable in the mineral market, especially as the high-grade deposits are depleted and mining has expanded to lower grade ores. At the beginning of the 20th century, for example, the grade of low-grade gold was 10 grams per metric ton (ppm), but high market demand and record high prices have brought the grade down to around 1.3 grams per metric ton (ppm). The same scenario applies to copper ore, the content of which fell from 4% in 1900 to 1.07% in 2010 (Faqir Yar, 2024).

Low-grade iron ore is mined for the same reasons. In the 20th century, the price and demand on the market for iron was stable and relatively low. Until the 1970s, the cut-off grade was over 60% Fe and 65% Fe, but in the 21st century, the market is no longer stable, the demand and price are high, so the cut-off grade changes and drops to 60%. With some modern technological improvements, in some parts of the world the ore is mined down to an average of 40% or 35%. In central Iran, the optimal threshold for low concentrations is 34% for the Bafgh Lakeh Siah iron mine (Mousavi et al., 2022). In a study by Ali Rezaei et al. (2022), 86 million tons of iron deposits with an average grade of 41.9% Fe were estimated in Sangan, northeastern Iran.

The iron ore deposit in this study was divided into three types of grades: low grade (15% Fe), medium grade (30% Fe) and high grade (57% Fe) ore bodies.

The distribution of iron grades within the ore deposit is presented in the form of histograms and tabulated data as follows: high grade ore body in Figure 4.3 and Table 4.1, medium grade ore body in Figure 4.4 and Table 4.2 and low-grade ore body in Figure 4.5 and Table 4.3.

The geological characteristics of the iron ore deposit are characteristically similar to the iron ore deposits mined in the eastern parts of Iran. The proposed mine is located in close proximity to these mines and may face the same environmental and political problems. So, the current situation may point the way to mining high and medium grade ore. In an essay published in the Financial Tribune (URL-4), the Supreme Audit Office of Iran's concern about the depletion of iron ore reserves was mentioned. Saeed Asgarzadeh, secretary of the Iron Ore Association of Iran, recommended lowering the cut-off grade to 20%.

From these reports, it was deduced that the high-grade ore bodies with 57% average Fe and the medium grade ore bodies with 30% average Fe are financially reasonable and recoverable. On the other hand, the low-grade ore body with an average Fe grade of 15% is not affordable for beneficiation and further processing.

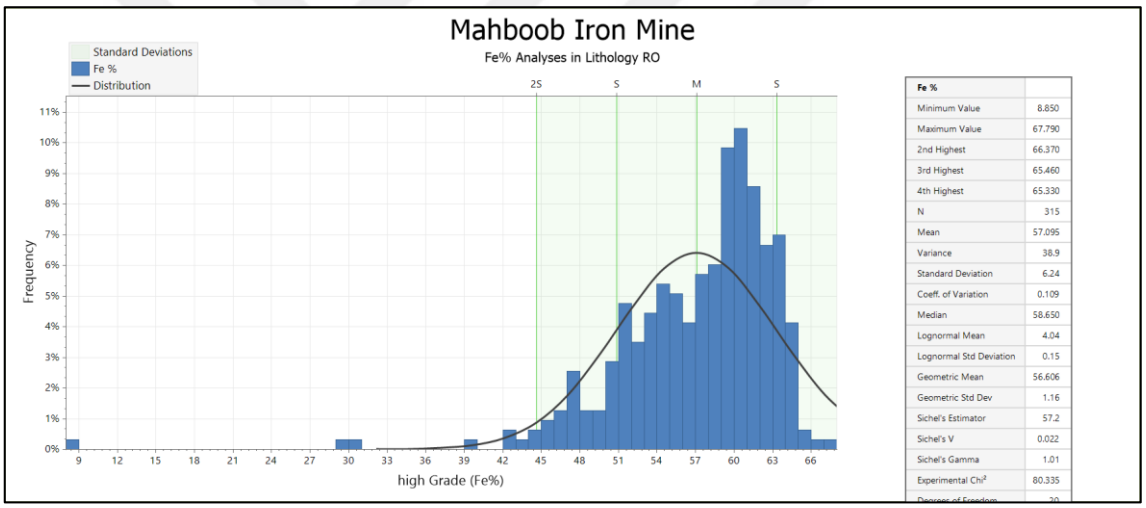

Figure 4.3 Grade distribution histogram of high grade iron ore analyses

Table 4.1 Descriptive statistics for the high grade iron ore

Analyzed data	: 315	Variance	: 38.9
Maximum grade	: 67.97	Lognormal average	: 4.04
Minimum grade	: 8.85	Lognormal Std deviation	: 0.15
Average	: 57.095	Geometric average	: 56.606
Median	: 58.65	Geometric standard deviation	: 1.16
Standard deviation	: 6.24		

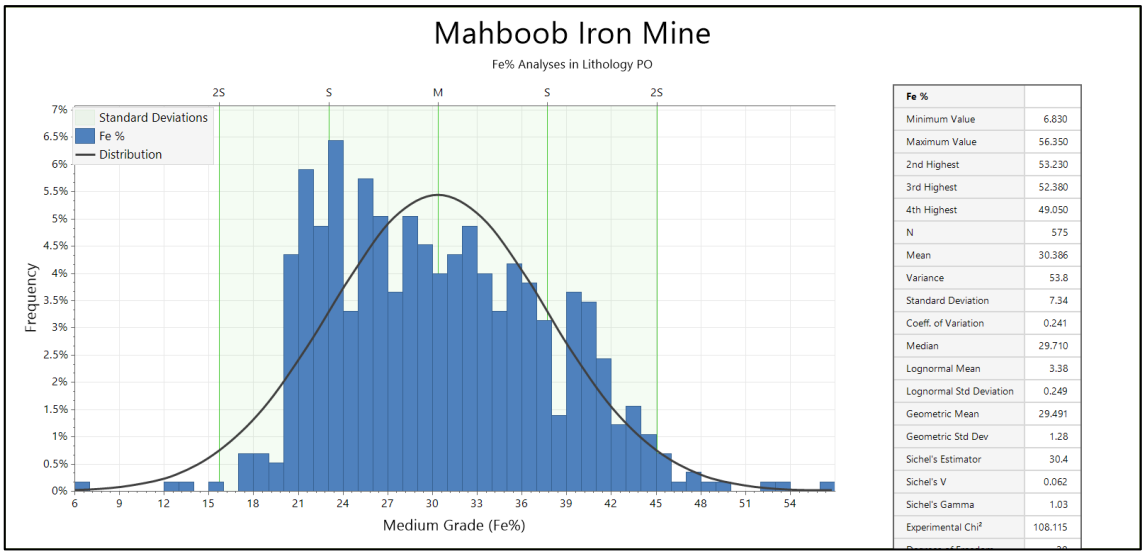

Figure 4.4 Grade distribution histogram of medium grade iron ore analyses

Table 4.2 Descriptive statistics for the medium grade iron ore

Analyzed data	: 575	Variance	: 53.8
Maximum grade	: 56.35	Lognormal average	: 3.38
Minimum grade	: 6.83	Lognormal Std deviation	: 0.249
Average	: 30.386	Geometric average	: 29.491
Median	: 29.710	Geometric standard deviation	: 1.28
Standard deviation	: 7.34		

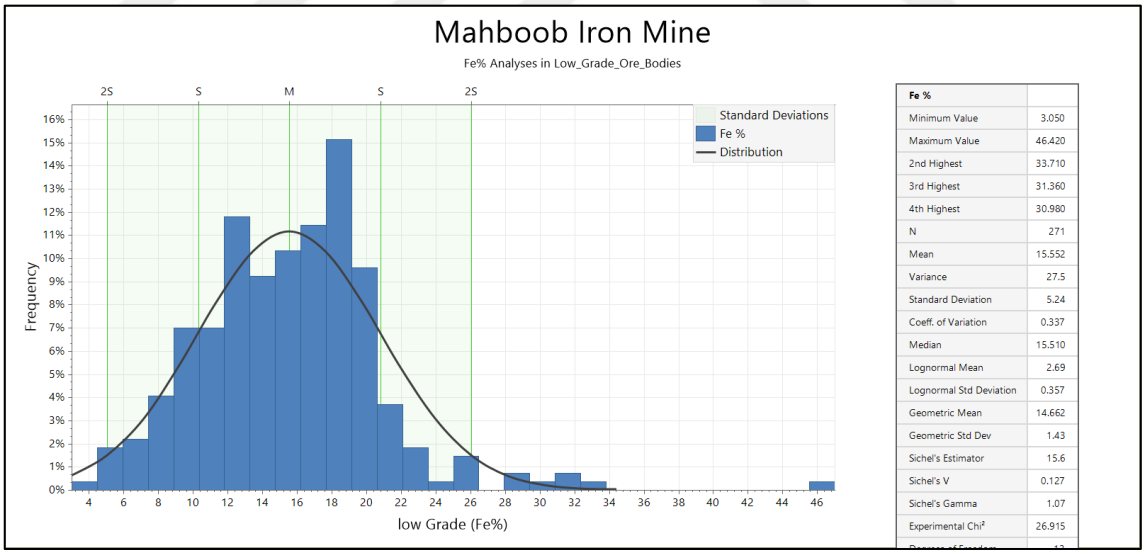

Figure 4.5 Grade distribution histogram of low grade iron ore analyses

Table 4.3 Descriptive statistics for the low grade iron ore

Analyzed data	: 271	Variance	: 27.5
Maximum grade	: 46.42	Lognormal average	: 2.69
Minimum grade	: 3.05	Lognormal Std deviation	: 0.357
Average	: 15.552	Geometric average	: 14.662
Median	: 15.51	Geometric standard deviation	: 1.43
Standard deviation	: 5.24		

Lithologies intersected by the drill holes include high-grade ore (RO), medium grade ore (PO), low-grade ore (MM, DD, CZ, MM and MP) and the waste rock (W). Figure 4.6 shows a perspective view of the site for better visualization. The most abundant samples belong to the high-grade ores, followed by the medium-grade ores and the low-grade ores. The ore-bearing drill holes are surrounded by empty drill holes everywhere. A high column of high-grade ore is concentrated in the drill holes along the southern boundary of the orebody. Figure 4.7 illustrates the situation.

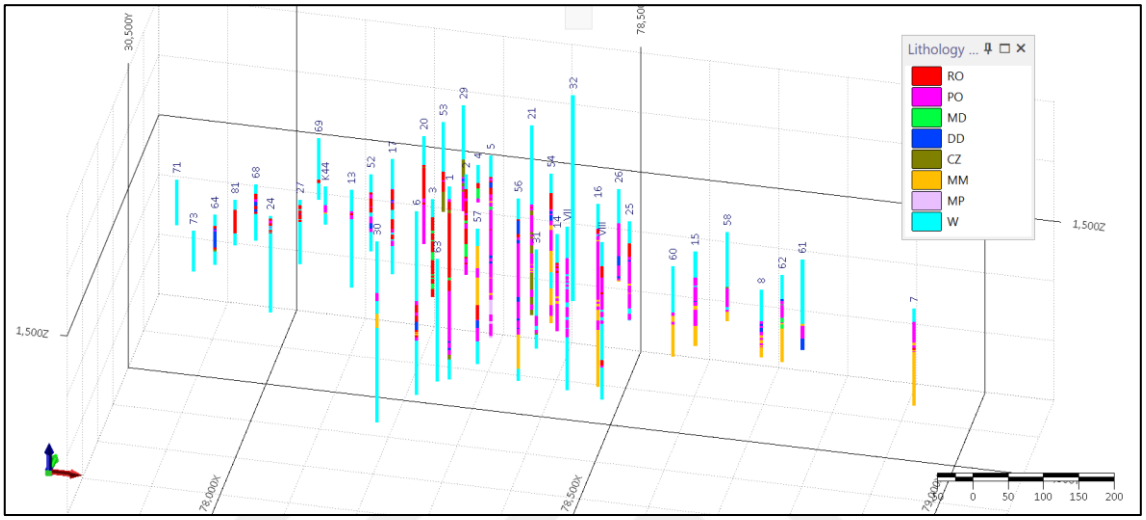

Figure 4.6 Ore and rock layers intersected by drillholes

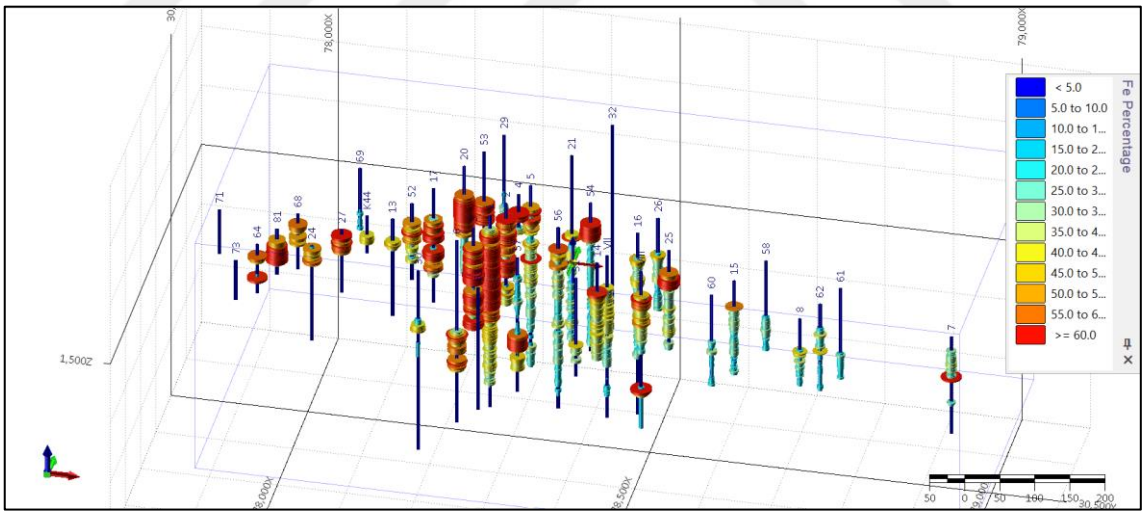

Figure 4.7 The distribution of ore grades in drill holes

4.3. Geostatistical Evaluation

4.3.1. Orebody modeling

In order to assign grade values to the ore blocks, we should have solid body wireframes of the mineral body(ies)and rock layers. For solid modeling, one needs a search ellipsoid with defined dimensions and parameters representing the axes of the search ellipsoid, including strike, dip direction, dip, and plunge. On the other hand, the number of sectors the ellipsoid should have and

the maximum number of analyzes each sector must capture and the minimum total number of analyzes the ellipsoid must capture were determined and presented in Table 4.4. The search ellipsoid to be used in the solid modeling is shown in Figure 4.8.

The strike of the ore body in the field is N111° and the plunge of orebody along the same direction is approximately NW9°-10°. When the sections are taken along WNW-ESE direction from the existing drillhole data the dip of the orebody appears as SW15°-30° and NE9-20°.

Table 4.4 The geometry of the search ellipsoid formed in accordance with the data parameters

Max samples per sector	Min samples for ellipsoid	1st axis (m)	2nd axis (m)	3rd axis (m)	Azimuth (°)	Plunge (°)	Dip (°)
150	4	65	33	20	111	9-10	15-30

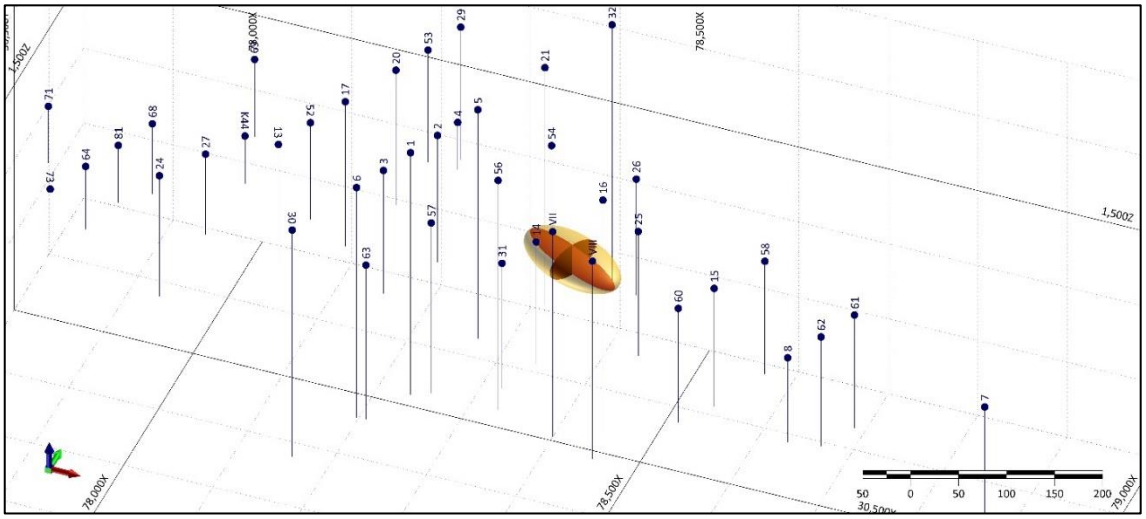

Figure 4.8 The designed search ellipsoid for solid body modeling

Using the above ellipsoid on the drilling data, we have created wireframes representing solid models of all layers. Using this method, the properties of the ore body model are shown in Table 4.5 and Figure 4.9. The cross sections of orebody models, including the host rock layers, are shown in Figure 4.10.

Table 4.5 The characteristics of the solid body model of the ore body

Wireframe model	X min (m)	X max (m)	Y min (m)	Y max (m)	Z min (m)	Z max (m)	Volume (m³)
Ore body	77913	79716	30165	30640	1309	1673	

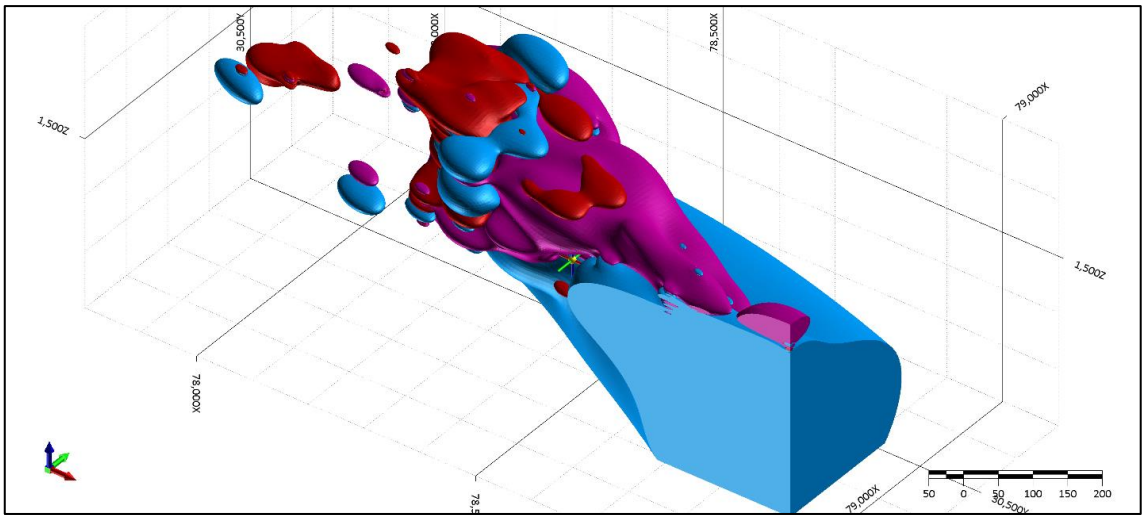

Figure 4.9 The solid body model of the ore body

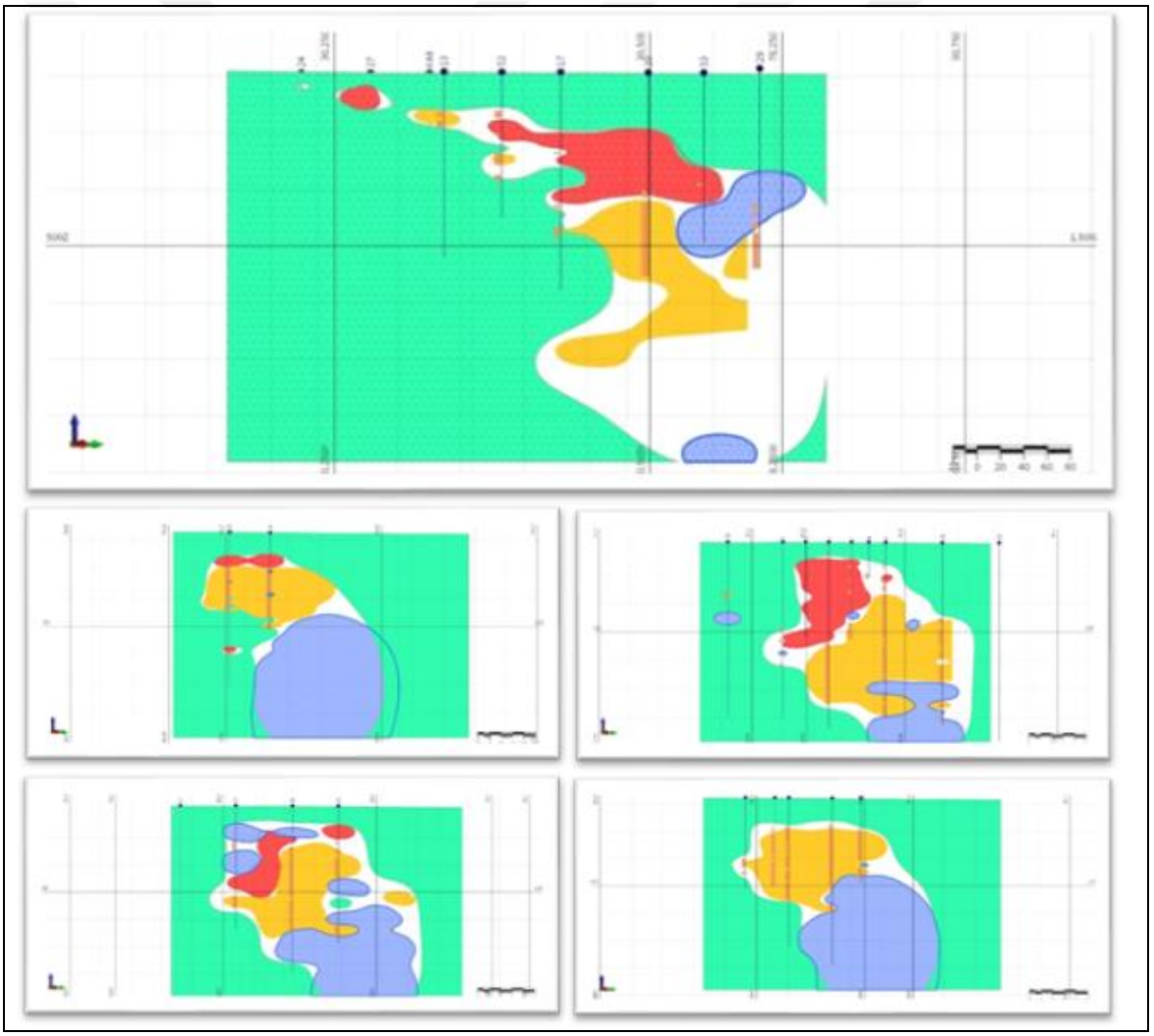

Figure 4.10 Cross-sections from the solid body model of the ore body and host rock

4.3.2. Blank and geologic block models

A block model is representative of earth elements and mineral deposits and consists of a combination of blocks or a 3D grid of small cubes. Each block contains specific information such as rock or mineral types, ore grade(s), density, geologic zone and spatial coordinates obtained from drill hole samples. According to computer-aided programs, a complete block model cannot be designed before preparing a blank and a geological block model. In this study, the blank block model was created with an equivalent dimension of 5 m along all axes. A full block therefore has a volume of 125 m³, as can be seen in Figure 4.11.

The blank block model is the base for the geologic block model and the ore body is divided into elements by grade, i.e. high-grade ore (RO), medium grade ore (PO) and low-grade ore (LGO) and waste, as illustrated in Figure 4.12.

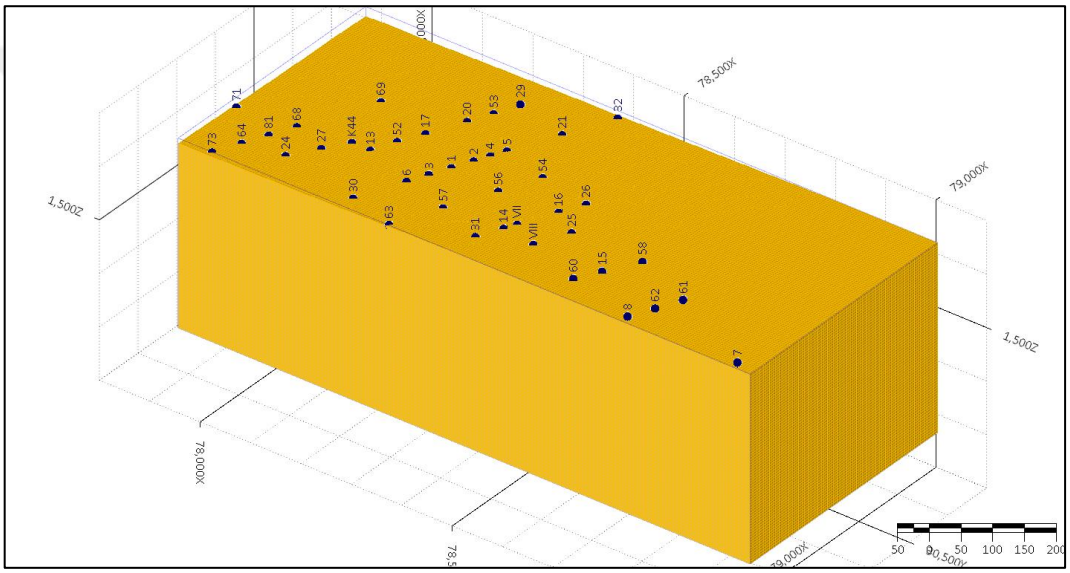

Figure 4.11 Blank block model

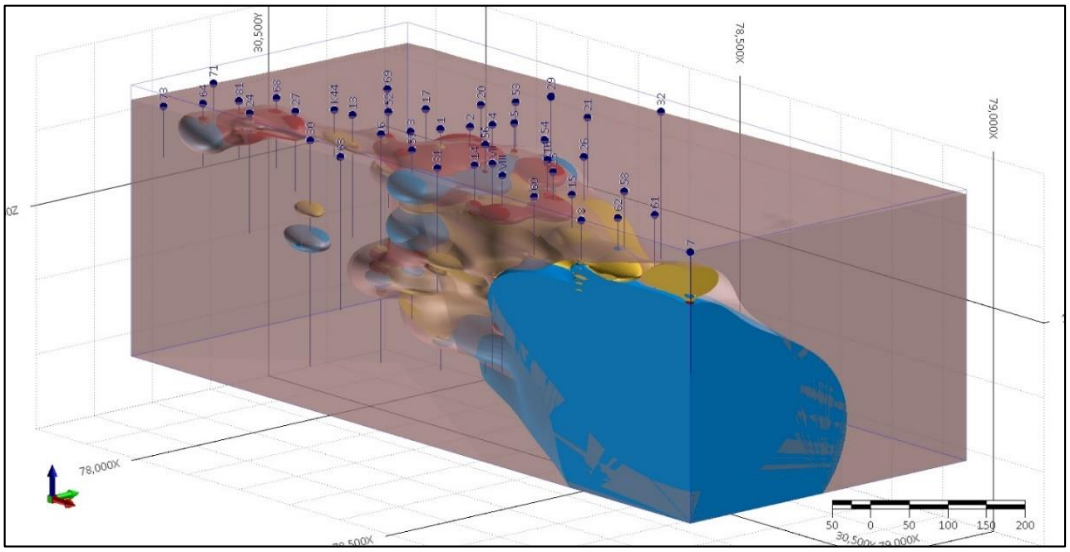

Figure 4.12 Geologic block model

5. RESOURCE ESTIMATION

5.1. Compositing of Drillhole Data

Compositing or regularization of drillhole data is a common practice in mineral resource estimation and is considered a necessary step in producing unbiased estimates of mineral resources and reserves. Typically, data is collected over irregular distances as the relative thicknesses of drilled lithologies or sampling and assaying strategies vary. This necessitates a transformation of the data into regular lengths of equal size to ensure that all data have the same sampling basis (Palmer, 2024). For this reason, since it is necessary to organize the grades to avoid biased predictions over the regular lengths, we perform the compositing operation before the resource estimation.

As we have divided our drillhole data into high grade, medium grade and low-grade orebodies and waste, we have composited the individual ore body compartments separately. The composite histogram of the high-grade ore body is shown in Figure 5.1 with the parameter values listed in Table 5.1. The arithmetic mean and median of the analysis data are 2.54 m and 2 m respectively. It can be observed that the peak of the data is at 2 m - 2.4 m, where over 50% of the total data is in this range. This is where the median lies and the long tail extends to the right towards 5.5 m where some high intervals of Fe pull the mean upwards and the data deviates a little from normality. Nevertheless, the data quality is good enough for geostatistical modeling and a compositing interval of 2 m is accepted for geostatistical modeling.

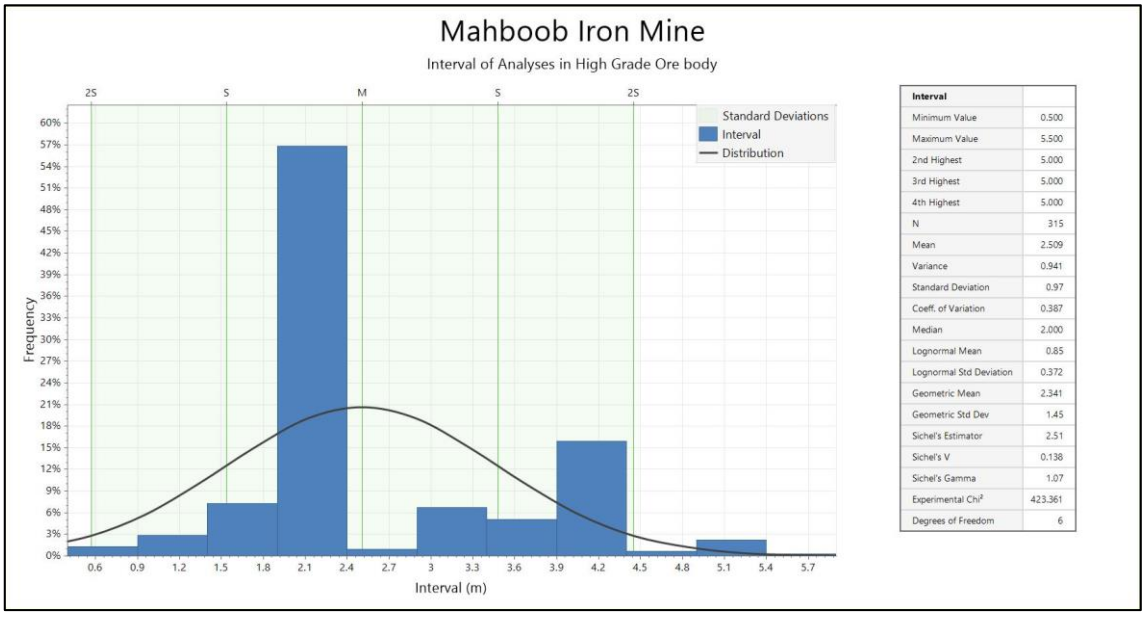

Figure 5.1 Sampling interval length distribution of high grade orebody

Table 5.1 Descriptive statistics for compositing of the high-grade ore body

Samples: 315	Standard deviation: 0.97
The shortest analyzed thickness: 0.5 m	Composited thickness: 2.0 m
The longest analyzed thickness: 5.5 m	Median: 2 m
Mean: 2.51 m	Skewness(visual): Right-skewed

For medium grade orebody, the sampling interval data is almost symmetrical and less skewed than for high grade orebody as you can see in Figure 5.2. The descriptive statistics for the data are shown in Table 5.2, where the mean is 3.033 and the median is 3. A few values above 5.5 may act as outliers, but do not dominate. Finally, the data is of good quality for geostatistical modeling and a compositing interval of 2 m is accepted for geostatistical modeling.

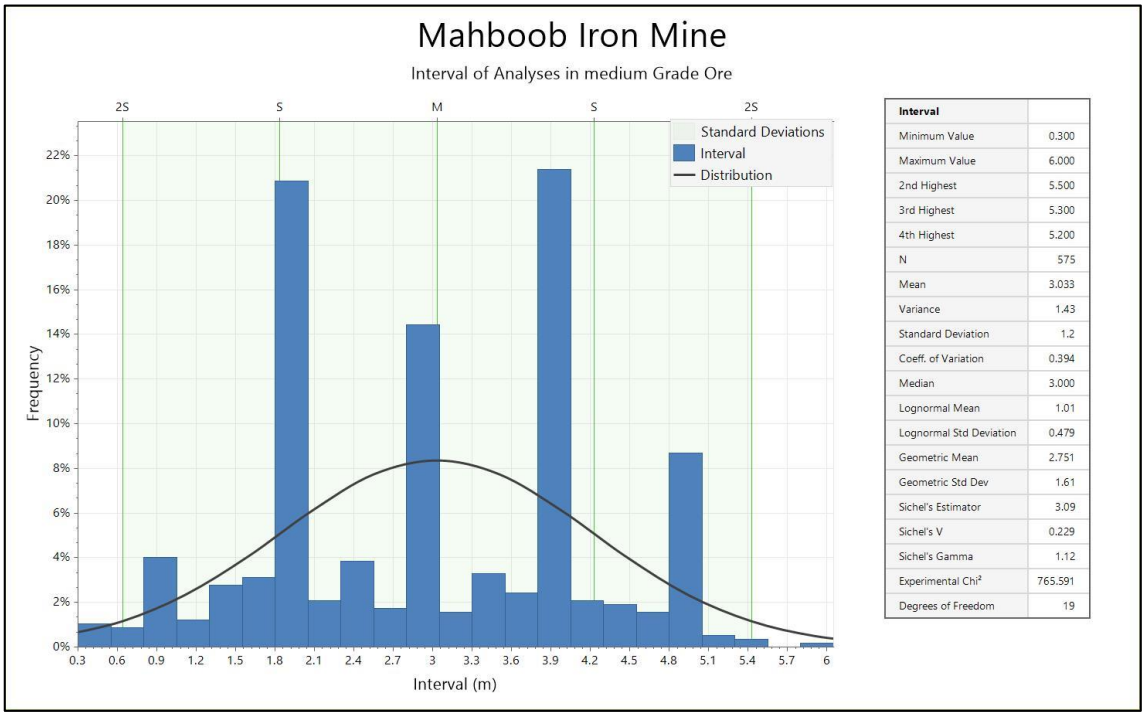

Figure 5.2 Sampling interval length distribution of medium grade orebody

Table 5.2 Descriptive statistics for compositing of the medium grade orebody

Samples: 575	Standard deviation: 1.2
The shortest analyzed thickness: 0.3 m	Composited thickness: 2.0 m
The longest analyzed thickness: 6 m	Median: 3.0 m
Mean: 3.03 m	Skewness(visual): Non-skewed

For the low-grade orebody, the sampling interval data has accumulated in the range of 1 m to 6 m and is right skewed, as shown in Figure 5.3. The descriptive statistics for the data are shown in Table 5.3. The mean value is 3.41 m and the median is 3.2 m. A compositing interval of 3 m is accepted for geostatistical modeling.

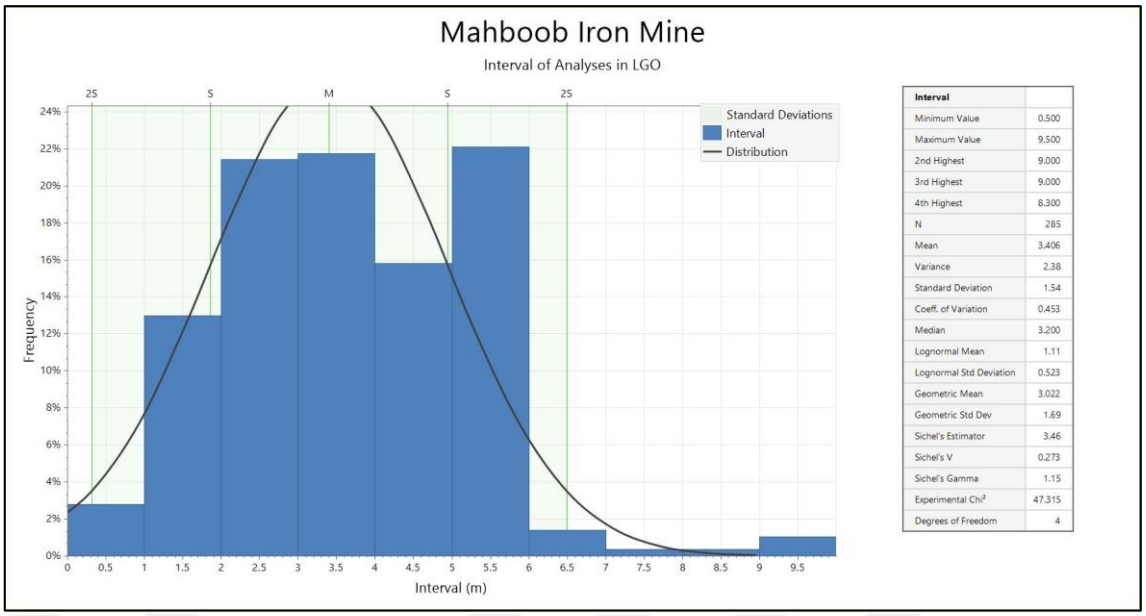

Figure 5.3 Sampling interval length distribution of low grade orebody

Table 5.3 Descriptive statistics for compositing of the low grade orebody

Samples: 285	Standard deviation: 1.54
The shortest analyzed thickness: 0.5 m	Composited thickness: 3.0 m
The longest analyzed thickness: 9.5 m	Median: 3.2 m
Mean: 3.41 m	Skewness(visual): Right-skewed

5.2. Variogram Analyses

Before you assign grades to the ore blocks, the dimensions of the search ellipsoid must be determined. If a large ellipsoid is used, resulting from an inappropriate design, the majority of the orebody falls into the "measured" resource category and is designated as "reserve" that can guarantee the exploitability of the orebody. Consequently, the financial return of the mine in feasibility analyzes can be significantly higher than what it should be in the real situation. In contrast, if a small search ellipsoid is used, the majority of the ore body is classified as an "indicated" or "probable" resource. This can lead to the NPV of the mine being understated due to over-planning, which in turn can lead to sub-optimal utilization of the underground resources, a national treasure. As is well known, the National Resources and Reserves Reporting Committee (UMREK) code, the system adopted by Türkiye for classifying resources and reserves, does not recommend the use of "probable" resources in feasibility analyses. Therefore, semi-variogram maps were created to determine the distance of influence of the samples intersected in drillholes.

The strike, pitch, and dip angles of the orebody given in Section 4.3.1 were plotted on the variogram maps of the high-grade orebody and 36 10° slices were used for each of the three axes. In addition, a 50 m step interval was defined for strike and pitch, and a 2 m step interval for dip. In this way, the relationship between the sample pairs was examined over distances of 725 m for the strike and dip and 121 m for the dip. These distances were also measured on the map

and confirmed to accurately reflect the extent of the orebody. The variogram mapping results for the high grade orebody (RO) are shown in Figure 5.4.

An exponential semi variogram model was fitted to the sample pair data with the value of nugget and sill being 2.2 and 27, respectively (Figure 5.5). The dip direction of the search ellipsoid is N200° with a dip of 90°. The pitch is 180°. The radii of the axes of the search ellipsoid, therefore, generated by the above approach is as follows: Axis 1 → 106 m, Axis 2 → 26 m, and Axis 3 → 90 m. The search ellipsoid has quadrants, each of which must catch at least one sample with the maximum number of samples in each sector unlimited.

The medium grade orebody was divided into 72 5° slices, which allowed examining sample pairs along the strike of N295°. The step distance was selected as 70 m along 735 m of extent of the medium grade orebody. There were 36 10° slices along the dip and pitch directions. Likewise, a 2 m step interval was assigned along the dip and 50 m along the pitch direction. By this way, the relationship between the sample pairs was examined over distances of 90.5 m along the dip and 775 m along the pitch. Variogram mapping results for the medium grade orebody (PO) are shown in Figure 5.6.

A spherical semi variogram model was fitted to the sample pair data with the value of nugget and sill being 0.0 and 31, respectively (Figure 5.7). The dip direction of the search ellipsoid is N25° with a dip of 20°. The pitch is 170°. The radii of the axes of the search ellipsoid are 200 m for Axis 1, 50 m for Axis 2 and 100 m for Axis 3.

The low-grade orebody was divided into 72 5° slices, which allowed examining sample pairs along the strike of N290°, the dip direction of 20° and the pitch direction of 5°. The step distance was selected as 70 m along 735 m of extent of the low-grade orebody. Similarly, a 3 m step interval was assigned along the dip and 70 m along the pitch direction. By this way, the relationship between the sample pairs was examined over distances of 181 m along the dip and 735 m along the pitch. Variogram mapping results for the low grade orebody (LGO) are shown in Figure 5.8.

A spherical semi variogram model was fitted to the sample pair data with the value of nugget and sill being 2.7 and 49.6, respectively (Figure 5.9). The dip direction of the search ellipsoid is N195° with a dip of 90°. The pitch is 175°. The radii of the axes of the search ellipsoid are 209 m for Axis 1, 90 m for Axis 2 and 85 m for Axis 3.

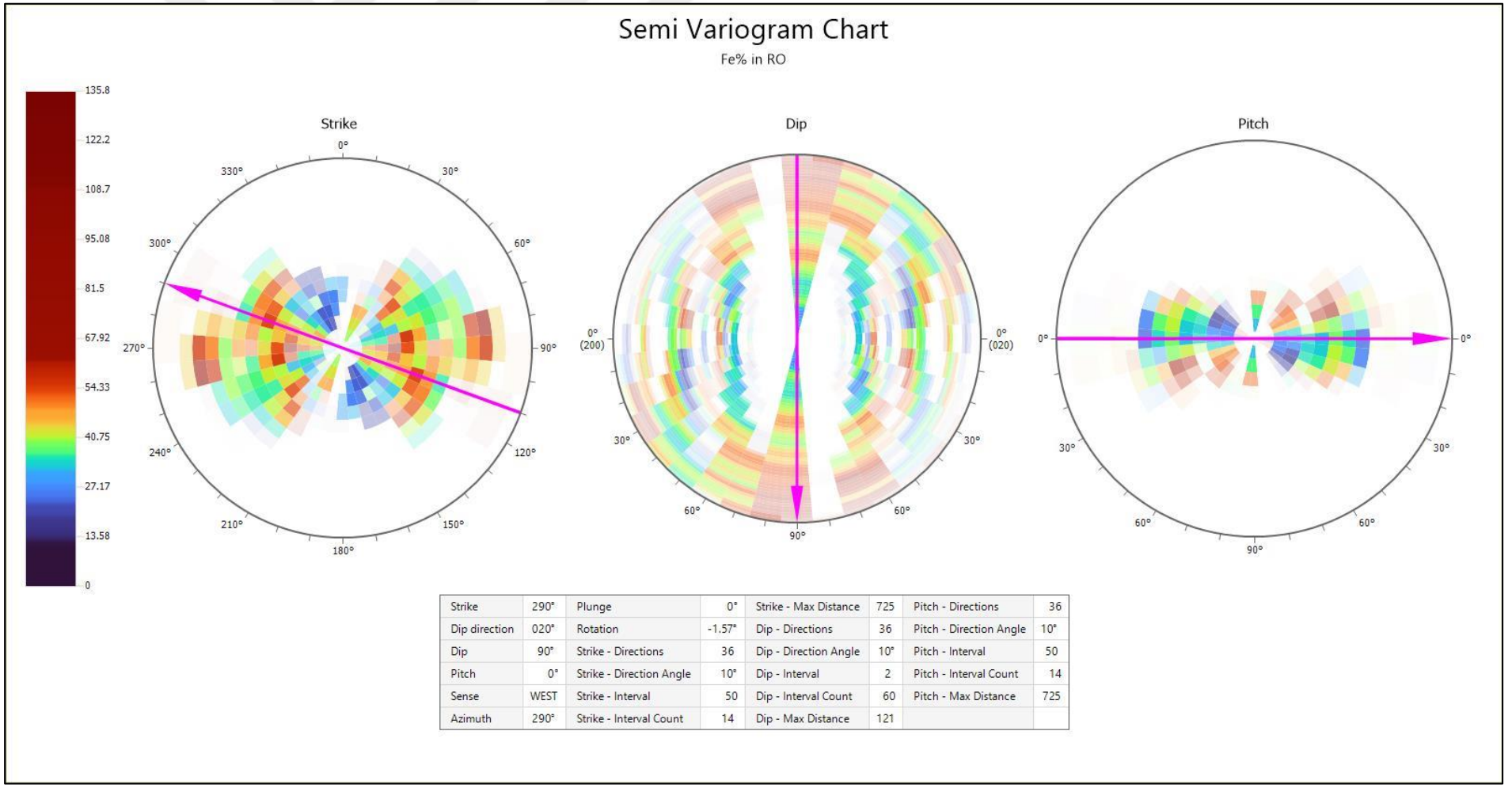

Strike	290°	Plunge	0°	Strike - Max Distance	725	Pitch - Directions	36
Dip direction	020°	Rotation	-1.57°	Dip - Directions	36	Pitch - Direction Angle	10°
Dip	90°	Strike - Directions	36	Dip - Direction Angle	10°	Pitch - Interval	50
Pitch	0°	Strike - Direction Angle	10°	Dip - Interval	2	Pitch - Interval Count	14
Sense	WEST	Strike - Interval	50	Dip - Interval Count	60	Pitch - Max Distance	725
Azimuth	290°	Strike - Interval Count	14	Dip - Max Distance	121		

Figure 5.4 Variogram maps of the high grade orebody

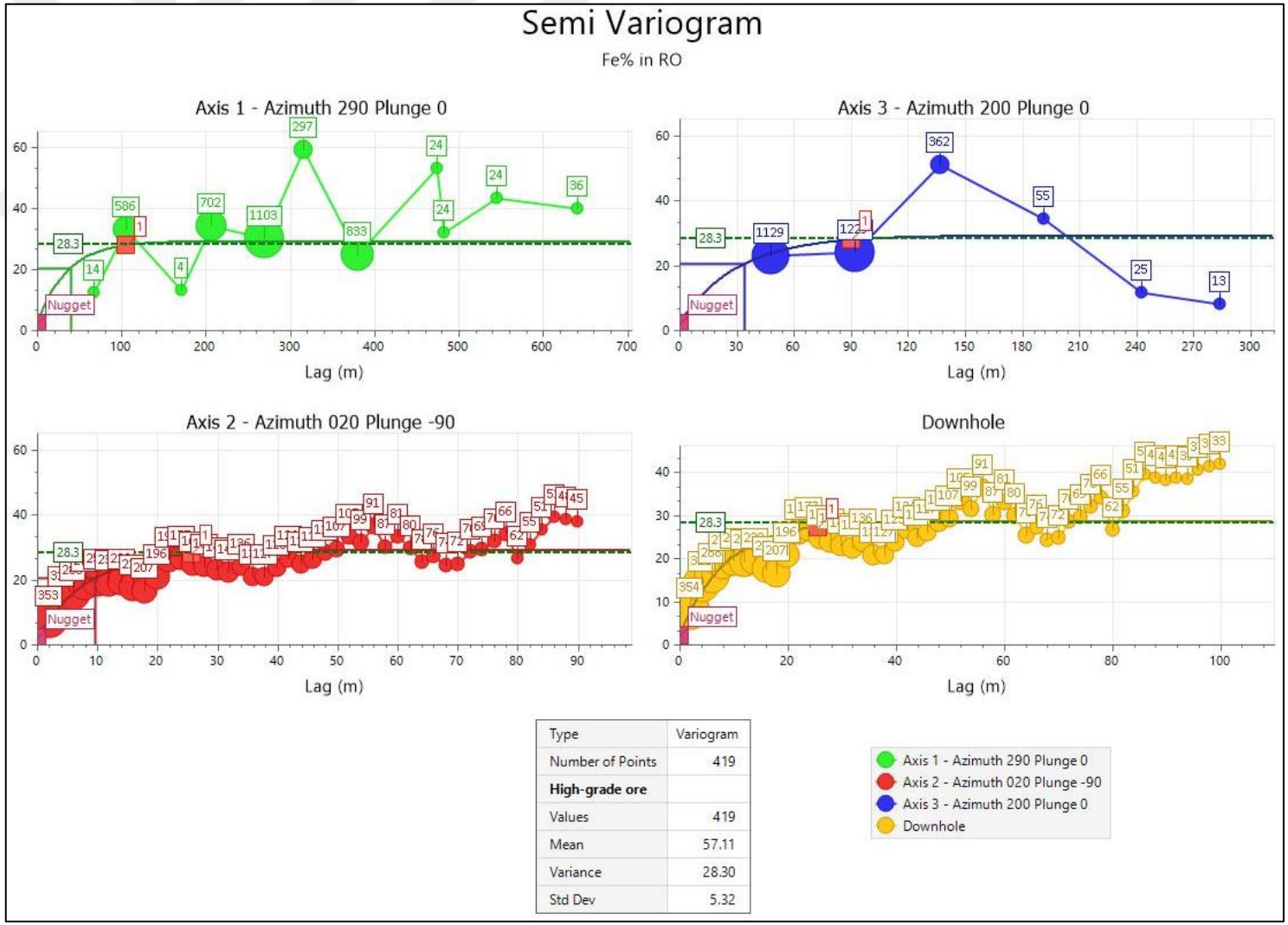

Figure 5.5 Semi variograms of the high-grade orebody

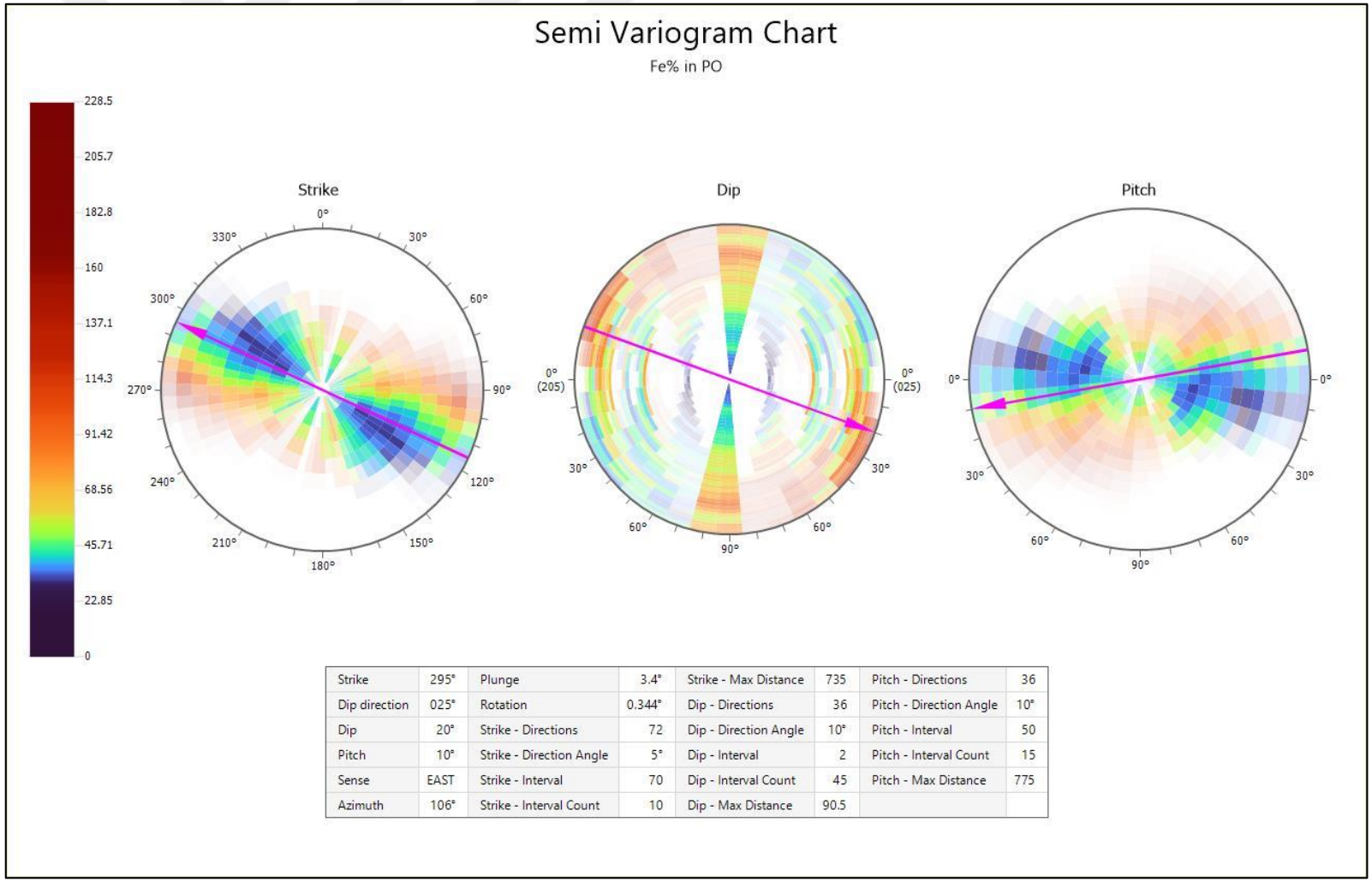

Strike	295°	Plunge	3.4°	Strike - Max Distance	735	Pitch - Directions	36
Dip direction	025°	Rotation	0.344°	Dip - Directions	36	Pitch - Direction Angle	10°
Dip	20°	Strike - Directions	72	Dip - Direction Angle	10°	Pitch - Interval	50
Pitch	10°	Strike - Direction Angle	5°	Dip - Interval	2	Pitch - Interval Count	15
Sense	EAST	Strike - Interval	70	Dip - Interval Count	45	Pitch - Max Distance	775
Azimuth	106°	Strike - Interval Count	10	Dip - Max Distance	90.5		

Figure 5.6 Variogram maps of the medium grade orebody

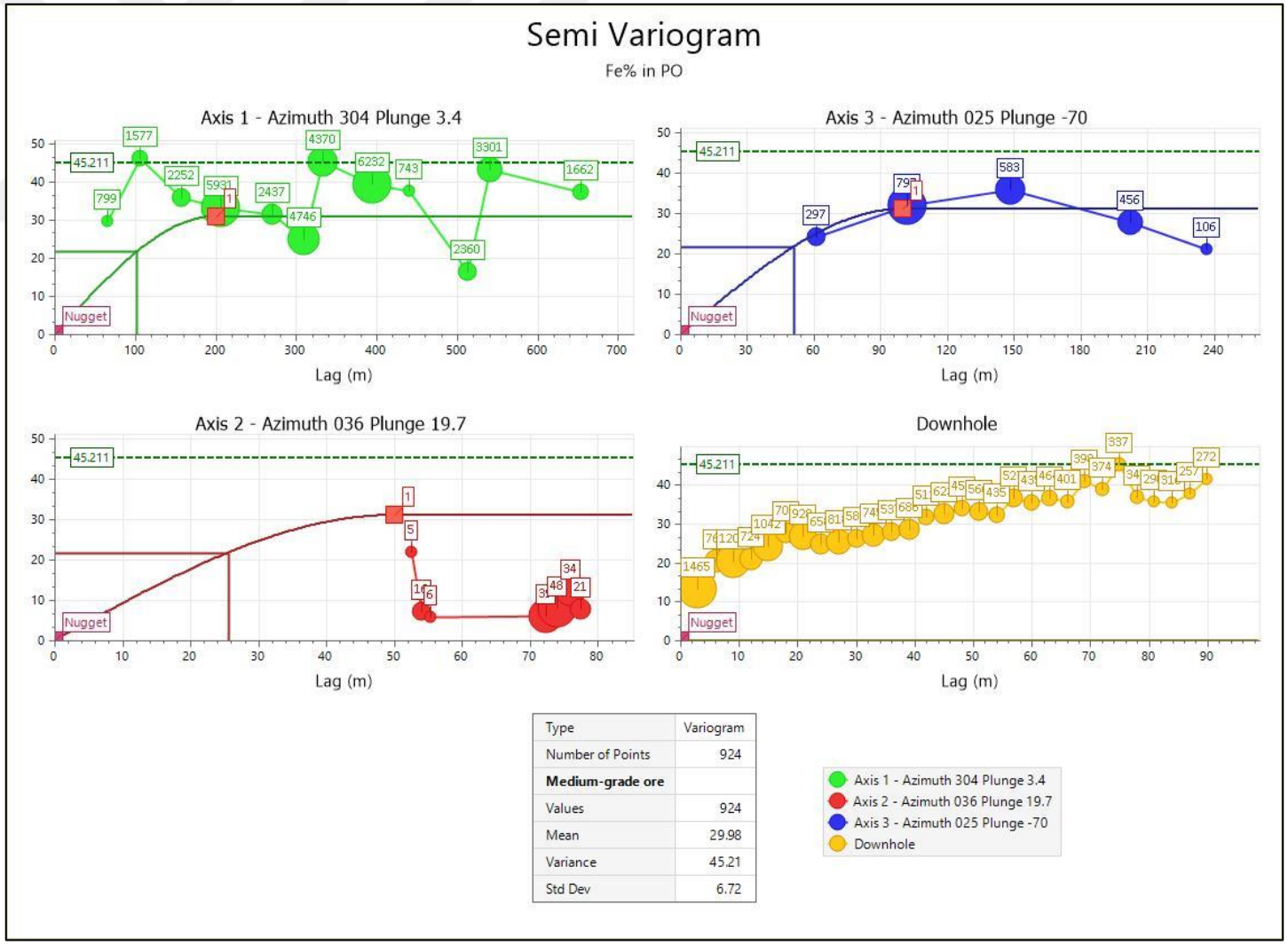

Figure 5.7 Semi variograms of the medium grade orebody

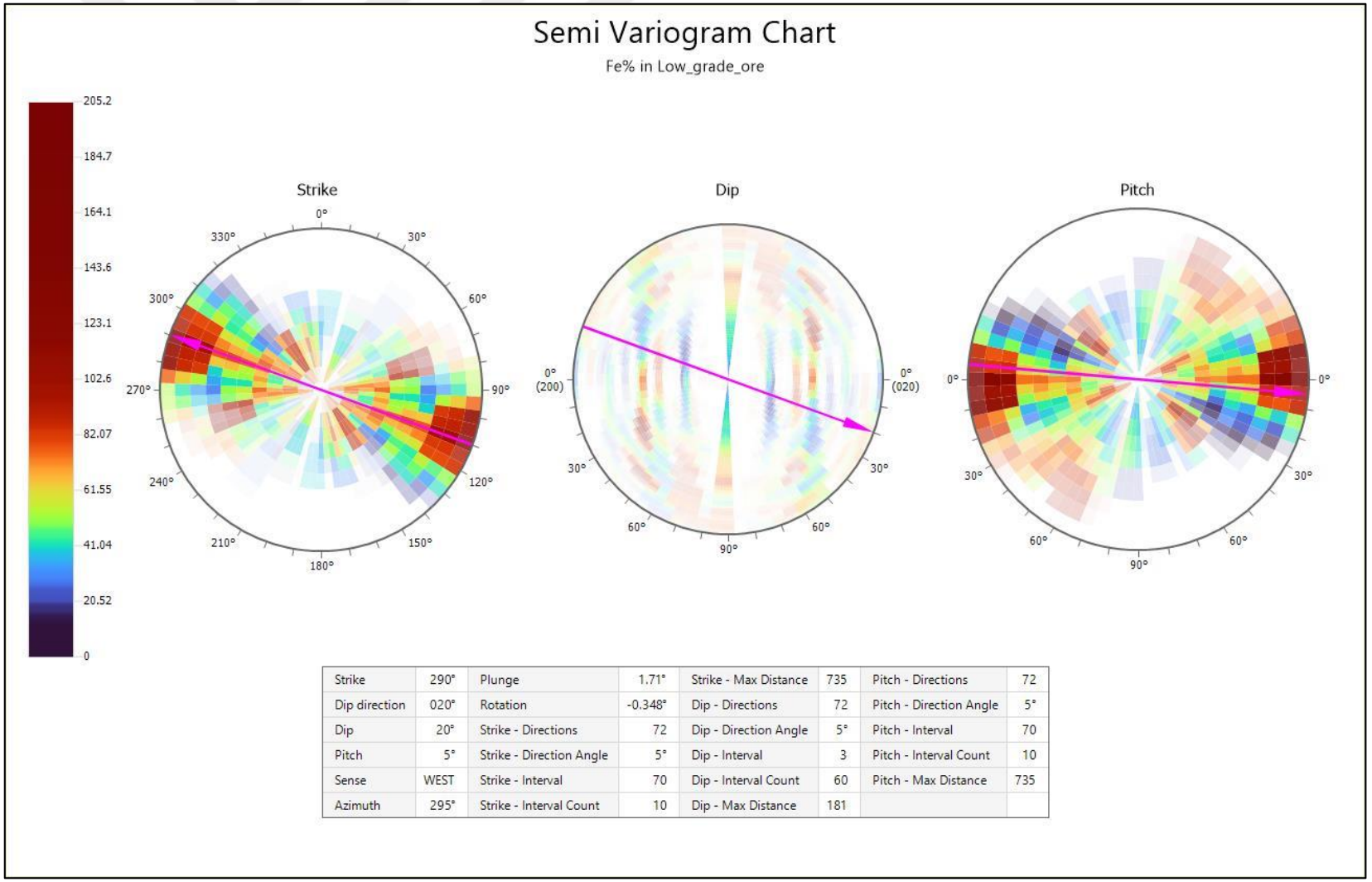

Strike	290°	Plunge	1.71°	Strike - Max Distance	735	Pitch - Directions	72
Dip direction	020°	Rotation	-0.348°	Dip - Directions	72	Pitch - Direction Angle	5°
Dip	20°	Strike - Directions	72	Dip - Direction Angle	5°	Pitch - Interval	70
Pitch	5°	Strike - Direction Angle	5°	Dip - Interval	3	Pitch - Interval Count	10
Sense	WEST	Strike - Interval	70	Dip - Interval Count	60	Pitch - Max Distance	735
Azimuth	295°	Strike - Interval Count	10	Dip - Max Distance	181		

Figure 5.8 Variogram maps of the low grade orebody

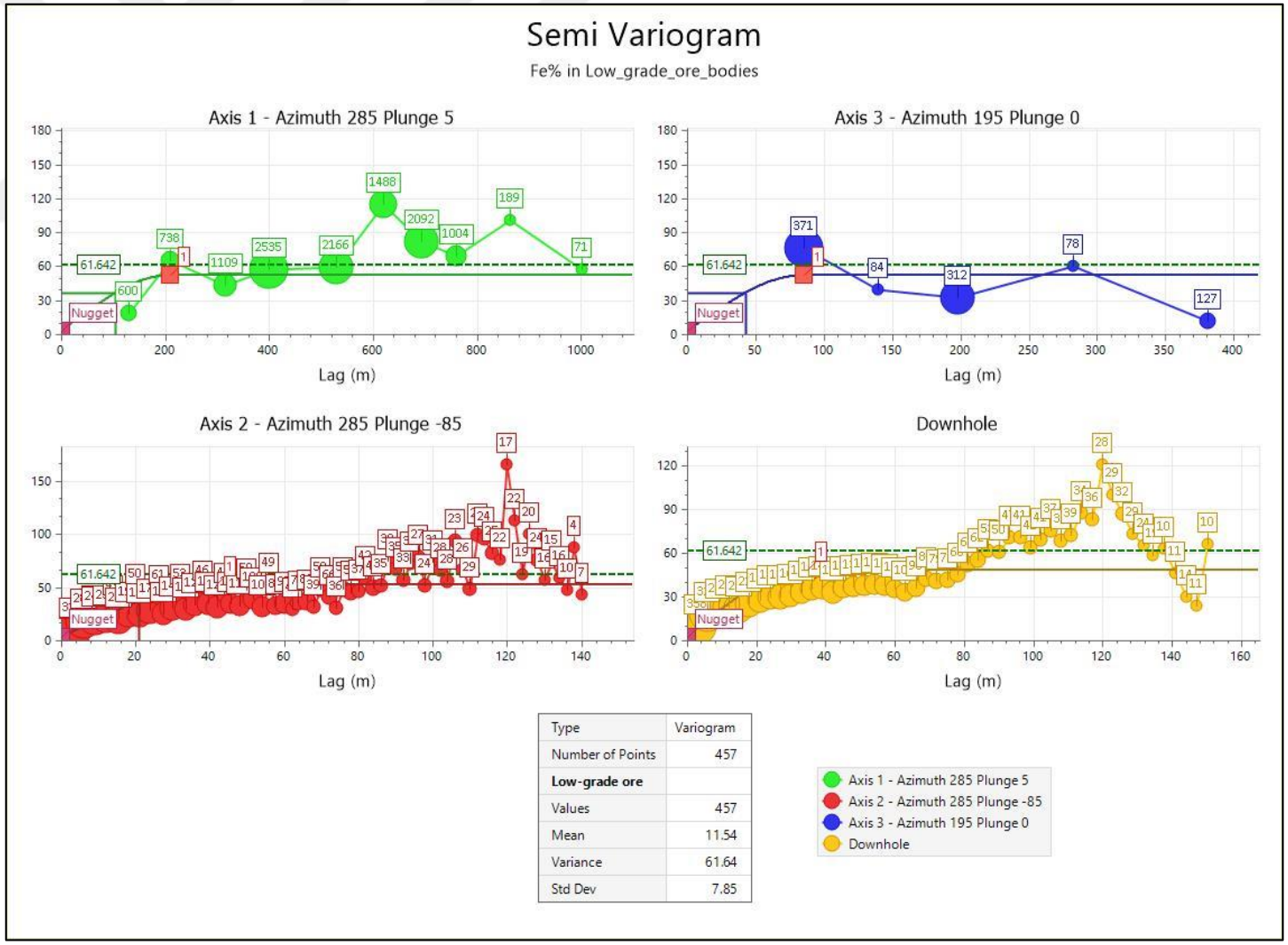

Figure 5.9 Semi variograms of the low-grade orebody

5.3. Cross Validation of the Models

Before creating geostatistical models, a variogram model and a kriging type must be selected. Cross-validation makes it possible to assess the influence of the choice of variogram model, kriging type and search strategies. Therefore, cross validation is a way of testing the validity of the model prior to using it for kriging or IDW estimation (www.micromine.com; accessed 11.07.2025). For the estimation, the estimated values are plotted against the true values and the scenario with the highest correlation coefficient is sought.

Cross-validation is performed for the respective scenario and then the results are compared. Sample points are successively omitted from the data set and estimated using the remaining data and suitable scenario parameters. During estimation, the error is calculated as the residual of the estimated value minus the true value. These error values can be analyzed in different ways. The most common methods for interpreting the error values are as follows:

- A scatterplot of the true values versus the estimated values. There should be few outliers and the correlation coefficient should be high.
- The histogram of the errors should be symmetrical, with a mean of zero in the middle, and the standard deviation should be as low as possible.
- The plot of the error versus the estimated value should be centered around the zero-error line. This is referred to as “conditional unbiasedness” (Oz and Deutsch).

The cross validation diagrams of the high-grade ore are shown in Figure 5.10. There is a high correlation (R ~79%) between the true values and the estimated values with only a few outliers. The histogram of the standard errors is symmetrical and centered at zero. Finally, the plot of the error versus the estimated value is centered around the zero-error line, indicating a well-designed model.

Figure 5.11 illustrates the cross-validation plots of the medium ore. There is also a high correlation (R ~84%) between the true values and the estimated values with some outliers. The histogram of standard errors is symmetrical and centered at zero. Finally, the plot of the error versus the estimated value is centered around the zero-error line, indicating a well-developed model.

Figure 5.12 shows the cross-validation plots for the low-grade ore. The highest correlation (R ~87%) between the true values and the estimated values is achieved with this model. The histogram of standard errors is symmetrical and centered at zero. Finally, the plot of the error versus the estimated value is centered around the zero-error line, indicating a well-established model.

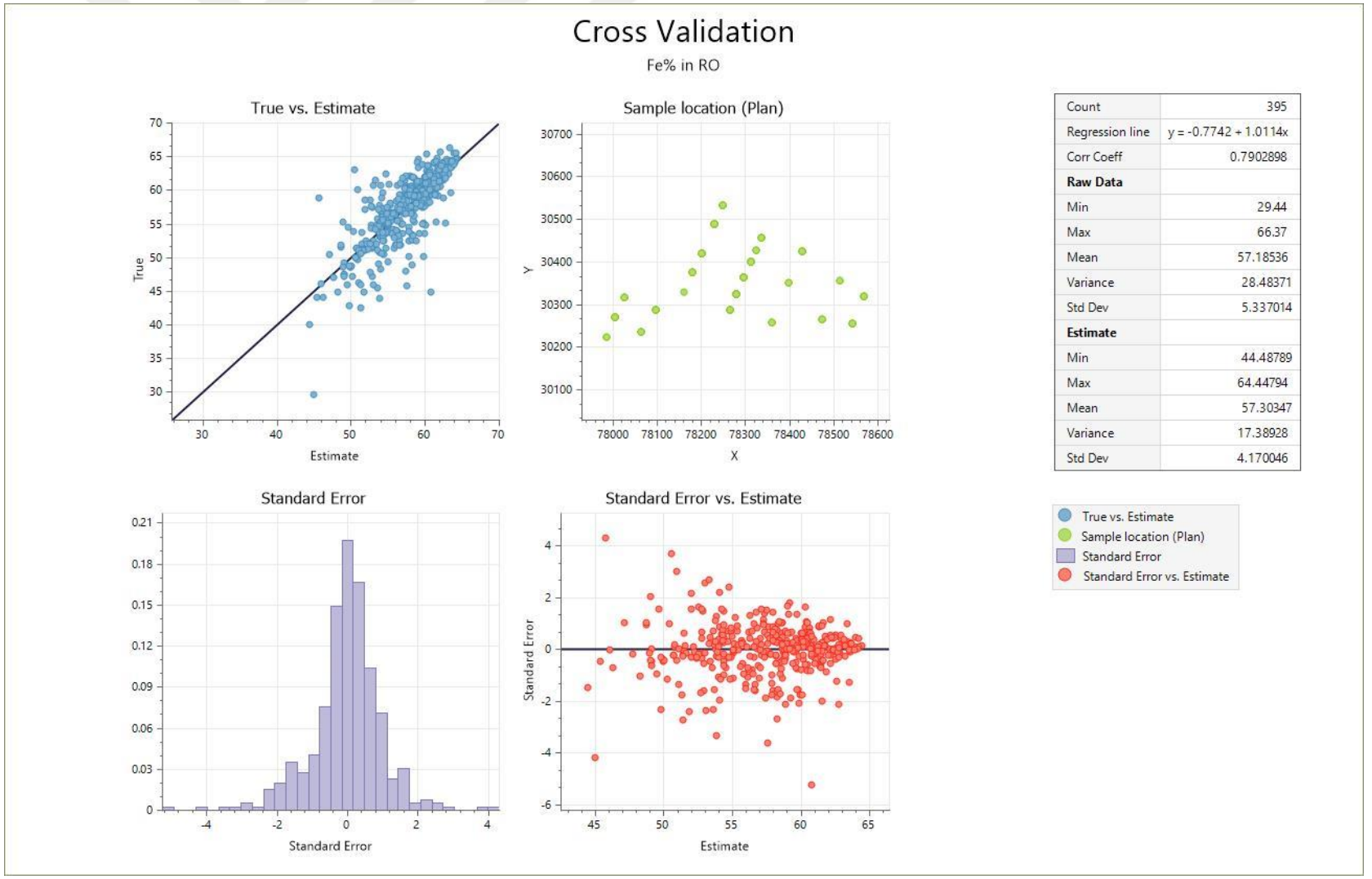

Figure 5.10 Cross validation plots of the high grade orebody

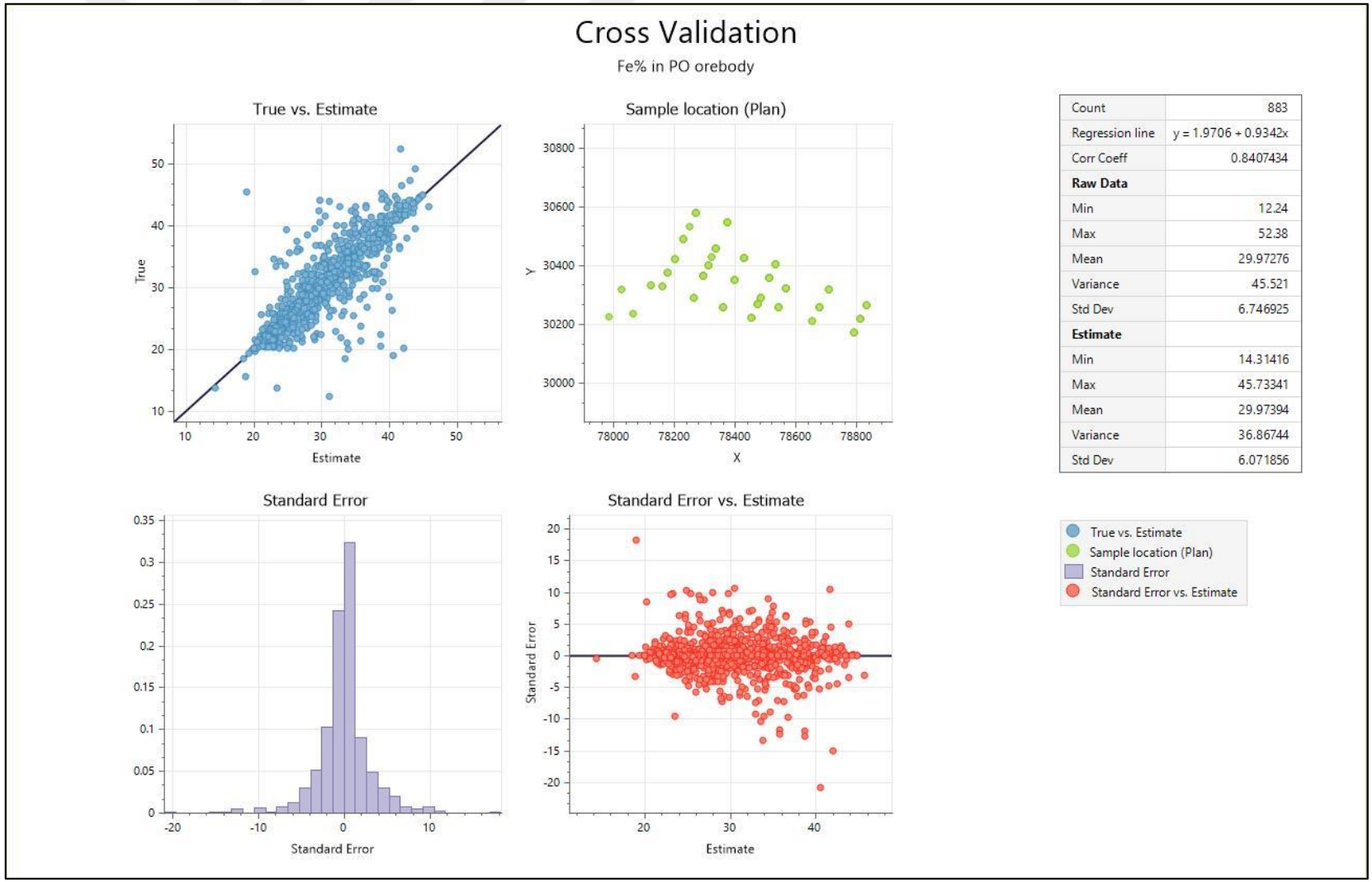

Figure 5.11 Cross validation plots of the medium grade orebody

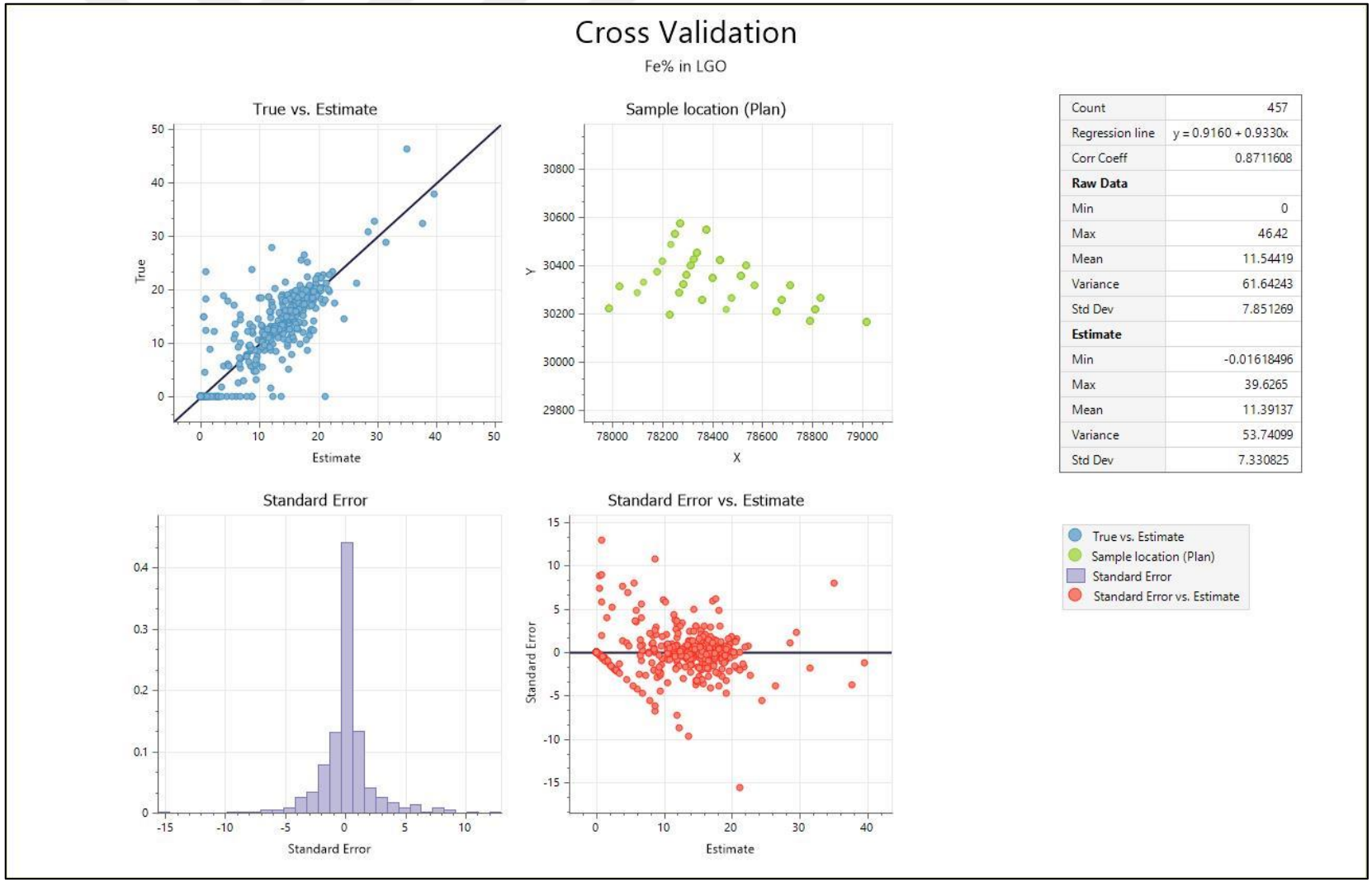

Figure 5.12 Cross validation plots of the low grade orebody

5.4. Grade Assignment for the High Grade Orebody

In this work, the assignment of grades to the blocks in the ore bodies was carried out using two commonly used tools: the deterministic interpolation method of the IDW (inverse distance weighting) algorithm and the geostatistical tool of kriging, which are based on statistical models that include autocorrelation, i.e. the statistical relationships between the measured points.

Inverse distance weighting (IDW) is one of the most commonly used methods in geostatistical analysis and modeling. It is a deterministic spatial interpolation method that estimates values at unsampled locations and is based on the principle that closer points have a greater influence than points further away (https://support.esri.com/en-us/gis-dictionary/inverse-distance-weighted-interpolation; accessed 13.07.2025).

Kriging assumes that the distance or direction between sample points reflects a spatial correlation that can be used to explain variation in the surface. The Kriging tool fits a mathematical function to a specified number of points or to all points within a specified radius to determine the output value for each location. It is a multi-step process that includes exploratory statistical analysis of the data, variogram modeling, surface creation, and (optionally) exploration of a variance surface. Kriging is most appropriate when the data is known to have a spatially correlated distance or directional variance (https://pro.arcgis.com/en/pro-app/latest/tool-reference/3d-analyst/how-kriging-works.htm%23ESRI_SECTION1_E112B7FAED26453D8DA4B9AEC3E4E9BF; accessed 13.07.2025).

Firstly, the anisotropic IDW method of power 2 was used to assign grades to the ore blocks using the composited analysis data. The parameter values of the search ellipsoid used by both algorithms are listed in Table 5.4. For a block to be registered as measured, samples must be taken from at least two drillholes while sample values from a single drill hole are sufficient for the indicated resources. The search ellipsoids generated by the semivariogram analysis have four sectors (quadrants). To assign a grade value to any block, each sector must use at least one analysis value, whereby a maximum of 150 analyzes are permitted.

Modeling was followed with the ordinary kriging method where grade values were assigned to individual blocks within the orebody. The same search ellipsoid was used in the estimation process.

It should be noted that boundaries of blank block models are created based on the furthest samples along the principal directions, which may ultimately result in a massive block. A conservative approach was taken to avoid assigning unrealistic grade values to large orebodies for which assay data was not available and to avoid inappropriately large tonnages for the resource. Accordingly, the orebody was constrained by the drillholes that defined it and the ore block model was constructed accordingly.

Table 5.4 Parameter values of the search ellipsoid used by the estimation algorithms for the high-grade orebody

Category	Axis-1 (m)	Axis-2 (m)	Axis-3 (m)	Azimuth (°)	Plunge (°)	Rotation (°)
Measured	156.54	114.81	88.90			
Indicated	313.08	229.62	177.80	251.52	9.85	17.50
Inferred	469.62	344.43	266.70			

The tonnage calculated based on grade ranges of the high-grade iron ore using the IDW and kriging estimation algorithms are presented in Tables 5.5 and 5.6, respectively. The block model of the ore body based on grade categories with kriging is shown in Figure 5.13.

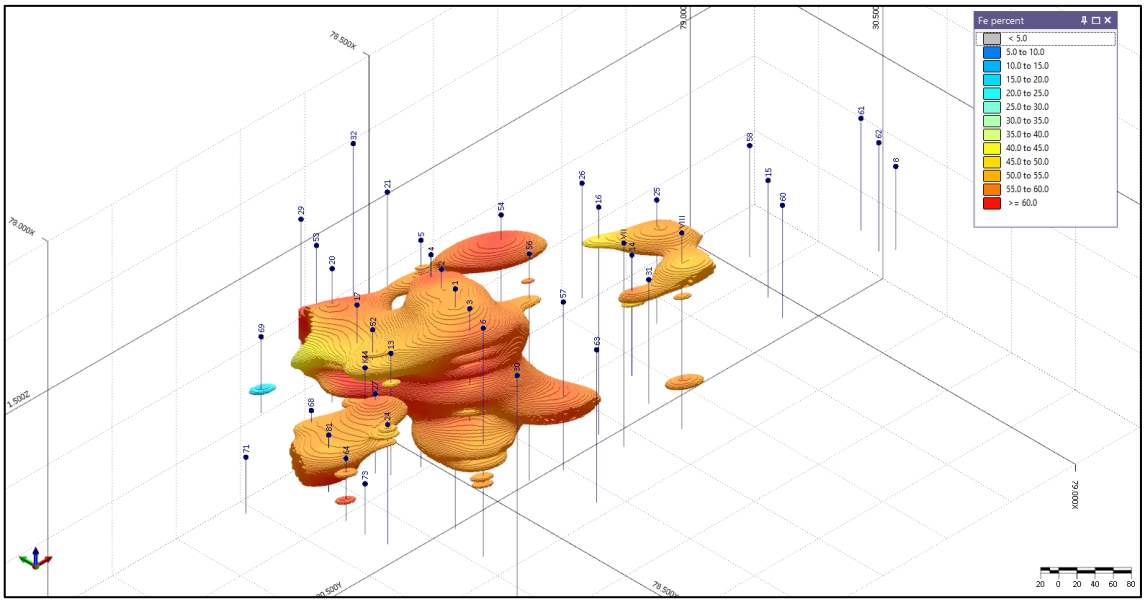

Figure 5.13 The high-grade orebody with grades assigned to blocks with kriging

The deposit contains 8,153,165 tons of iron ore with an average Fe grade of 58.02%, yielding approximately 4,730,335 tons of extractable iron, according to the IDW method. Of the total resource, 99.83% falls into the measured category, while only 0.17% is classified as Indicated, which typically has a lower geological confidence than Measured. This high proportion of measured resources indicates that the search ellipsoid used in the resource estimation was relatively tight, and that many samples met the criteria for classification with high confidence.

Although the total volume and tonnage figures for the high-grade orebody were consistent with the IDW method (8,153,165 tons of ore and 4,656,037 tons of extractable iron content), the average Fe grade estimated by kriging was slightly lower at 57.11%. The kriging method assigned slightly lower grades to the "measured" blocks and higher grades to the "indicated" blocks.

Table 5.5 Estimated tonnage of resources by the IDW algorithm for the high grade orebody

							Cumulative					
From Fe% (%)	To Fe% (%)	Volume (m³)	Density (t/m³)	Tonnage (t)	Fe % (%)	Iron content (t)	Volume (m³)	Tonnage (t)	Density (t/m³)	Fe% (%)	Iron content (t)	Resource type
60	70	0	0.00	0	0.00	0	0	0	0.00	0.00	0	Indicated
50	60	4984	2.65	13208	53.79	7105	4984	13,208	2.65	53.79	7105	Indicated
40	50	195	2.65	517	49.19	254	5179	13,724	2.65	53.62	7359	Indicated
30	40	0	0.00	0	0.00	0	5179	13,724	2.65	53.62	7359	Indicated
20	30	0	0.00	0	0.00	0	5179	13,724	2.65	53.62	7359	Indicated
10	20	0	0.00	0	0.00	0	5179	13,724	2.65	53.62	7359	Indicated
0	10	0	0.00	0	0.00	0	5179	13,724	2.65	53.62	7359	Indicated
60	70	184,337	2.65	488,493	60.71	296,564	184,337	488,493	2.65	60.71	296,564	Measured
50	60	2,879,216	2.65	7,629,922	57.90	4,417,895	3,063,553	8,118,415	2.65	58.07	4,714,459	Measured
40	50	6261	2.65	16592	47.95	7956	3,069,814	8,135,007	2.65	58.05	4,722,415	Measured
30	40	0	0.00	0	0.00	0	3,069,814	8,135,007	2.65	58.05	4,722,415	Measured
20	30	117	2.65	310	22.17	69	3,069,931	8,135,317	2.65	58.05	4,722,484	Measured
10	20	1155	2.65	3061	12.68	388	3,071,086	8,138,378	2.65	58.03	4,722,872	Measured
0	10	401	2.65	1063	9.75	104	3,071,487	8,139,441	2.65	58.03	4,722,976	Measured
60	70	184,337	2.65	488,493	60.71	296,564	184,337	488,493	2.65	60.71	296,564	TOTAL
50	60	2,884,200	2.65	7,643,130	57.90	4,425,000	3,068,537	8,131,623	2.65	58.06	4,721,564	TOTAL
40	50	6456	2.65	17108	47.99	8211	3,074,993	8,148,731	2.65	58.04	4,729,774	TOTAL
30	40	0	0.00	0	0.00	0	3,074,993	8,148,731	2.65	58.04	4,729,774	TOTAL
20	30	117	2.65	310	22.17	69	3,075,110	8,149,042	2.65	58.04	4,729,843	TOTAL
10	20	1155	2.65	3061	12.68	388	3,076,265	8,152,102	2.65	58.02	4,730,231	TOTAL
0	10	401	2.65	1063	9.75	104	3,076,666	8,153,165	2.65	58.02	4,730,335	TOTAL

Table 5.6 Estimated tonnage of resources by the ordinary kriging algorithm for the high grade orebody

							Cumulative					
From Fe% (%)	To Fe% (%)	Volume (m^3)	Density (t/m^3)	Tonnage (t)	Fe % (%)	Iron content (t)	Volume (m^3)	Tonnage (t)	Density (t/m^3)	Fe% (%)	Iron content (t)	Resource type
60	70	0	0.00	0	0.00	0	0	0	0.0000	0.00	0	Indicated
50	60	5179	2.65	13,724	53.98	7408	5179	13,724	2.6500	53.98	7408	Indicated
40	50	0	0.00	0	0.00	0	5179	13,724	2.6500	53.98	7408	Indicated
30	40	0	0.00	0	0.00	0	5179	13,724	2.6500	53.98	7408	Indicated
20	30	0	0.00	0	0.00	0	5179	13,724	2.6500	53.98	7408	Indicated
10	20	0	0.00	0	0.00	0	5179	13,724	2.6500	53.98	7408	Indicated
0	10	0	0.00	0	0.00	0	5179	13,724	2.6500	53.98	7408	Indicated
60	70	321,344	2.65	851,562	60.82	517,919	321,344	851,562	2.6500	60.82	517,919	Measured
50	60	2,711,143	2.65	7,184,529	56.83	4,082,734	3,032,487	8,036,091	2.6500	57.25	4,600,653	Measured
40	50	37,131	2.65	98,397	47.93	47,161	3,069,618	8,134,488	2.6500	57.14	4,647,815	Measured
30	40	196	2.65	519	39.38	205	3,069,814	8,135,007	2.6500	57.14	4,648,019	Measured
20	30	0	0.00	0	0.00	0	3,069,814	8,135,007	2.6500	57.14	4,648,019	Measured
10	20	1673	2.65	4433	13.77	610	3,071,487	8,139,441	2.6500	57.11	4,648,630	Measured
0	10	0	0.00	0	0.00	0	3,071,487	8,139,441	2.6500	57.11	4,648,630	Measured
60	70	321,344	2.65	851,562	60.82	517,919	321,344	851,562	2.6500	60.82	517,919	TOTAL
50	60	2,716,322	2.65	7,198,253	56.82	4,090,142	3,037,666	8,049,815	2.6500	57.24	4,608,061	TOTAL
40	50	37,131	2.65	98,397	47.93	47,161	3,074,797	8,148,212	2.6500	57.13	4,655,223	TOTAL
30	40	196	2.65	519	39.38	205	3,074,993	8,148,731	2.6500	57.13	4,655,427	TOTAL
20	30	0	0.00	0	0.00	0	3,074,993	8,148,731	2.6500	57.13	4,655,427	TOTAL
10	20	1673	2.65	4433	13.77	610	3,076,666	8,153,165	2.6500	57.11	4,656,037	TOTAL
0	10	0	0.00	0	0.00	0	3,076,666	8,153,165	2.6500	57.11	4,656,037	TOTAL

5.5. Grade Assignment for the Medium Grade Orebody

The parameter values of the search ellipsoid generated by the semivariogram analysis are listed in Table 5.7. As we had similar concerns about uncontrolled dispersion of the orebody, a boundary string was applied to solve this problem. In this way, the medium grade orebody was significantly reduced in size. Modeling was continued in the same way as for the high-grade orebody.

The tonnage calculated based on grade ranges of the medium grade iron ore using the IDW and kriging estimation algorithms are presented in Tables 5.8 and 5.9, respectively. The block model of the ore body based on grade categories with kriging is shown in Figure 5.14.

Table 5.7 Parameter values of the search ellipsoid used by the estimation algorithms for the medium grade orebody

Category	Axis-1 (m)	Axis-2 (m)	Axis-3 (m)	Azimuth (°)	Plunge (°)	Rotation (°)
Measured	200.00	50.00	100.00			
Indicated	400.00	100.00	200.00	105.59	3.41	19.72
Inferred	600.00	150.00	300.00			

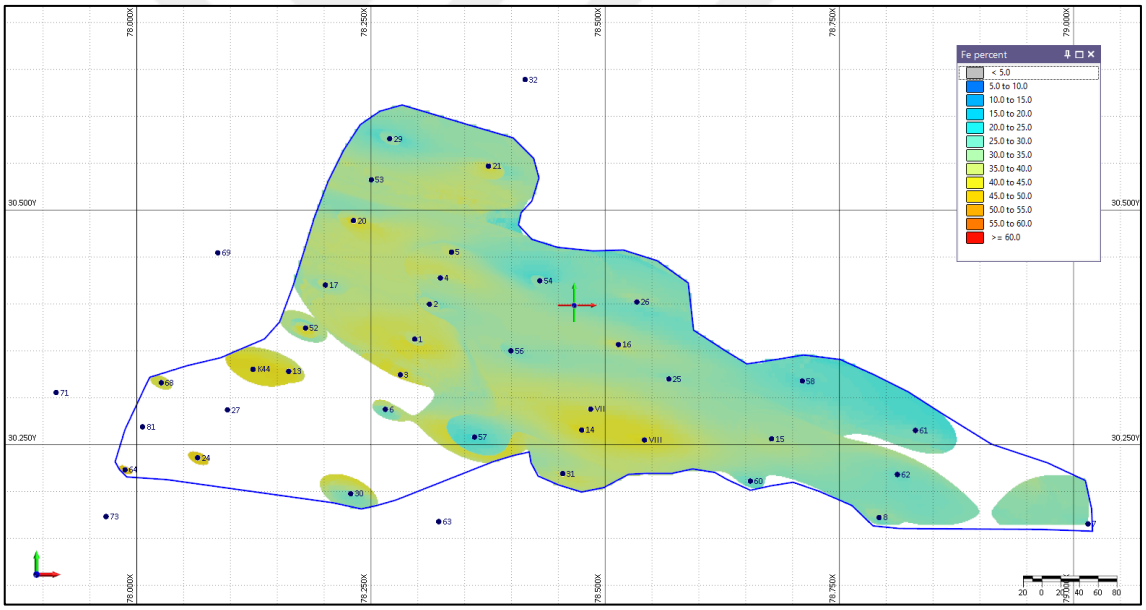

Figure 5.14 The medium grade orebody with grades assigned to blocks with kriging

The deposit contains 34,405,668 tons of iron ore with an average Fe grade of 29.22%, yielding approximately 10,051,658 tons of extractable iron, according to the IDW method. Of the total resource, 93.68% falls into the measured category, while only 6.32% is classified as Indicated, which typically has a lower geological confidence than Measured.

Although the total volume and tonnage figures for the high-grade orebody were quite similar to the IDW method (34,405,668 tons of ore and 10,080,834 tons of extractable iron content), the average Fe grade estimated by kriging was slightly higher at 29.30%.

Table 5.8 Estimated tonnage of resources by the IDW algorithm for the medium grade orebody

							Cumulative					
From Fe% (%)	To Fe% (%)	Volume (m³)	Density (t/m³)	Tonnage (t)	Fe % (%)	Iron content (t)	Volume (m³)	Tonnage (t)	Density (t/m³)	Fe% (%)	Iron content (t)	Resource type
60	70	0	0.00	0	0.00	0	0	0	0.00	0.00	0	Indicated
50	60	0	0.00	0	0.00	0	0	0	0.00	0.00	0	Indicated
40	50	776	2.65	2056	40.98	843	776	2056	2.65	40.98	843	Indicated
30	40	119,019	2.65	315,400	32.14	101,364	119,795	317,457	2.65	32.20	102,207	Indicated
20	30	700,492	2.65	1856,304	27.17	504,357	820,287	2,173,761	2.65	27.90	606,564	Indicated
10	20	0	0.00	0	0.00	0	820,287	2,173,761	2.65	27.90	606,564	Indicated
0	10	0	0.00	0	0.00	0	820,287	2,173,761	2.65	27.90	606,564	Indicated
60	70	0	0.00	0	0.00	0	0	0	0.00	0.00	0	Measured
50	60	0	0.00	0	0.00	0	0	0	0.00	0.00	0	Measured
40	50	18,748	2.65	49,682	41.40	20,566	18,748	49,682	2.65	41.40	20,566	Measured
30	40	4,030,783	2.65	10,681,575	33.00	3,524,524	4,049,531	10,731,257	2.65	33.04	3,545,091	Measured
20	30	8,113,353	2.65	21,500,385	27.44	5,899,951	12,162,884	32,231,643	2.65	29.30	9,445,042	Measured
10	20	100	2.65	265	19.70	52	12,162,984	32,231,908	2.65	29.30	9,445,094	Measured
0	10	0	0.00	0	0.00	0	12,162,984	32,231,908	2.65	29.30	9,445,094	Measured
60	70	0	0.00	0	0.00	0	0	0	0.00	0.00	0	TOTAL
50	60	0	0.00	0	0.00	0	0	0	0.00	0.00	0	TOTAL
40	50	19,524	2.65	51,739	41.38	21,409	19,524	51,739	2.65	41.38	21,409	TOTAL
30	40	4,149,802	2.65	10,996,975	32.97	3,625,888	4169,326	11,048,714	2.65	33.01	3,647,297	TOTAL
20	30	8,813,845	2.65	23,356,689	27.42	6,404,308	12,983,171	34,405,403	2.65	29.22	10,051,606	TOTAL
10	20	100	2.65	265	19.70	52	12,983,271	34,405,668	2.65	29.22	10,051,658	TOTAL
0	10	0	0.00	0	0.00	0	12,983,271	34,405,668	2.65	29.22	10,051,658	TOTAL

Table 5.9 Estimated tonnage of resources by the kriging algorithm for the medium grade orebody

From Fe% (%)	To Fe% (%)	Volume (m³)	Density (t/m³)	Tonnage (t)	Fe % (%)	Iron content (t)	Cumulative Volume (m³)	Cumulative Tonnage (t)	Cumulative Density (t/m³)	Cumulative Fe% (%)	Cumulative Iron content (t)	Resource type
60	70	0	0.00	0	0.00	0	0	0	0.00	0.00	0	Indicated
50	60	0	0.00	0	0.00	0	0	0	0.00	0.00	0	Indicated
40	50	3711	2.65	9834	41.47	4078	3711	9834	2.65	41.47	4078	Indicated
30	40	101,794	2.65	269,754	31.61	85,267	105,505	279,588	2.65	31.96	89,346	Indicated
20	30	714,782	2.65	1,894,172	28.23	534,687	820,287	2,173,761	2.65	28.71	624,033	Indicated
10	20	0	0.00	0	0.00	0	820,287	2,173,761	2.65	28.71	624,033	Indicated
0	10	0	0.00	0	0.00	0	820,287	2,173,761	2.65	28.71	624,033	Indicated
60	70	0	0.00	0	0.00	0	0	0	0.00	0.00	0	Measured
50	60	0	0.00	0	0.00	0	0	0	0.00	0.00	0	Measured
40	50	34,851	2.65	92,355	41.08	37,940	34,851	92,355	2.65	41.08	37,940	Measured
30	40	4,818,023	2.65	12,767,761	33.08	4,224,146	4,852,874	12,860,116	2.65	33.14	4,262,086	Measured
20	30	7,309,225	2.65	19,369,446	26.82	5,194,272	12,162,099	32,229,562	2.65	29.34	9,456,357	Measured
10	20	885	2.65	2345	18.92	444	12,162,984	32,231,908	2.65	29.34	9,456,801	Measured
0	10	0	0.00	0	0.00	0	12,162,984	32,231,908	2.65	29.34	9,456,801	Measured
60	70	0	0.00	0	0.00	0	0	0	0.00	0.00	0	TOTAL
50	60	0	0.00	0	0.00	0	0	0	0.00	0.00	0	TOTAL
40	50	38,562	2.65	102,189	41.12	42,018	38,562	102,189	2.65	41.12	42,018	TOTAL
30	40	4,919,817	2.65	13,037,515	33.05	4,309,413	4,958,379	13,139,704	2.65	33.12	4,351,431	TOTAL
20	30	8,024,007	2.65	21,263,619	26.94	5,728,959	12,982,386	34,403,323	2.65	29.30	10,080,390	TOTAL
10	20	885	2.65	2345	18.92	444	12,983,271	34,405,668	2.65	29.30	10,080,834	TOTAL
0	10	0	0.00	0	0.00	0	12,983,271	34,405,668	2.65	29.30	10,080,834	TOTAL

5.6. Grade Assignment for the Low Grade Orebody

The parameter values of the search ellipsoid generated by the semivariogram analysis are listed in Table 5.10. Due to the same concerns about uncontrolled spatial extent of the orebody, a boundary string was applied to solve this problem. In this way, the low-grade orebody was significantly reduced in size. Modeling was continued in the same way as in previous approaches.

The tonnage calculated based on grade ranges of the low-grade iron ore using the IDW and kriging estimation algorithms are presented in Tables 5.11 and 5.12, respectively. The block model of the ore body based on grade categories with kriging is shown in Figure 5.15.

Table 5.10 Parameter values of the search ellipsoid used by the estimation algorithms for the low-grade orebody

Category	Axis-1 (m)	Axis-2 (m)	Axis-3 (m)	Azimuth (°)	Plunge (°)	Rotation (°)
Measured	250.00	120.00	140.00			
Indicated	500.00	240.00	280.00	294.70	1.71	-19.93
Inferred	750.00	360.00	420.00			

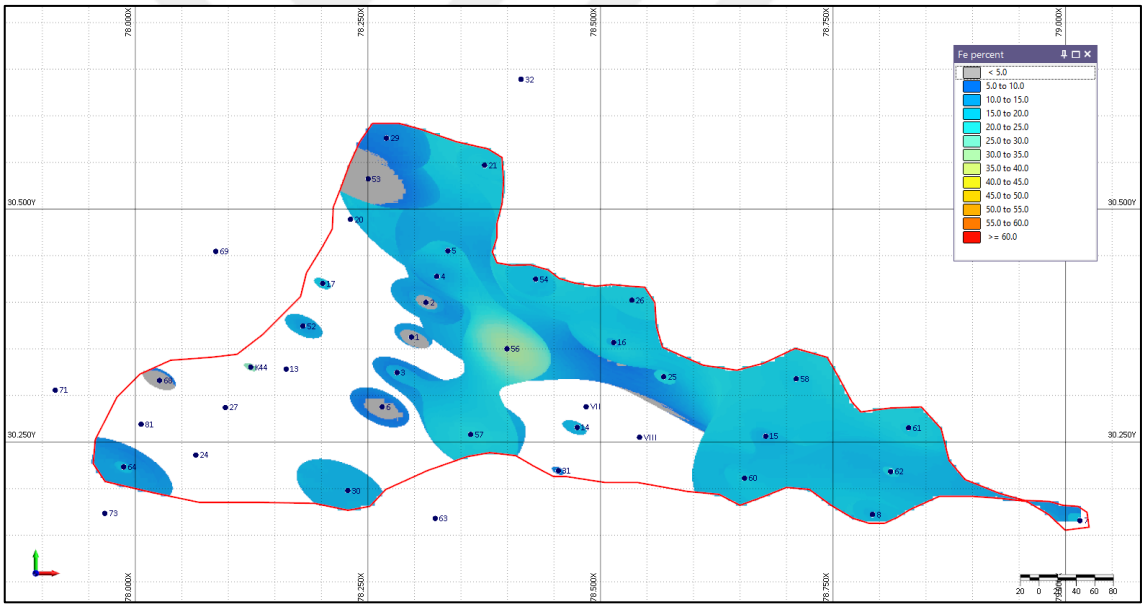

Figure 5.15 The low-grade orebody with grades assigned to blocks with kriging

The deposit contains 38,666,815 tons of iron ore with an average Fe grade of 10.80%, yielding approximately 4,175,225 tons of extractable iron, according to the IDW method. Of the total resource, 83.35% falls into the measured category, while only 16.65% is classified as Indicated, which typically has a lower geological confidence than Measured.

Although the total volume and tonnage figures for the high-grade orebody were quite similar to the IDW method (38,666,815 tons of ore and 4,698,803 tons of extractable iron content), the average Fe grade estimated by kriging was slightly higher at 12.15%.

Table 5.11 Estimated tonnage of resources by the IDW algorithm for the low-grade orebody

							Cumulative					
From Fe% (%)	To Fe% (%)	Volume (m³)	Density (t/m³)	Tonnage (t)	Fe % (%)	Iron content (t)	Volume (m³)	Tonnage (t)	Density (t/m³)	Fe% (%)	Iron content (t)	Resource type
60	70	0	0.00	0	0.00	0	0	0	0.00	0.00	0	Indicated
50	60	0	0.00	0	0.00	0	0	0	0.00	0.00	0	Indicated
40	50	0	0.00	0	0.00	0	0	0	0.00	0.00	0	Indicated
30	40	0	0.00	0	0.00	0	0	0	0.00	0.00	0	Indicated
20	30	0	0.00	0	0.00	0	0	0	0.00	0.00	0	Indicated
10	20	769,854	2.65	2,040,113	10.34	210,873	769,854	2,040,113	2.65	10.34	210,873	Indicated
0	10	1,659,736	2.65	4,398,300	9.30	408,917	2,429,590	6,438,414	2.65	9.63	619,791	Indicated
60	70	0	0.00	0	0.00	0	0	0	0.00	0.00	0	Measured
50	60	0	0.00	0	0.00	0	0	0	0.00	0.00	0	Measured
40	50	0	0.00	0	0.00	0	0	0	0.00	0.00	0	Measured
30	40	6467	2.65	17,138	31.54	5406	6467	17,138	2.65	31.54	5406	Measured
20	30	76,171	2.65	201,853	24.11	48,672	82,638	218,991	2.65	24.69	54,078	Measured
10	20	7,825,218	2.65	20,736,828	13.97	2,896,717	7,907,856	20,955,818	2.65	14.08	2,950,795	Measured
0	10	4,253,805	2.65	11,272,583	5.36	604,639	12,161,661	32,228,402	2.65	11.03	3,555,434	Measured
60	70	0	0.00	0	0.00	0	0	0	0.00	0.00	0	TOTAL
50	60	0	0.00	0	0.00	0	0	0	0.00	0.00	0	TOTAL
40	50	0	0.00	0	0.00	0	0	0	0.00	0.00	0	TOTAL
30	40	6467	2.65	17,138	31.54	5406	6467	17,138	2.65	31.54	5406	TOTAL
20	30	76,171	2.65	201,853	24.11	48,672	82,638	218,991	2.65	24.69	54,078	TOTAL
10	20	8,595,072	2.65	22,776,941	13.64	3,107,590	8,677,710	22,995,932	2.65	13.75	3,161,668	TOTAL
0	10	5,913,541	2.65	15,670,884	6.47	1,013,557	14,591,251	38,666,815	2.65	10.80	4,175,225	TOTAL

Table 5.12 Estimated tonnage of resources by the kriging algorithm for the low grade orebody

							Cumulative					
From Fe% (%)	To Fe% (%)	Volume (m^3)	Density (t/m^3)	Tonnage (t)	Fe % (%)	Iron content (t)	Volume (m^3)	Tonnage (t)	Density (t/m^3)	Fe% (%)	Iron content (t)	Resource type
60	70	0	0.00	0	0.00	0	0	0	0.00	0.00	0	Indicated
50	60	0	0.00	0	0.00	0	0	0	0.00	0.00	0	Indicated
40	50	0	0.00	0	0.00	0	0	0	0.00	0.00	0	Indicated
30	40	0	0.00	0	0.00	0	0	0	0.00	0.00	0	Indicated
20	30	0	0.00	0	0.00	0	0	0	0.00	0.00	0	Indicated
10	20	2,350,449	2.65	6,228,690	11.94	743,396	2,350,449	6,228,690	2.65	11.94	743,396	Indicated
0	10	79,141	2.65	209,724	9.44	19,795	2,429,590	6,438,414	2.65	11.85	763,191	Indicated
60	70	0	0.00	0	0.00	0	0	0	0.00	0.00	0	Measured
50	60	0	0.00	0	0.00	0	0	0	0.00	0.00	0	Measured
40	50	0	0.00	0	0.00	0	0	0	0.00	0.00	0	Measured
30	40	7407	2.65	19,629	31.84	6251	7407	19,629	2.65	31.84	6251	Measured
20	30	177,367	2.65	470,023	21.89	102,877	184,774	489,651	2.65	22.29	109,128	Measured
10	20	8,258,290	2.65	21,884,469	15.17	3,320,285	8,443,064	22,374,120	2.65	15.33	3,429,413	Measured
0	10	3,718,597	2.65	9,854,282	5.14	506,198	12,161,661	32,228,402	2.65	12.21	3,935,611	Measured
60	70	0	0.00	0	0.00	0	0	0	0.00	0.00	0	TOTAL
50	60	0	0.00	0	0.00	0	0	0	0.00	0.00	0	TOTAL
40	50	0	0.00	0	0.00	0	0	0	0.00	0.00	0	TOTAL
30	40	7407	2.65	19,629	31.84	6251	7407	19,629	2.65	31.84	6251	TOTAL
20	30	177,367	2.65	470,023	21.89	102,877	184,774	489,651	2.65	22.29	109,128	TOTAL
10	20	10,608,739	2.65	28,113,158	14.45	4,063,681	10,793,513	28,602,809	2.65	14.59	4,172,809	TOTAL
0	10	3,797,738	2.65	10,064,006	5.23	525,993	14,591,251	38,666,815	2.65	12.15	4,698,803	TOTAL

5.7. Combining the Orebodies

In the approaches presented above, grades were assigned to blocks in three separate ore bodies — high, medium and low grade – using IDW and kriging methods. However, as not all ore bodies could be included in the design during the planning phase of the open pit, the ore bodies were combined into one.

The data on volume, tonnage, density and iron content of the combined orebody can be found in Table 5.13. The block model of the combined orebody is shown in Figure 5.16. The total volume of the combined orebody is 30,374,815 m³. With a grade-weighted density of 3.29 t/m³, the mass of the orebody reaches 99,988,131 tons. The average grade is 26.14% Fe and the mineable iron content is 26,132,549 tons.

It should be remembered that the mass of the individual orebodies amounts to a total of 81,225,648 tons. The difference is due to the fact that when calculating the tonnage of the individual orebodies, the ore density was assumed to be 2.65 t/m³, regardless of the grade, which could mislead the planner. In contrast, when calculating the tonnage of the combined ore body, the density of each block was assigned a unique value based on the Equation 5.1. Nevertheless, the volume of the combined orebody and the sum of the volumes of the individual orebodies are very close to each other with a difference of 276,373 m³, which corresponds to a value of only 0.91%.

$$Density = 0.036 \cdot Grade + 2.4327 \quad [5.1]$$

The majority of the ore (~90%) belongs to the measured category. The average grade of this category is also higher than that of the indicated category, with ore concentrated in the 10% to 40% iron range. Similarly, the ore in the indicated category contains between 10% and 30% iron.

When evaluating the resource as a whole, the largest portion falls within the 10%-40% Fe grade range. This trend is also observed within the measured category. However, the measured resources are most concentrated in the broader 20%–60% Fe range, indicating that a significant portion of high-confidence resources are of medium grade. Overall, the deposit can be classified as hosting a medium-grade iron ore resource. Additionally, there is a clear decrease in resource tonnage as the Fe grade increases from lower to higher ranges.

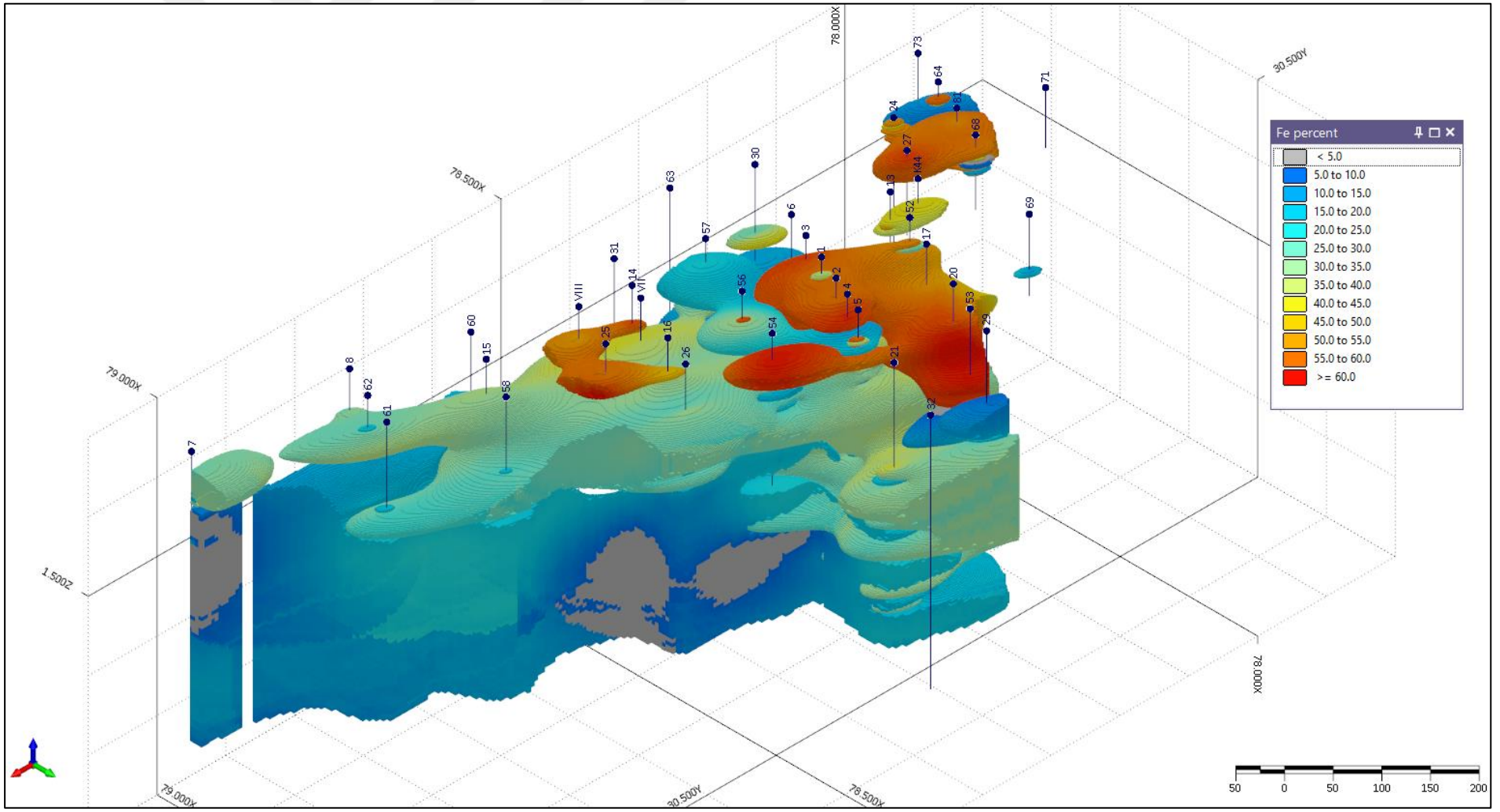

Figure 5.16 The combined orebody

Table 5.13 Estimated tonnage of resources for the combined orebody

							Cumulative					
From Fe% (%)	To Fe% (%)	Volume (m³)	Density (t/m³)	Tonnage (t)	Fe % (%)	Iron content (t)	Volume (m³)	Tonnage (t)	Density (t/m³)	Fe% (%)	Iron content (t)	Resource type
60	70	0	0.00	0	0.00	0	0	0	0.000	0.00	0	Indicated
50	60	5135	4.38	22,474	54.01	12,138	5135	22,474	4.38	54.01	12,138	Indicated
40	50	3711	3.93	14,568	41.48	6042	8846	37,042	4.19	49.08	18,180	Indicated
30	40	101,648	3.57	362,954	31.65	114,870	110,494	399,996	3.62	33.26	133,050	Indicated
20	30	666,557	3.45	2,299,018	28.25	649,399	777,051	2,699,014	3.47	28.99	782,449	Indicated
10	20	2,350,449	2.86	6,727,834	11.94	803,391	3,127,500	9,426,848	3.01	16.82	1,585,840	Indicated
0	10	79,141	2.77	219,418	9.44	20,716	3,206,641	9,646,266	3.01	16.65	1,606,556	Indicated
60	70	321,152	4.62	1,484,437	60.82	902,891	321,152	1,484,437	4.62	60.82	902,891	Measured
50	60	2,680,920	4.48	12,006,282	56.86	6,826,731	3,002,072	13,490,718	4.49	57.30	7,729,622	Measured
40	50	71,524	4.04	,288,814	44.72	129,146	3,073,596	13,779,533	4.48	57.03	7,858,768	Measured
30	40	4,778,294	3.62	17,317,114	33.15	5,740,160	7,851,890	31,096,647	3.96	43.73	13,598,928	Measured
20	30	7,336,868	3.39	24,903,239	26.76	6,664,327	15,188,758	55,999,887	3.69	36.18	20,263,255	Measured
10	20	8,260,819	2.98	24,608,083	15.25	3,751,926	23,449,577	80,607,969	3.44	29.79	24,015,181	Measured
0	10	3,718,597	2.62	9,733,896	5.25	510,812	27,168,174	90,341,865	3.33	27.15	24,525,993	Measured
60	70	321,152	4.62	1,484,437	60.82	902,891	321,152	1,484,437	4.62	60.82	902,891	TOTAL
50	60	2,686,055	4.48	12,028,755	56.85	6,838,869	3,007,207	13,513,192	4.49	57.29	7,741,760	TOTAL
40	50	75,235	4.03	303,382	44.56	135,188	3,082,442	13,816,574	4.48	57.01	7,876,948	TOTAL
30	40	4,879,942	3.62	17,680,069	33.12	5,855,030	7,962,384	31,496,643	3.96	43.60	13,731,978	TOTAL
20	30	8,003,425	3.40	27,202,258	26.89	7,313,727	15,965,809	58,698,901	3.68	35.85	21,045,705	TOTAL
10	20	10,611,268	2.95	31,335,917	14.54	4,555,317	26,577,077	90,034,817	3.39	28.43	25,601,021	TOTAL
0	10	3,797,738	2.62	9,953,314	5.34	531,528	30,374,815	99,988,131	3.29	26.14	26,132,549	TOTAL

6. PIT OPTIMIZATION and DESIGN

6.1. Ultimate Pit Optimization

One of the greatest challenges in mining technology is the pit limit optimization. As early as 1965, Lerchs and Grossmann were working on this problem and developed a method named after them, the Lerchs and Grossmann algorithm. The optimal design of the open-pit mine geometry is still in use today. The Lerchs-Grossmann algorithm can develop an open pit boundary that maximizes the net present value of a mine's yield over a given period of time or its lifetime. Using this algorithm, therefore, the objective of this chapter was defined as determining a profitable pit limit for mining that maximizes the net present value for the largest possible portion of the iron ore deposits in the area.

Some data is important to optimize the horizontal and vertical expansion of the pit. Most of the data, including mining, reclamation and processing costs, ore and waste density, and final pit slope angles, were collected from similar current operations. Since the topography of the mine site is quite flat, a single angle of 40° was used for the overall pit slope. It should be noted that the slope angles are not based on geotechnical evaluations and therefore may not be realistic assumptions due to a lack of geotechnical information on the country rocks and mineral. The parameter values used for the optimization of the final pit are listed in Table 6.1.

Table 6.1 Input parameter values used in ultimate pit optimization

Pit type	Ultimate
Revenue adjustment factor (RAF)	1
Ore mining costs (US$/t)	1.0
Waste mining cost (US$/t)	1.0
Environmental rehabilitation cost (US$/t)	0.0
Ore mining cost adjustment factor (MCAF)	1
Waste mining cost adjustment factor (MCAF)	1
Rehabilitation cost adjustment factor (RCAF)	1
Ore density, default (t/m³)	3.94
Ore density (determined as a function of ore grade, t/m³)	2.433-4.722
Cut-off grade for mining (% Fe)	10
Waste density (t/m³)	2.5
Ore dilution during operating stage (waste/ore, %)	10
Ore recovery during operating stage (%)	85
Final slope angles (°)	40
Ore processing costs (US$/t)	10
Ore processing cost adjustment factor (PCAF)	1
General and administration cost (US$/t)	1
Ore recovery during processing (%)	85
Ore selling price after processing (US$/t)	105
Selling cost (US$/t)	2

The parameters calculated by the optimization algorithm, which are listed in Table 6.2, are formulated below.

A. Pit bottom elevation: determined by the modeler.
B. Pit top elevation: determined by the modeler.
C. Volume in situ:

$$C = E + G$$

D. Volume diluted recovered:

$$D = F + H$$

E. Ore volume in situ: determined by the modeler.

F. Ore volume diluted recovered: Ore is diluted with some waste during operations (10% in Table 6.1) and cannot be extracted in full (85% in Table 6.1).

$$F = E \cdot \left(\frac{1 + Dilution}{100}\right) \cdot \frac{Recovery}{100}$$

G. Waste volume in situ: determined by the modeler.
H. Waste volume diluted recovered:

$$H = C - F$$

İ. Density:

$$I = \left(\frac{P + R}{F + H}\right)$$

J. Ore density: Weighted value, determined by the modeler.
K. Waste density: Weighted value, determined by the modeler.
L. Total mass of ore & waste, in situ:

$$L = C \cdot I$$

M. Total mass of ore & waste, diluted recovered:

$$M = D \cdot I$$

N. Stripping ratio:

$$N = \frac{R}{P}$$

O. Ore mass, in situ:

$$N = E \cdot J$$

P. Ore mass, diluted recovered:

$$P = F \cdot J$$

Q. Waste mass, in situ:

$$Q = G \cdot K$$

R. Waste mass, diluted recovered:

$$R = H \cdot K$$

S. Mining cost: Ore (US$ 1/t in Table 6.1) and waste (US$ 1/t in Table 6.1) mining unit costs are taken into account.

$$S = (P \cdot Ore\ mining\ unit\ cost) + (R \cdot Waste\ mining\ unit\ cost)$$

T. Ore mining cost:

$$T = O \cdot Ore\ mining\ unit\ cost$$

U. Waste mining cost:

$$U = Q \cdot Waste\ mining\ unit\ cost$$

V. Processing cost: The unit cost (US$ 10/t in Table 6.1) is taken into account.

$$V = P \cdot Processing\ unit\ cost$$

W. Additional processing cost: -

X. General and administration cost: The unit cost (US$ 1/t in Table 6.1) is taken into account.

$$W = P \cdot General\ and\ administration\ unit\ cost$$

Y. Selling cost: The unit cost (US$ 2/t in Table 6.1) is taken into account.

$$W = HH \cdot Administation\ unit\ cost$$

Z. Rehabilitation cost: -

AA. Total cost:

$$AA = S + V + X + Y$$

BB. Total revenue: The selling price (US$ 105/t in Table 6.1) is taken into account.

$$BB = HH \cdot Processed\ ore\ selling\ price$$

CC. Net value:

$$CC = BB - AA$$

DD. Iron by mass in situ:

$$DD = (O + Q) \cdot II$$

EE. Iron by ore mass in situ:

$$EE = (O + Q) \cdot JJ$$

FF. Iron by mass diluted recovered:

$$FF = M \cdot LL$$

GG. Iron by ore mass diluted recovered:

$$GG = P \cdot MM$$

HH. Iron by mass processed recovered: The recovery ratio (85% in Table 6.1) is taken into account.

$$HH = GG \cdot Recovery\ ratio$$

İİ. Iron by mass, in situ:

$$II = \frac{DD}{L}\%$$

JJ. Iron by ore mass, in situ:

$$JJ = \frac{EE}{O}\%$$

KK. Iron diluting grade: -

LL. Iron by mass, diluted recovered:

$$LL = \frac{FF}{M}\%$$

MM. Iron by ore mass, diluted recovered:

$$MM = \frac{GG}{P}\%$$

NN. Iron by volume, in situ:

$$NN = \frac{DD}{C}\%$$

OO. Iron by ore volume, in situ:

$$OO = \frac{EE}{E}\%$$

PP. Iron by volume, diluted recovered:

$$PP = \frac{FF}{D}\%$$

QQ. Iron by ore volume, diluted recovered:

$$QQ = \frac{GG}{F}\%$$

RR. Iron revenue: The selling price (US$ 105/t in Table 6.1) is taken into account.

$$RR = HH \cdot Processed\ ore\ selling\ price$$

SS. MB Fe volume: -

TT. MB Fe volume, diluted recovered:

$$TT = E + AAA$$

UU. MB Fe mass, in situ: -

VV. MB Fe mass diluted recovered: -

WW. MB Fe costs:

$$WW = S + V + X + Y + EEE$$

XX. MB Fe revenue: The selling price (US$ 105/t in Table 6.1) is taken into account.

$$XX = HH \cdot Processed\ ore\ selling\ price$$

YY. MB Fe net revenue:

$$YY = XX - WW$$

ZZ. MB Unclassified material volume, in situ: determined by the modeler.

AAA. MB Unclassified material volume, diluted recovered: determined by the modeler.

BBB. MB Unclassified material mass, in situ:

$$BBB = ZZ \cdot I$$

CCC. MB Unclassified material mass, diluted recovered:

$$CCC = AAA \cdot I$$

DDD. MB Unclassified material density: -

EEE. MB Unclassified material costs: The waste mining cost (US$ 1/t in Table 6.1) is taken into account.

$$EEE = BBB \cdot Waste\ mining\ cost$$

FFF. MB Unclassified material revenue: No ore is mined in this part, so there is no revenue.

GGG. MB Unclassified material net revenue: This item is actually cost of extra waste disposal.

$$GGG = BBB \cdot Waste\ mining\ cost$$

HHH. MB DEFAULT volume, in situ: determined by the modeler.

İİİ. MB DEFAULT volume, diluted recovered: determined by the modeler.

JJJ. MB DEFAULT mass, in situ: The waste density (2.65 t/m³ in Table 6.1) is taken into account.

$$JJJ = HHH \cdot Waste\ density$$

KKK. MB DEFAULT mass, diluted recovered: The waste density (2.65 t/m³ in Table 6.1) is taken into account.

$$KKK = III \cdot I$$

LLL. MB DEFAULT costs: The waste mining cost (US$ 1/t in Table 6.1) is taken into account.

$$LLL = JJJ \cdot Waste\ mining\ cost$$

MMM. MB DEFAULT revenue: No ore is mined in this part, so there is no revenue.

NNN. MB DEFAULT net revenue: This item is actually cost of extra waste disposal.

$$NNN = JJJ \cdot Waste\ mining\ cost$$

The final (ultimate) pit, shown on the isometric and sectional images in Figures 6.1 and 6.2, has a depth of 320 meters from its base at 1355 meters to its highest point at 1675 meters. Based on an average in-situ density of 2.76918 t/m³, the total mineable material in the pit is 194,358,607 tons. Of this, 55,116,039.35 tons are diluted recovered ore, while 139,242,568 tons are diluted recovered waste, resulting in a stripping ratio of 2.52635. Although the total in-situ iron mass is 21,109,961 tons, the diluted recovered iron mass is 17,702,602 tons. Assuming an 85% recovery from the processing plant, the final processed iron production is 15,047,212 tons.

The mining costs for the open pit are estimated at USD 194,358,607, of which USD 58,947,636 is for the ore and USD 135,410,971 for the waste. The processing costs for the diluted ore amount to USD 551,160,393, while the general administration costs and distribution costs amount to USD 55,116,039 and USD 30,094,424, respectively. Thus, the pit's total costs amount to USD 830,729,464 and total revenues to USD 1,579,957,260, resulting in a net value before taxes of USD 749,227,796. It should be noted that the revenue and cost figures are not time-dependent and have not been discounted to present value.

Table 6.2 The results of ultimate pit optimization

A	Pit bottom elevation (m)	1355
B	Pit top elevation (m)	1675
C	Volume in situ (m^3)	70,186,226
D	Volume, diluted recovered (m^3)	70,186,226
E	Ore volume in situ (m^3)	16,138,749
F	Ore volume, diluted recovered (m^3)	15,089,730
G	Waste volume in situ (m^3)	54,047,477
H	Waste volume, diluted recovered (m^3)	55,096,496
I	Density (t/m^3)	2.76918
J	Ore density (t/m^3)	3.65255
K	Waste density (t/m^3)	2.50541
L	Total mass of ore & waste, in situ (t)	194,358,607
M	Total mass of ore & waste, diluted recovered (t)	194,358,607
N	Stripping ratio (t/t)	2.52635
O	Ore mass, in situ (t)	58,947,636
P	Ore mass, diluted recovered (t)	55,116,039
Q	Waste mass, in situ (t)	135,410,971
R	Waste mass, diluted recovered (t)	139,242,568
S	Mining cost ($)	194,358,607
T	Ore mining cost ($)	58,947,636
U	Waste mining cost ($)	135,410,971
V	Processing cost ($)	551,160,393
W	Additional processing cost ($)	-
X	General and administration cost ($)	55,116,039
Y	Selling cost ($)	30,094,424
Z	Rehabilitation cost ($)	-
AA	Total cost ($)	830,729,464
BB	Total revenue ($)	1,579,957,260
CC	Net Value ($)	749,227,796
DD	Iron by mass in situ (t)	21,109,961
EE	Iron by ore mass in situ (t)	20,826,591
FF	Iron by mass, diluted recovered (t)	17,943,467
GG	Iron by ore mass, diluted recovered (t)	17,702,602
HH	Iron by mass, processed recovered (t)	15,047,212
II	Iron by mass, in situ (%)	10.86135
JJ	Iron by ore mass, in situ (%)	35.33066
KK	Iron diluting grade (%)	-
LL	Iron by mass, diluted recovered (%)	9.23214
MM	Iron by ore mass, diluted recovered (%)	32.11879
NN	Iron by volume, in situ (t/m^3)	0.30077
OO	Iron by ore volume, in situ (t/m^3)	1.29047
PP	Iron by volume, diluted recovered (t/m^3)	0.25566
QQ	Iron by ore volume, diluted recovered (t/m^3)	1.17316
RR	Iron revenue ($)	1,579,957,260
SS	MB Fe volume, in situ (m^3)	16,744,272
TT	MB Fe volume, diluted recovered (m^3)	16,744,272
UU	MB Fe mass, in situ (t)	60,678,410
VV	MB Fe mass diluted recovered (t)	60,678,410
WW	MB Fe costs ($)	697,049,267
XX	MB Fe revenue ($)	1,579,957,260
YY	MB Fe net revenue ($)	882,907,993
ZZ	MB Unclassified material volume, in situ (m^3)	429,160
AAA	MB Unclassified material volume, diluted recovered (m^3)	429,160
BBB	MB Unclassified material mass, in situ (t)	1,148,213
CCC	MB Unclassified material mass, diluted recovered (t)	1,148,213
DDD	MB Unclassified material density (t/m^3)	-
EEE	MB Unclassified material costs ($)	1,148,213
FFF	MB Unclassified material revenue ($)	-
GGG	MB Unclassified material net revenue ($)	1,148,213
HHH	MB DEFAULT volume, in situ (m^3)	53,012,794
III	MB DEFAULT volume, diluted recovered (m^3)	53,012,794
JJJ	MB DEFAULT mass, in situ (t)	132,531,985
KKK	MB DEFAULT mass, diluted recovered (t)	132,531,985
LLL	MB DEFAULT costs ($)	132,531,985
MMM	MB DEFAULT revenue ($)	-
NNN	MB DEFAULT net revenue ($)	132,531,985

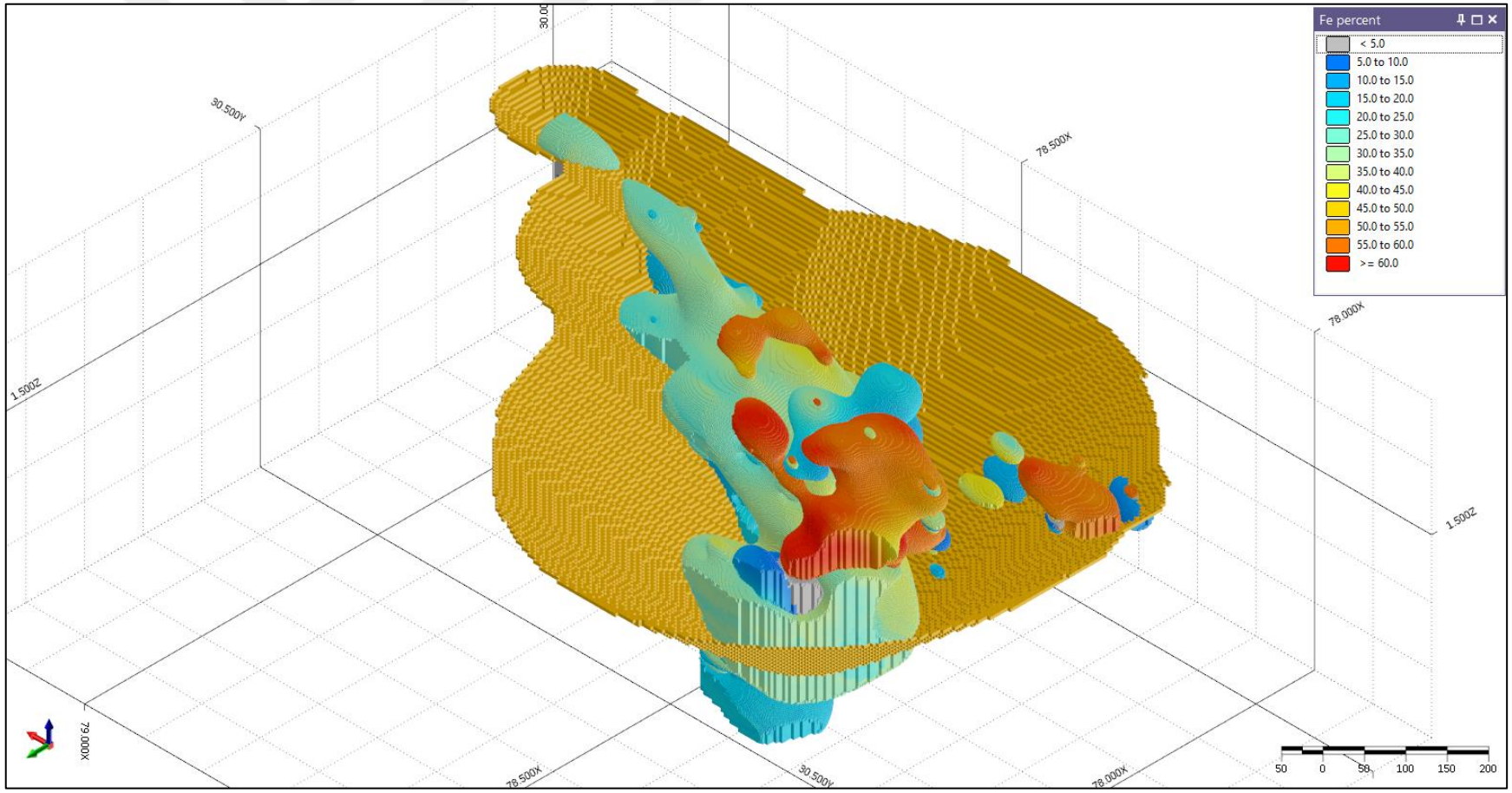

Figure 6.1 The ultimate pit (isometric view to the southeast)

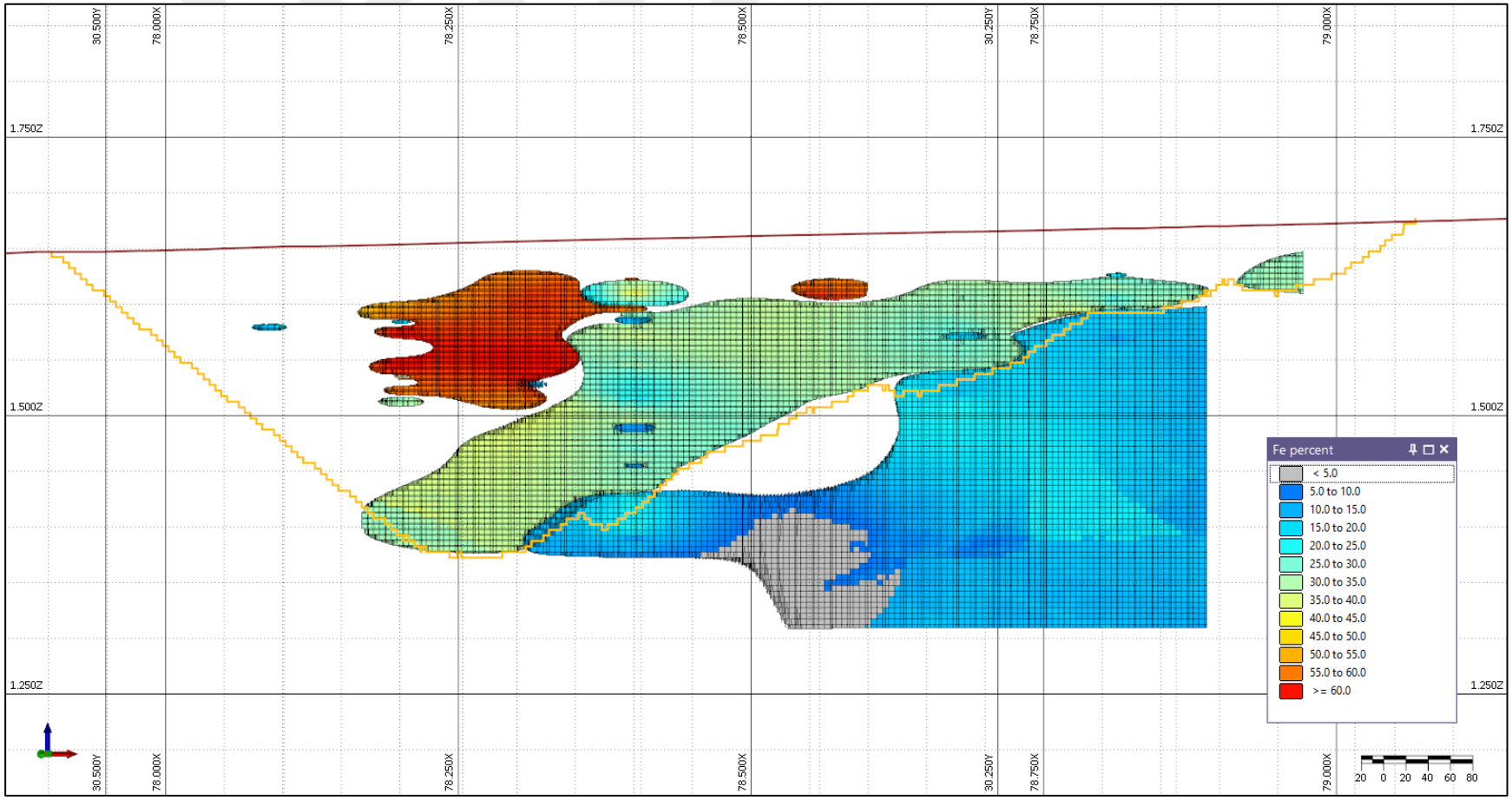

Figure 6.2 The ultimate pit and the block model of the combined orebody (cross-section view)

6.2. Nested Pit Optimization

The optimization of nested pits is the decisive process in the planning and design of mines. The selection of a profitable and economic pit from a series of pits located below or above the final pit is the essential process and determines how the economic limits of an open pit mine expand under different economic conditions.

Computerized programs such as Micromine™ can be used to create nested pits or the pit shells for different operating conditions. In today's fluctuating market conditions, ore prices are very flexible for a number of reasons. Since mining operations can last for decades and the selling price is unpredictable over the decades of mine operation, the Revenue Adjustment Factor (RAF) needs to be modified. Therefore, we generated a series of nested pits to account for the unpredictability of market prices. In the analyses, the RAF ranged from 0.5 (for the case where the selling price of enriched ore is halved, US$ 52.5) to 1.2 (the selling price is increased by 20%, US$ 126) with increments of 10%. Another constraint included in the analyses was that each nested pit must have produced at least 50,000 tons of material, including waste and ore, for the next nested pit to be produced. Otherwise, a pit would not be created for a given RAF.

As can be seen in Figures 6.3 and 6.4, 8 nested pits were created, each corresponding to a specific RAF. By evaluating the nested pits in terms of ore production and waste extraction figures and NPV, the optimal pit that meets the management's strategic objectives and fulfills the necessary criteria can be selected.

The analyses of the changes in production and cash flow in various phases and periods were carried out under the "constant lag" scenario for mining activities. An investment of US$ 200,000,000 is made, with US$ 50,000,000 allocated to years 0, 1, 2 and 3. A discount rate of 5% is used for the revenues generated in subsequent years. A maximum annual production of 20,000,000 tons (ore + overburden) is allowed yearly. Of this production, 6,667,000 tons will be processed in the ore processing plant and the enriched ore will be destined for sale without being held in stock.

While the production and cash flow figures are shown cumulatively for each subsequent "stage", they are shown on an annual basis for the "periods". From a mining perspective, the worst-case scenarios are designed such that all ore and waste at a given level (bench) within the pit limit is fully mined before proceeding to the level below. The constant lag scenario however, allows operations to continue at multiple levels simultaneously, similar to the real world. In this study, mining is carried out simultaneously on three levels.

The analyses performed with the pit optimizer based on stages of pit (each nested pit) and periods (years) are shown in Figures 6.5 and 6.6, respectively. According to the multivariable economic and production analysis across different stages (pit shells) shown in Figure 6.5, it can be observed that a negative cash flow starts at stage zero and then a rapid jump from negative to positive cash flow is realized until the peak, about 0.9 RAF. After that, the cash flow decreases slightly, which

means that the optimal cash flow is 0.9. The present value of the cash flow follows almost the same trend.

Revenue increased rapidly in stages. However, the cumulative revenues associated with iron ore indicate that revenues decrease after stage 1, as total costs increase with each stage as more material needs to be transported. It should be noted that stages with significant tonnages of waste and ore result in a rapid and significant increase in costs. As you can see from Figure 6.5, the large jump in waste tonnage between Stage 1 and Stage 1.2 has led to a rapid increase in overall costs. From the analyzes performed, it can thus be summarized that the optimal stage should be around stages 0.9 and 1, as the incremental increase in ore production declines slightly. In addition, the cash flow and present value of revenues peak at these stages and the costs and waste volumes are manageable.

The 'Nested Pits by Period' diagram in Figure 6.6 presents a time-based (period-by-period) breakdown of the performance metrics from the nested pit analysis. It complements the previous stage-based chart by showing how finances, revenues, costs and tonnage evolve over the operating periods. Due to the initial investment, cash flow is negative in period 0, but rises rapidly after period 2 and peaks around periods 9 and 13. The present value of revenues is negative at the beginning, but like cash flow, it rises from period 2 to peak in periods 3 to 5 and then falls slowly, but not alarmingly.

Revenues are high in periods 2 to 5 and then start to fall rapidly. This means that the high-grade iron ore was mined earlier. In Figure 6.4, the section through the nested pits, the high-grade ore is close to the surface, which is why the revenues decreases quickly. On the other hand, the total cost starts moderately, increases slightly, then flattens out and slowly decreases. From the NPV perspective, this early peak means that a significant portion of revenues is generated in these periods.

The waste handling is concentrated in the initial phase. It decreases in period 2, but shows an almost steady and constant production behavior until period 9. Then the volume of waste disposal gradually decreases between periods 10 and 13. Ore production increases gradually from period 2 and reaches its maximum between periods 10-12. The mine mainly produces ore after period 2. To summarize, periods 0 to 2 are costly, but in the middle phase, between periods 3 to 6, high-grade ore was mined. The cash flow is maximized in subsequent years due to the higher ore tonnage, even though the NPV decreases due to time discounting.

The evaluation of the analysis of the nested pits with regard to profitability and the main operating parameters shows that pit no. 9 is economically suitable. In addition, pit No. 9 is very close to the ultimate pit. After evaluating the economic conditions of the ultimate pit, it is selected as the optimum pit as it offers better financial conditions. Therefore, further work on the pit design and planning of the iron mine will continue with the ultimate pit structure.

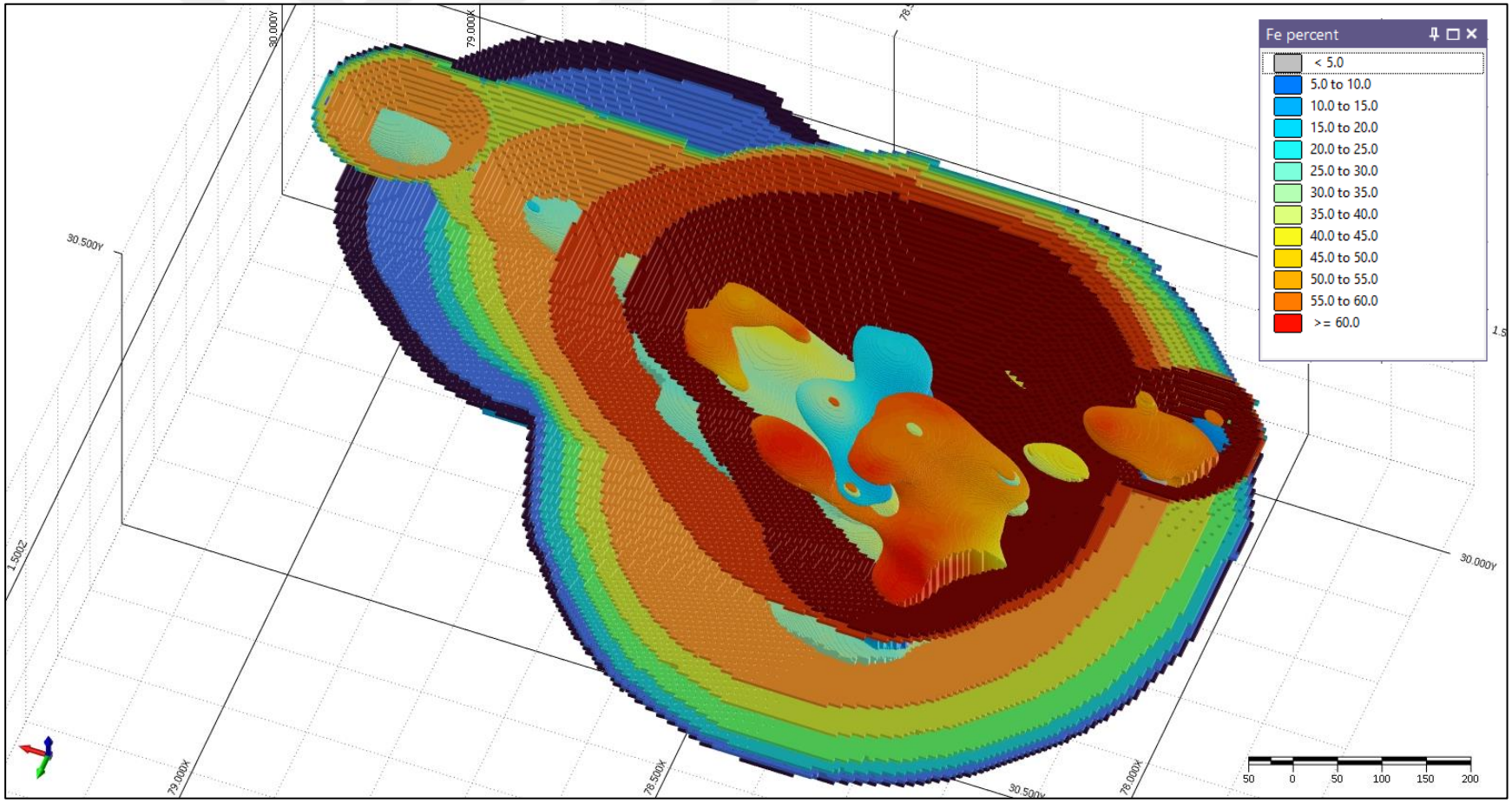

Figure 6.3 The nested pits and the block model of the combined orebody (isometric view to the southeast)

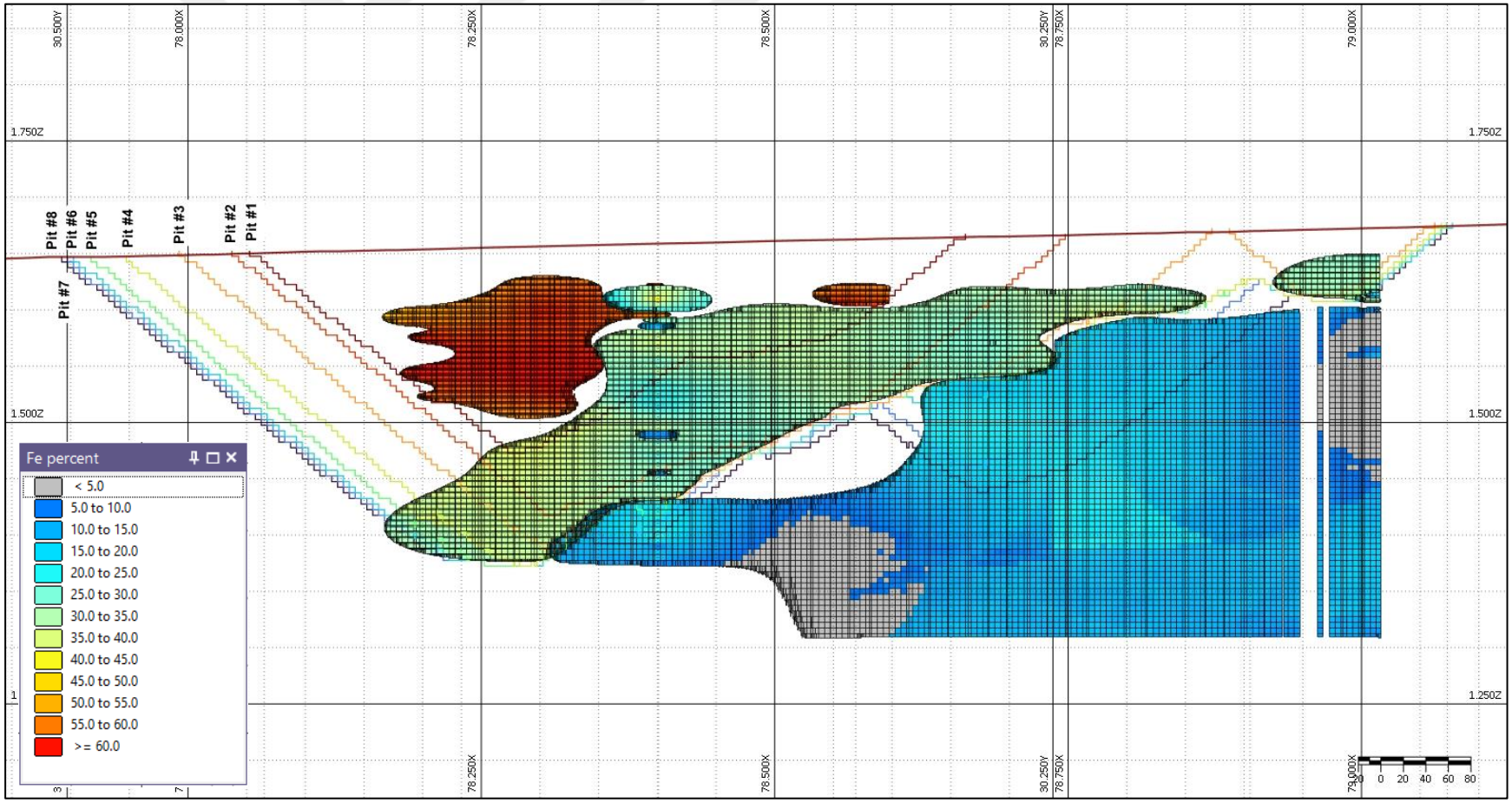

Figure 6.4 The nested pits and the block model of the combined orebody (cross section view)

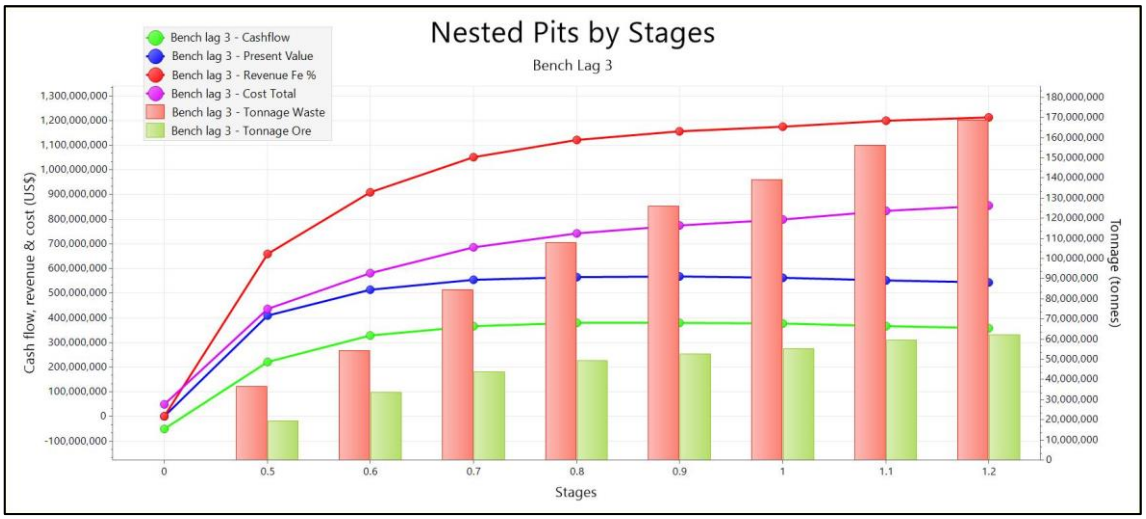

Figure 6.5 The optimization scenario of nested pits by stages (bench lagging)

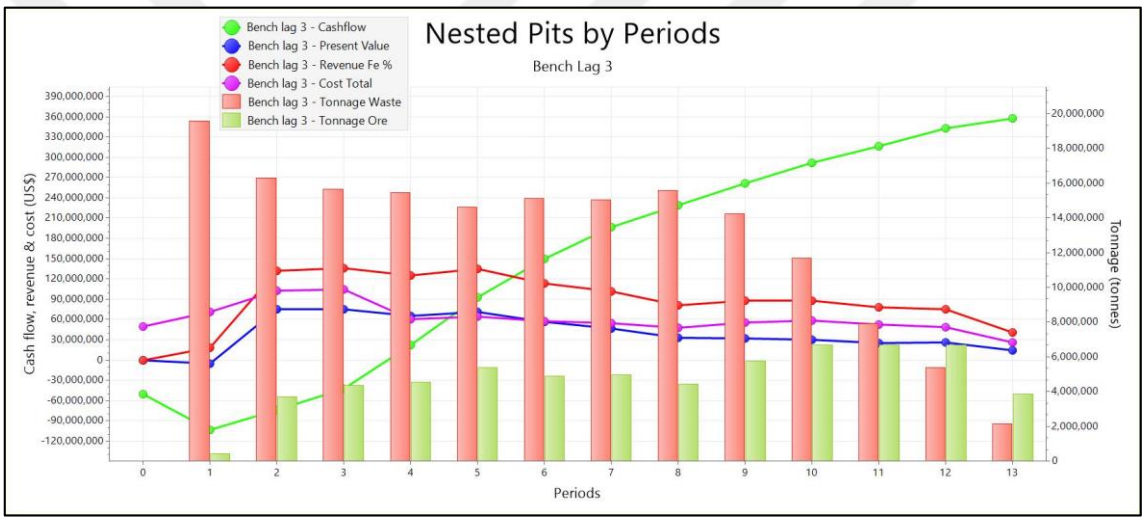

Figure 6.6 The optimization scenario of nested pits by periods (bench lagging)

6.3. Pit Design

After the theoretical work and research that has been carried out up to this point, from the processing of borehole data to solid modeling, resource modeling, pit optimization and finally the selection of the optimum pit, the practical implementation of the planned pit in the mine is finally carried out. In this way, economic ore extraction can be ensured by optimizing the shape, depth and layout of the mine and ensuring safety and structural stability.

Since we consider the ultimate pit to be the most suitable pit for mining (the optimum pit) under operational and financial conditions, the pit is designed from the bottom up, intersecting the topography with benches arranged in successive levels (Figure 6.7). In this upward development, each bench was defined with a batter height of 10 meters, a batter slope of 75° and a berm width of 9 meters. With this configuration, the total pit slope angle reaches approximately 40.57° as calculated by the mine design package. The bench and berm arrangement are designed to ensure both operational efficiency and slope stability.

It should be noted that the interramp angle between the ramps is a guide value and has not been tested for geotechnical stability. Future changes to this angle based on rock mechanical investigations or analyzes of slope stability would require a new optimization of the pit geometry.

Figure 6.8 shows that the pit was modeled as a single-phase development where the benches and berms were generated simultaneously from the bottom of the pit upwards. The resulting geometry produces a V-shaped pit profile when viewed in cross-section in Figure 6.9.

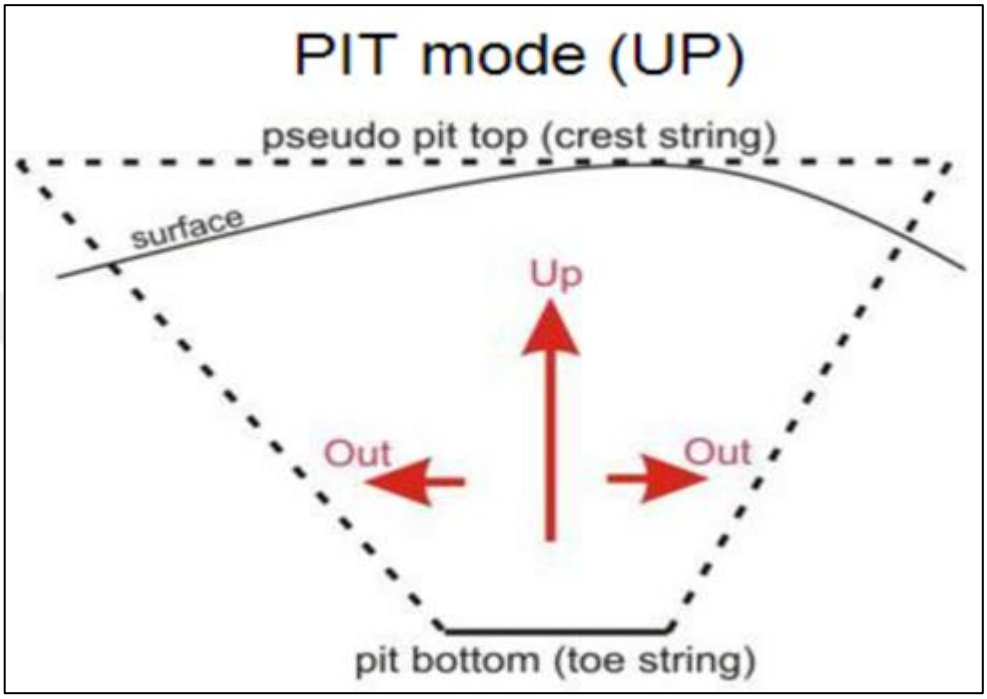

Figure 6.7 The up mode pit design by the package

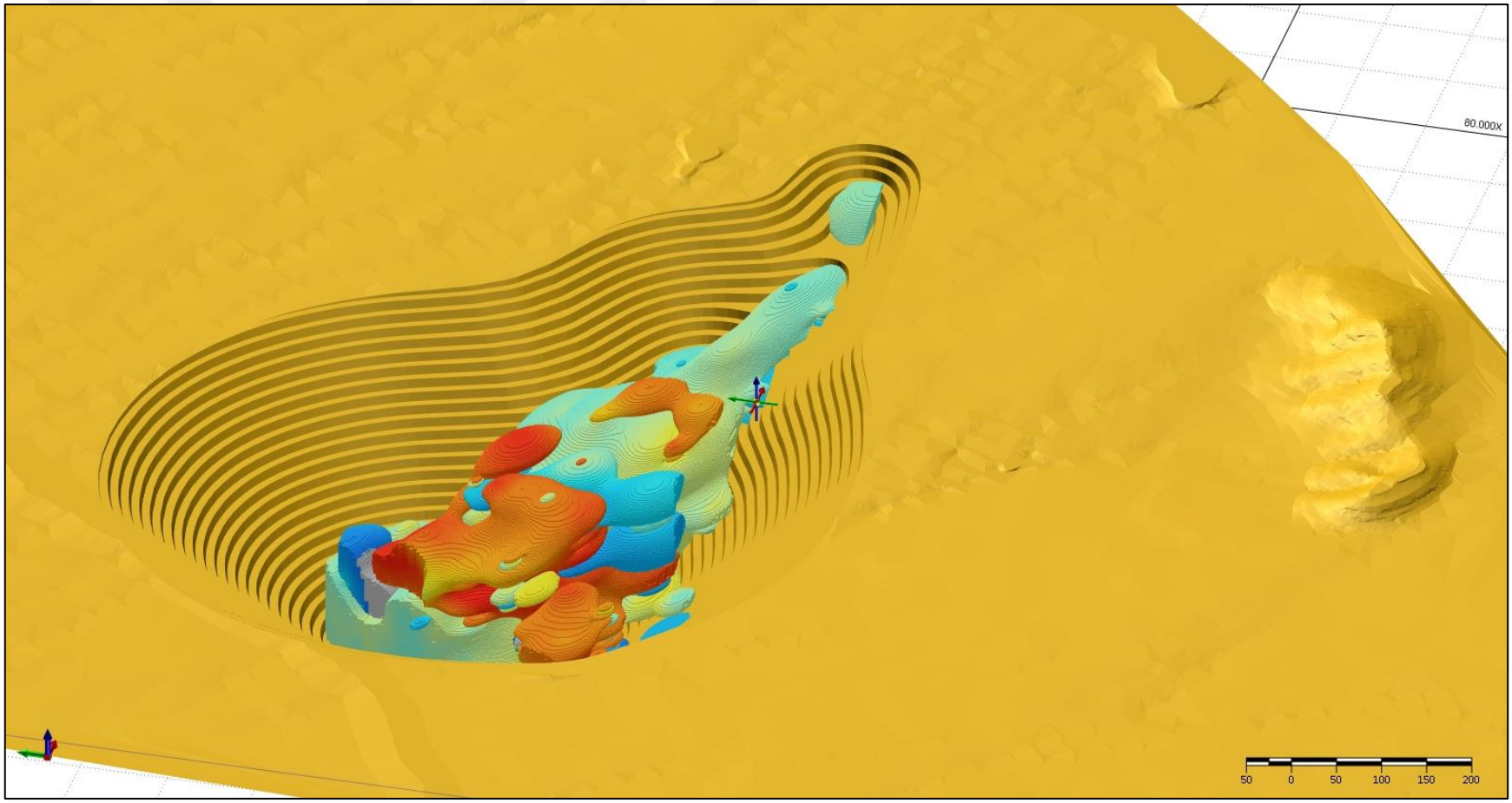

Figure 6.8 The designed open-pit mine and the block model of the combined orebody (isometric view to the northeast)

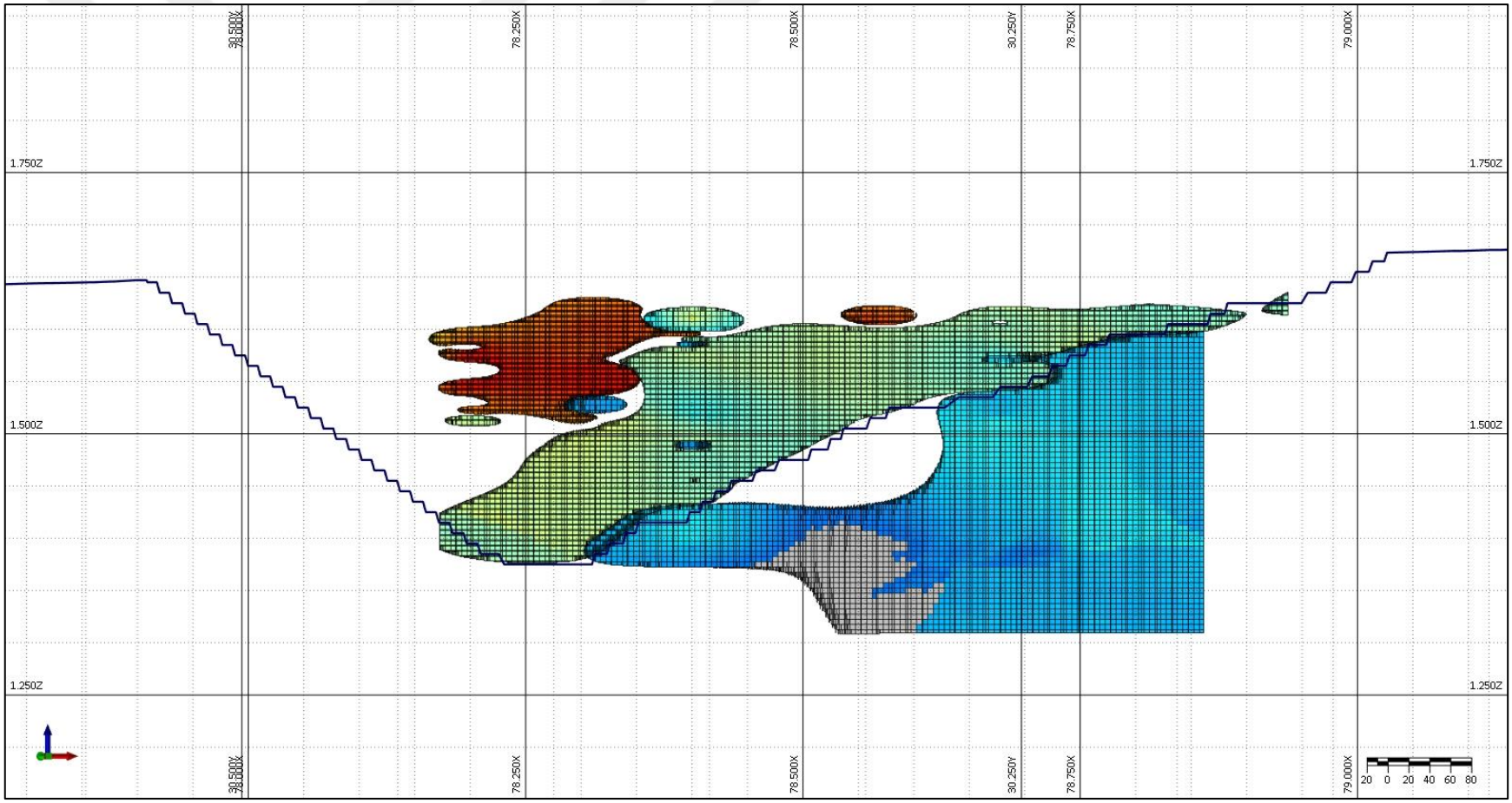

Figure 6.9 The cross section view of the designed open-pit mine and the block model of the combined orebody

7. GRADE-TONNAGE OPERATIONS

7.1. Creating Mining Blocks

The volume of the final pit is 67,476,297 m³ and we have divided it into small mining blocks to extract the ore. Therefore, each block measures 40 m along the X-axis and 50 m along the Y-axis.

The dimensions of all the mining blocks within the final pit must be compatible with each other. Each mining block has an area of 2,000 m² and a height of 10 m, resulting in a volume of 20,000 m³. In this design, blocks in isolated corners with a volume of less than 5,000 m³ are combined with neighboring blocks. After tonnage control, 3772 ore and waste blocks were created. This design includes 32 benches from the pit floor. The mining blocks are shown isometrically in Figure 7.1 and in section in Figure 7.2.

7.2. Grade-Tonnage Processes

The following attributes were defined for the mining blocks and the values assigned to them in the resource block model were determined. The specifications in Table 7.1 were defined for the planned mining blocks, whereby the corresponding resource quantities were derived from the mining blocks. According to the data presented in Table 7.1, a total of 16,573,572 cubic meters of ore with an average density of 3.21 t/m³ was identified, corresponding to approximately 59,858,578 tons of ore. The average iron (Fe) content in these ore blocks is estimated at 33.34%, which corresponds to a total iron content of 20,632,577 tons. In addition to the ore, the blocks also contain 50,902,725 cubic meters of waste material with a density of 2.50 t/m³, which corresponds to a total waste mass of 127,256,812 tons. This brings the total volume of material within the modeled area to 67,476,297 cubic meters and the combined total mass of ore and waste to approximately 187,115,389 tons. The estimated 20.63 million tons of contained iron within the ore forms the basis for further mine planning.

- Bench name
- Ore density (t/m³)
- Volume (m³)
- Waste density (t/m³)
- Column
- Ore grade, diluted (%)
- Overall density (t/m³)
- Level (m)
- Ore mass (t)
- Waste mass (t)
- Row
- Ore grade (%)
- Total mass (t)

Table 7.1 Ore and waste quantities of mining blocks in the ultimate pit

Category	Volume (m³)	Density (t/m³)	Mass (t)	Grade%	Total Fe (t)
Ore	16,573,572	3,21	59,858,578	33.34	20,632,577
Waste	50,902,725	2,50	127,256,812	-	-
Total	67,476,297	2,77	187,115,389	11.03	20,632,577

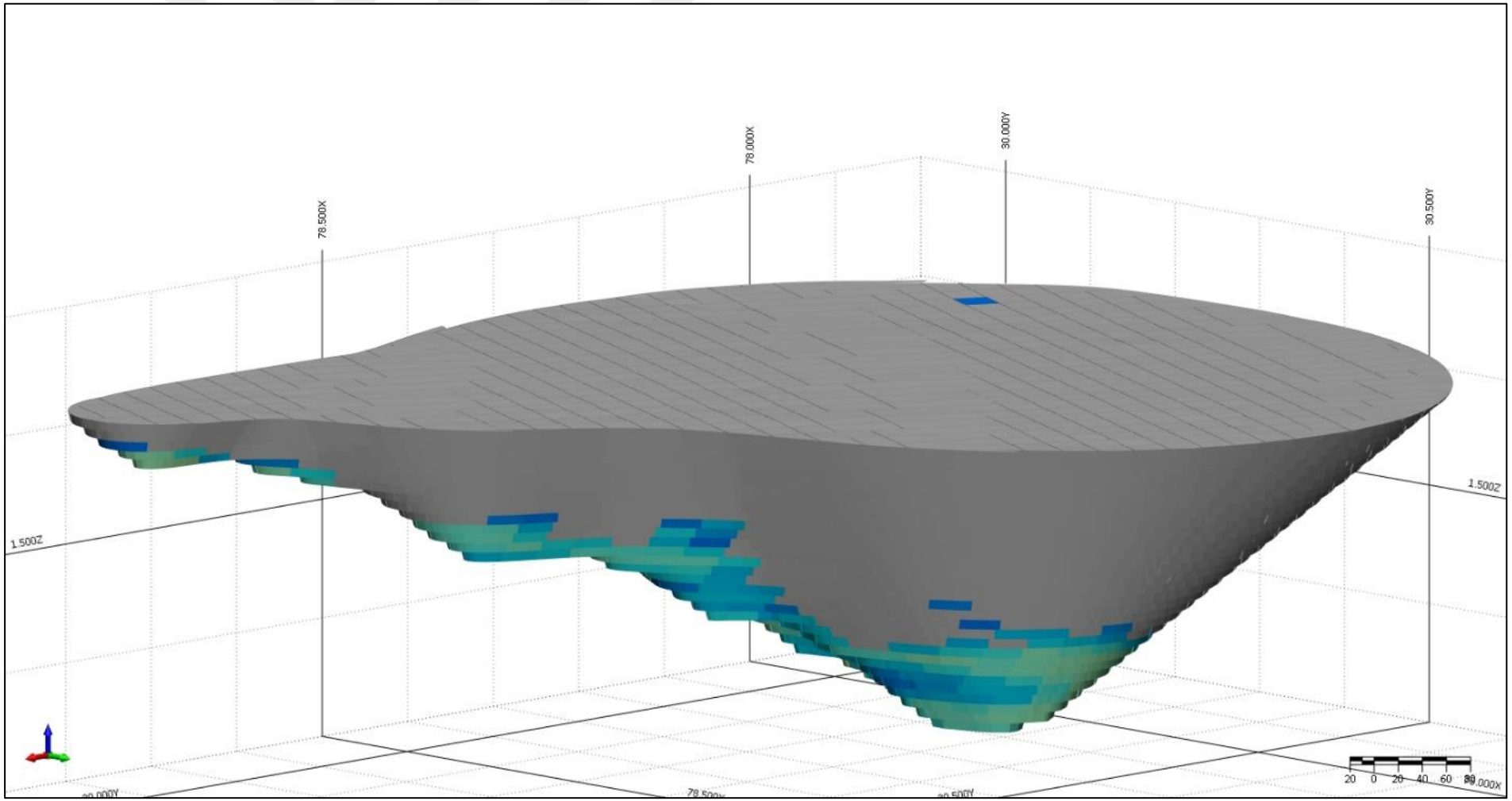

Figure 7.1 The mining blocks in the optimum pit (isometric view to the southwest)

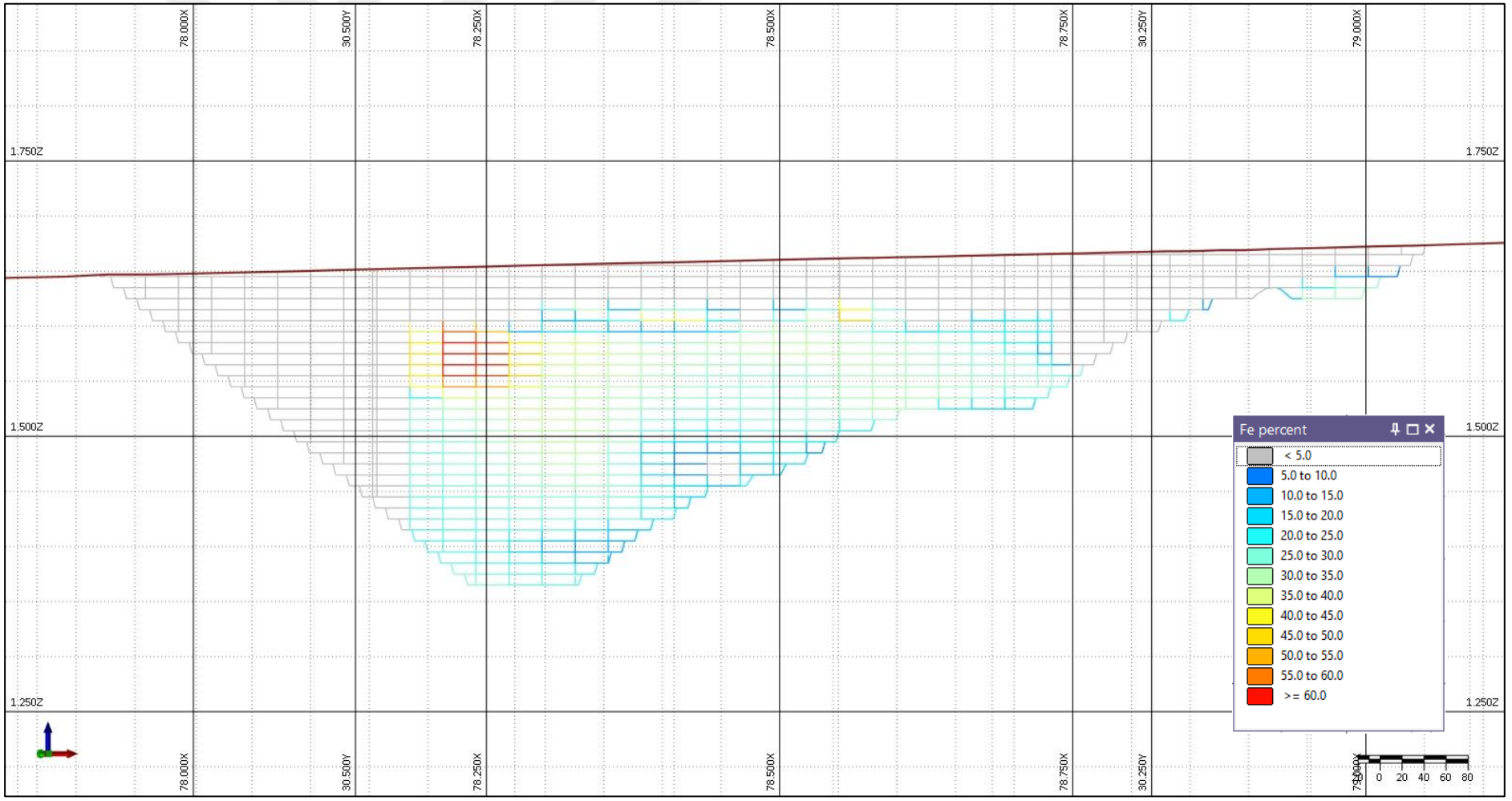

Figure 7.2 The cross section view of the mining blocks in the optimum pit

7.3. Production Scheduling

After the attribute values were assigned to the mining blocks in Section 7.2, it was decided to mine at a rate maximum rate of 25,000,000 tons per year at a production rate of 2850 ton/h and to start production on February 2, 2025. In the following step, first the vertical dependencies of the 3772 mining blocks within the mine were determined on a level basis and then the horizontal dependencies of all blocks within each level, starting from a specific starting block.

According to the schedule, production in the iron mine started in 2025 and the extraction of all blocks was completed in 2039. The mine was in operation for 15 years. Annual and monthly production figures can be found in Tables 7.2 and 7.3.

Table 7.2 Yearly production figures of the iron mine

Years	Ore mass (t)	Iron mass (t)	Iron grade (%)	Waste mass (t)	Total mass (t)
2025	102,308	29,031	28.376	2,431,370	2,533,678
2026	186,610	52,036	27.885	9,258,772	9,445,382
2027	1,082,686	382,871	35.363	18,582,053	19,664,739
2028	3,936,954	1,521,475	38.646	23,851,338	27,788,291
2029	8,046,853	2,960,696	36.793	17,154,372	25,201,225
2030	8,935,063	3,405,770	38.117	16,376,579	25,311,643
2031	6,837,610	2,628,616	38.443	12,520,941	19,358,551
2032	5,620,332	2,089,834	37.183	9,987,999	15,608,331
2033	5,149,540	1,759,372	34.166	6,703,526	11,853,066
2034	4,393,895	1,459,669	33.220	4,647,065	9,040,960
2035	5,111,981	1,565,387	30.622	3,696,987	8,808,968
2036	4,191,266	1,179,648	28.145	1,671,824	5,863,089
2037	3,762,245	949,364	25.234	334,774	4,097,019
2038	2,156,440	559,148	25.929	31,177	2,187,616
2039	344,794	89,660	26.004	6,923	351,717
Totals	**59,858,578**	**20,632,577**		**127,255,697**	**187,114,275**

From the start of production in February 2025, only overburden removal work was carried out for five months; regular ore extraction did not begin until later. Production until mid-2027 was characterized by low-grade ore, but the situation changed in the following years when a weighted average of 35% Fe was produced. However, from 2035 to 2039, when the mine ceased operations, the ore grade remained at only 25%.

Table 7.3 Monthly production figures of the iron mine

Date	Total mass (t)	Ore mass (t)	Waste mass (t)	Iron mass (t)	Ore grade (%)
February 2025	44,933	-	44,933	-	0.000
March 2025	81,327	-	81,327	-	0.000
April 2025	112,509	-	112,509	-	0.000
May 2025	159,003	-	159,003	-	0.000
June 2025	197,257	-	197,257	-	0.000
July 2025	234,019	985	233,034	272	27.659
August 2025	214,918	10,080	204,838	2,788	27.659
September 2025	264,120	6,262	257,858	1,745	27.862
October 2025	245,313	7,339	237,974	2,078	28.314
November 2025	295,392	29,602	265,791	8,384	28.322
December 2025	326,942	26,864	300,078	7,653	28.488
January 2026	357,944	21,176	336,768	6,111	28.857
February 2026	439,210	35,827	403,383	10,340	28.860
March 2026	454,777	7,204	447,573	2,087	28.974
April 2026	564,131	32,376	531,756	9,472	29.255
May 2026	675,231	22,345	652,887	6,444	28.839
June 2026	665,491	2,070	663,420	575	27.792
July 2026	784,748	-	784,748	-	0.000
August 2026	869,583	4	869,579	1	16.896
September 2026	868,406	5,110	863,296	1,339	26.196
October 2026	926,057	2,141	923,916	503	23.500
November 2026	992,108	23,299	968,809	6,120	26.266
December 2026	1,112,524	26,711	1,085,813	7,123	26.668
January 2027	1,093,116	29,524	1,063,592	8,033	27.208
February 2027	1,048,963	42,599	1,006,364	11,711	27.491
March 2027	1,203,490	57,156	1,146,334	15,768	27.588
April 2027	1,297,584	62,331	1,235,252	17,778	28.522
May 2027	1,375,546	55,444	1,320,102	15,835	28.560
June 2027	1,444,980	67,227	1,377,753	19,464	28.953
July 2027	1,644,087	72,213	1,571,875	22,770	31.533
August 2027	1,770,543	96,008	1,674,535	34,420	35.852
September 2027	1,763,508	118,782	1,644,726	44,350	37.337
October 2027	1,960,399	139,894	1,820,505	50,898	36.383
November 2027	1,953,550	119,492	1,834,058	45,853	38.373
December 2027	2,051,739	105,534	1,946,205	41,875	39.679
January 2028	2,150,349	146,006	2,004,343	62,149	42.566
February 2028	2,087,976	133,207	1,954,769	58,867	44.192
March 2028	2,236,055	187,791	2,048,264	83,643	44.540
April 2028	2,250,754	184,559	2,066,195	83,503	45.245
May 2028	2,408,101	216,459	2,191,642	95,123	43.945
June 2028	2,387,993	240,094	2,147,899	100,888	42.020
July 2028	2,487,658	297,356	2,190,301	118,862	39.973
August 2028	2,399,138	315,321	2,083,817	115,328	36.575
September 2028	2,414,783	419,555	1,995,228	156,468	37.294
October 2028	2,393,746	436,109	1,957,637	159,656	36.609
November 2028	2,363,926	462,203	1,901,723	163,832	35.446
December 2028	2,192,494	492,370	1,700,124	182,068	36.978
January 2029	2,235,056	570,272	1,664,784	209,832	36.795
February 2029	1,877,214	493,889	1,383,325	178,098	36.060
March 2029	2,130,269	604,670	1,525,599	217,120	35.907
April 2029	1,907,580	573,276	1,334,305	207,000	36.108
May 2029	1,997,825	668,660	1,329,165	238,571	35.679
June 2029	1,940,696	673,191	1,267,505	258,461	38.393
July 2029	2,127,364	727,807	1,399,557	272,723	37.472
August 2029	2,157,037	743,656	1,413,380	275,604	37.061
September 2029	2,175,841	696,752	1,479,089	258,516	37.103
October 2029	2,292,729	723,146	1,569,582	264,228	36.539
November 2029	2,105,656	663,449	1,442,207	245,401	36.989
December 2029	2,227,680	728,637	1,499,043	261,654	35.910
January 2030	2,268,744	760,437	1,508,307	287,436	37.799
February 2030	2,002,890	752,346	1,250,544	277,140	36.837
March 2030	2,220,023	783,884	1,436,139	295,327	37.675
April 2030	2,314,735	794,717	1,520,018	292,439	36.798

Date	Total mass (t)	Ore mass (t)	Waste mass (t)	Iron mass (t)	Ore grade (%)
May 2030	2,270,599	690,093	1,580,506	255,738	37.059
June 2030	2,262,471	824,254	1,438,217	316,251	38.368
July 2030	2,064,198	683,420	1,380,778	264,303	38.674
August 2030	2,259,511	820,294	1,439,217	311,980	38.033
September 2030	2,078,065	698,624	1,379,441	275,427	39.424
October 2030	2,091,068	789,924	1,301,144	289,460	36.644
November 2030	1,915,687	699,843	1,215,843	289,109	41.310
December 2030	1,984,670	708,266	1,276,403	273,099	38.559
January 2031	1,827,610	681,490	1,146,120	263,395	38.650
February 2031	1,542,369	615,841	926,528	246,217	39.981
March 2031	1,744,865	618,217	1,126,648	227,797	36.848
April 2031	1,717,766	610,957	1,106,810	246,848	40.404
May 2031	1,690,872	560,634	1,130,238	227,791	40.631
June 2031	1,671,078	549,110	1,121,968	214,152	39.000
July 2031	1,724,996	628,922	1,096,074	245,592	39.050
August 2031	1,627,682	572,523	1,055,159	201,248	35.151
September 2031	1,543,635	549,759	993,876	215,063	39.120
October 2031	1,533,571	512,522	1,021,049	203,816	39.767
November 2031	1,636,461	568,252	1,068,209	214,605	37.766
December 2031	1,483,119	525,332	957,787	202,737	38.592
January 2032	1,438,253	525,027	913,226	181,723	34.612
February 2032	1,429,030	514,242	914,788	199,014	38.701
March 2032	1,471,756	495,594	976,161	192,061	38.754
April 2032	1,458,213	518,613	939,600	195,540	37.704
May 2032	1,368,839	536,006	832,833	198,266	36.990
June 2032	1,257,055	429,434	827,622	151,937	35.381
July 2032	1,378,680	492,507	886,173	181,311	36.814
August 2032	1,343,253	467,638	875,616	162,866	34.827
September 2032	1,241,113	465,266	775,847	167,117	35.919
October 2032	1,237,865	470,906	766,959	176,264	37.431
November 2032	1,151,336	396,449	754,886	144,196	36.372
December 2032	1,191,641	444,251	747,390	173,003	38.943
January 2033	1,093,950	393,291	700,659	149,452	38.000
February 2033	997,836	399,712	598,124	148,626	37.183
March 2033	1,036,937	421,926	615,011	158,935	37.669
April 2033	999,413	393,944	605,470	135,001	34.269
May 2033	1,020,025	498,356	521,668	176,754	35.467
June 2033	892,541	417,142	475,399	148,950	35.707
July 2033	971,793	458,107	513,685	158,030	34.496
August 2033	1,020,406	446,344	574,061	158,746	35.566
September 2033	974,187	419,901	554,286	132,646	31.590
October 2033	1,085,357	506,296	579,061	155,079	30.630
November 2033	903,753	370,898	532,855	120,270	32.427
December 2033	1,005,797	427,167	578,631	138,223	32.358
January 2034	935,421	387,333	548,088	126,512	32.662
February 2034	803,336	357,094	446,242	112,676	31.554
March 2034	886,314	397,088	489,226	133,981	33.741
April 2034	786,136	303,799	482,337	104,327	34.341
May 2034	875,554	355,405	520,149	123,923	34.868
June 2034	785,948	348,707	437,241	121,573	34.864
July 2034	724,376	305,876	418,500	105,682	34.551
August 2034	690,343	319,866	370,476	112,517	35.176
September 2034	631,780	285,882	345,898	97,741	34.189
October 2034	802,371	417,439	384,931	136,111	32.606
November 2034	662,214	408,191	254,023	135,575	33.214
December 2034	671,122	427,854	243,268	131,968	30.844
January 2035	707,066	473,608	233,457	145,115	30.640
February 2035	691,023	452,538	238,485	137,291	30.338
March 2035	806,035	556,042	249,994	174,634	31.407
April 2035	726,056	414,761	311,295	131,239	31.642
May 2035	819,978	531,773	288,205	170,873	32.133
June 2035	759,723	416,953	342,771	134,375	32.228
July 2035	838,062	465,839	372,222	144,188	30.952
August 2035	773,456	405,922	367,534	122,824	30.258
September 2035	773,432	432,213	341,219	127,712	29.548

Date	Total mass (t)	Ore mass (t)	Waste mass (t)	Iron mass (t)	Ore grade (%)
October 2035	730,882	346,965	383,917	104,012	29.978
November 2035	671,624	411,485	260,139	122,364	29.737
December 2035	603,057	328,142	274,914	96,425	29.385
January 2036	606,039	337,504	268,535	95,860	28.403
February 2036	516,143	240,131	276,012	71,269	29.679
March 2036	527,371	347,967	179,404	101,598	29.197
April 2036	466,171	294,302	171,869	88,180	29.963
May 2036	474,755	319,359	155,395	90,366	28.296
June 2036	462,791	295,555	167,236	82,066	27.767
July 2036	474,955	347,221	127,734	95,549	27.518
August 2036	482,573	376,304	106,269	108,178	28.747
September 2036	458,828	393,684	65,144	109,585	27.836
October 2036	530,938	417,255	113,683	114,074	27.339
November 2036	494,816	397,415	97,402	107,297	26.999
December 2036	546,651	401,687	144,964	113,322	28.212
January 2037	440,297	384,432	55,865	104,479	27.177
February 2037	440,247	367,719	72,528	102,471	27.867
March 2037	429,596	373,424	56,172	101,140	27.085
April 2037	399,010	319,447	79,564	87,446	27.374
May 2037	340,408	315,771	24,637	82,531	26.136
June 2037	348,372	327,808	20,564	82,065	25.034
July 2037	316,962	283,446	33,517	69,684	24.585
August 2037	314,990	294,851	20,139	68,123	23.104
September 2037	329,579	321,793	7,786	76,155	23.666
October 2037	268,024	260,853	7,171	63,867	24.484
November 2037	315,873	312,707	3,166	73,343	23.454
December 2037	292,951	290,047	2,905	71,227	24.557
January 2038	289,735	288,593	1,142	69,013	23.914
February 2038	251,878	251,303	575	65,272	25.973
March 2038	294,754	291,712	3,042	74,392	25.502
April 2038	217,270	215,423	1,847	50,715	23.542
May 2038	216,130	212,818	3,312	56,429	26.515
June 2038	230,037	226,564	3,473	59,445	26.237
July 2038	200,449	197,499	2,949	48,481	24.547
August 2038	185,658	180,826	4,832	47,509	26.273
September 2038	153,259	151,723	1,536	40,952	26.991
October 2038	157,552	152,894	4,657	41,054	26.851
November 2038	130,848	127,015	3,833	34,510	27.170
December 2038	67,535	66,528	1,007	18,580	27.928
January 2039	53,920	53,919	1	14,632	27.137
February 2039	53,458	53,456	2	14,259	26.675
March 2039	81,360	81,109	251	21,191	26.126
April 2039	71,895	71,487	408	18,285	25.578
May 2039	64,019	62,759	1,259	16,188	25.794
June 2039	69,109	64,561	4,548	16,757	25.955
July 2039	4,676	4,221	455	1,039	24.625
Totals	**187,114,275**	**59,858,578**	**127,255,697**	**20,632,577**	**34.469%**

8. CONCLUSIONS and RECOMMENDATIONS for FURTHER RESEARCH

8.1. Conclusions

This thesis focused on the long-term production planning of an open pit iron mine with the aim of developing an optimized and efficient framework for resource extraction, maximizing economic benefits and operational feasibility. Using geological data from 42 exploration drill holes with 1321 samples of drill material, orebody modeling and grade estimation were performed using inverse distance weighting (IDW) and kriging methods. These estimates formed a solid basis for mine planning, block modeling, pit boundary optimization and production scheduling.

The ore deposit was divided into three ore bodies based on the variation of iron content at depth. The high-grade ore body with an average iron content of 57% is located near the surface. Below this is the medium-grade ore body with an average iron content of 30% Fe and finally the low-grade ore body at greater depth with an average of 15% Fe. After classifying the ore grades, a geostatistical evaluation was carried out. This began with modeling the ore bodies using search ellipsoid parameters, resulting in the creation of a solid model for each ore body. A block modeling process was conducted to support mine planning and resource estimation. First, a blank block model was created with uniform dimensions of 5 meters along the X, Y and Z axes so that each block had a total volume of 125 m^3. A geologic block model was then developed by integrating geologic and grade data into the blank block model.

Estimation is at the heart of a mining plan and engineers must be careful because we collect drill hole data to estimate the quality of deposits and we estimate drillhole samples to design and plan mineable deposits. This means that selecting an appropriate method for just that type of deposit will lead us to a true estimate.

We can see the effectiveness of the two techniques. Kriging estimates the average grade of the high-grade orebody slightly lower (57.11%) than IDW (58.02%). Kriging therefore shows a tendency to smooth the grade distributions compared to IDW. While the IDW estimate of average iron content in medium and low grade ore bodies was 29.22% and 10.80% respectively, kriging estimated a slightly higher iron content of 29.30% and 12.15% in medium and low grade ore bodies.

Kriging provides more realistic estimates than IDW because it takes into account not only the distance between sample points but also the change in values with distance, whereas IDW estimates values based only on nearby sample points, which can lead to over- or underestimates. To be selective, we opted for the kriging method and combined all three ore bodies. The result is a total resource of 99.99 million tons and an average Fe grade of 26.14%, demonstrating the dominance of medium-grade ore in the deposit.

When optimizing the pit boundaries, we created ultimate and nested pits using the Lerchs-Grossmann algorithm. Since the topography of the surface was quite flat, we chose a slope of

40° for the overall pit, resulting in a V-shaped pit. The ultimate pit reaches a depth of 320 meters and contains approximately 194.36 million tons of waste and ore. With a stripping ratio of 2.53, 17.70 million tons of diluted iron will be extracted, resulting in 15.05 million tons of processed iron after recycling at the plant. The total cost of the project is estimated at USD 830.73 million, while the projected revenue is USD 1.58 billion, resulting in a net value of USD 749.23 million before tax. These results confirm the economic viability of open pit iron mining under the assumed parameters. A nested pit analysis was performed to assess the impact of market price fluctuations and production strategies on the profitability of the mine. Using the Revenue Adjustment Factor (RAF) and staged pit development, eight nested pits were created. The analysis showed that pit #9, which closely follows the ultimate pit, is the most economic option. At an RAF of 0.9, cash flow and NPV peaked, indicating an optimal balance between ore recovery and cost. Therefore, the ultimate pit was selected for final design and long-term production planning to ensure maximum economic return under realistic operating and market conditions.

To enable efficient mining, the 67.48 million m³ pit was divided into 3772 standardized mining blocks on 32 benches. This includes 59.86 million tons of ore with 33.34% Fe (20.63 million tons of iron) and 127.26 million tons of waste, a total of 187.12 million tons of material. The block model forms the basis for production planning and scheduling. From 2025 to 2039, the mine will produce almost 60 million tons of ore and 127 million tons of waste over 15 years. After an initial low grade production, production peaked between 2028 and 2032 at over 35% Fe–, followed by a decline to 25% Fe by closure. The schedule ensured efficient resource recovery and operational continuity.

8.2. Recommendations for Further Research

One of the biggest challenges in the accurate estimation of ores is the lack of sufficient drill hole data and sample information. Reliable and detailed geological data is essential for effective mine planning and design. Without adequate sampling and drilling, the spatial distribution of ore grades cannot be accurately modeled, which can lead to suboptimal mining strategies and financial losses.

The study also highlights the need for density adjustments based on grade to avoid tonnage discrepancies. These results provide a solid foundation for future mining planning, optimizing resource extraction and maximizing economic returns.

REFERENCES

Açan, H. (2013). Assessment of an iron ore deposit using Surpac integrated mining software (In Turkish). Master Thesis İstanbul technical University, Istanbul, 184p.

Akisa, D. M., Mireku-Gyimah, D. (2015). Application of Surpac and Whittle software in open pit optimisation and design. *Ghana Mining Journal*, 15(1), 35-43.

Asad, M. W. A. (2011). Topal, E. Net present value maximization model for optimum cut-off grade policy of open pit mining operations. *The Journal of The Southern African Institute of Mining and Metallurgy*, 111, 741-750.

Bise, C. J. (2013). *Mining engineering analysis*. Society for Mining, Metallurgy, and Exploration.

Caccetta, L., Hill, S. P. (2003). An application of branch and cut to open-pit mine scheduling. *Journal of Global Optimization*, 27(2-3), 349-365.

Choudhury, S. (2015). Comparative Study on Linear and Non-Linear Geo statistical Estimation Methods: A Case Study on Iron Deposit. *Global Challenges, Policy Framework & Sustainable Development for Mining of Mineral and Fossil Energy Resources (GCPF2015), 11, 131-139.*

Dagdelen, K. (2001). Open pit optimization-strategies for improving economics of mining projects through mine planning. *Proceedings of 17th International Mining Congress and Exhibition of Turkey*, 117-121.

Dimitrakopoulos, R. (2007). *Geostatistics for the next century*. Springer Science & Business Media.

Ergin, H., Kırmanlı, C., Erdoğan, T. (1998). *Classified reserve estimation of coal deposits according to quality by new computer techniques (In Turkish)*. Madencilik, 37(4), 13-22.

Faqir Yar, M. M. (2024). Long-term production planning of an open copper mine (In Turkish) Master Thesis, Sivas Cumhuriyet University, Sivas 93p.

Fenerli, U. R., Güven, S. (2019). Mine Planning and Its Importance (In Turkish). Madencilik Türkiye, 79, 86-95.

Hoek, E., Bray, J. W. (1981). *Rock slope engineering*. CRC Press.

Hustrulid, W., Kuchta, M., Martin, R. (2013). *Open pit mine planning and design*. 5.5, 450.

Journel, A. G., & Huijbregts, C. J. (1978). *Mining geostatistics*. Academic Press.

Karakurt, E. (2019). Mine scheduling for metallic open pit mines (In Turkish). Master Thesis, Dokuz Eylül University, Izmir, 51p.

Karaöz, B. (2014). A proposal on integer programming for mine planning and scheduling: Kar mining example (In Turkish). Master Thesis, Hacettepe University, Ankara 133p.

Kaydım, H. E. (2022). Long-term production scheduling optimization for a polymetallic open pit mine. Master of Science Thesis, Middle East Technical University, Ankara 104p.

Knudsen, H. P. (1975). A comparison of the geostatistical ore reserve estimation method over the conventional methods. The University of Arizona, (Master of Science Thesis), Arizona.

Lane, K. F. (1988). *The economic definition of ore: cut-off grades in theory and practice*. Mining Journal Books.

Lindi, O. T, Aladejare, A. E., Ozoji, T. M., Ranta, J. P. (2024). *Uncertainty Quantification in Mineral Resource Estimation*, 33(6), 2503-2526

Mai, L. M., Topal, E., Erten O., Sommerville, B. (2019). A new risk-based optimisation method for the iron ore production scheduling using stochastic integer programming. *Science Direct,* 62, 571-579.

Matheron, G. (1971). *The theory of regionalized variables and its applications*. Les Cahiers du Centre de Morphologie Mathématique de Fontainebleau.

Moharaj, M.C., Wangmo, Y. (2014). Ore body modeling and comparison of different reserve estimation techniques. *National Institute of Technology of Rourkela* (Bachelor of Technology Thesis), 42 p, India.

Mousavi, S.J., Shayestehfar, M., Maarefvand, P., Rezaei, A. (2022). Estimating the iron grade and separating the mineralization areas using fractal concentration-volume fractal model: a case study of Bafgh Lakeh Siah orebody, Central Iran. *Arabian Journal of Geosciences*. 15(21).

Newman, A., Rubio, E., Caro, R., Weintraub, A., & Eurek, K. (2010). A review of operations research in mine planning. *Interfaces*, 40(3), 222-245.

Osanloo, M., Gholamnejad, J. & Karimi, B. (2008). Long-term open pit mine production planning: a review of models and algorithms. *International Journal of Mining, Reclamation and Environment*, 22(1), 3-35. https://doi.org/10.1080/17480930601118947

Oz, B., Deutsch, C. V. (2000). Cross validation for selection of variogram model and kriging type: application to IP data from West Virginia. Report to Mining Firm.

Palmer, L. W. (2024). Compositing and regularization of drillhole data for geostatistical resource estimation. *Journal of the Southern African Institute of Mining and Metallurgy. 124(6) 331-338*

Dimitrakopoulos, R., Jewbali, A. (2013). Joint stochastic optimisation of short and long term mine production planning: method and application in a large operating gold mine, *Mining Technology*, 122:2, 110-123. https://doi.org/10.1179/1743286313Y.0000000040

Ramazan, S., Dimitrakopoulos, R. (2004). Stochastic optimization of long-term production scheduling for open pit mines with a new integer programming formulation. *Orebody Modelling and Strategic Mine Planning*, 14(1), 291-298.

Reazai, A., Hassani, H., Moarefvand, P. Golmohammadi, A., Jabbari, N. (2022). Three-dimensional Subsurface Modeling and Classification of Mineral Reserve: A Case Study of the C-North Iron Skarn Ore Reserve, Sangan, NE Iran. *Arabian Journal of Geosciences 15(373), 11.*

Rossi, M. E., Deutsch, C. V. (2014). *Mineral resource estimation*. Springer.

Shishvan, M. S., Sattarvand, J. (2015). Long term production planning of open pit mines by ant colony optimization. *European Journal of Operational Research*, 240(3), 825 836. https://doi.org/10.1016/j.ejor.2014.07.040

Topal, E., Ramazan, S. (2012). Strategic mine planning model using network flow model and real case application. *International Journal of Mining, Reclamation and Environment*, 26(1), 29-37.

URL-1 <https://worldpopulationreview.com/country-rankings/iron-ore-production-by-country accessed date 11.4.2025

URL-2 < https://oec.world/en/profile/hs/iron-ore accessed date 11.4.2025

URL-3 < https://github.com/furkankasa/Lerchs-Grossman-2-D-Algorithm

URL-4 *https://financialtribune.com/articles/domestic-economy/116788/iran-s-iron-ore-reserves-5-billion-tons-estimated-23-billion-tons#:~:text=I%20ran%E2%80%99s%20proven%20iron%20ore%20reserves%20have%20currently,Mehrdad%20Akbarian%2C%20the%20head%20of%20Iran%20Stone%20Association. Accessed 23.4.2025*

Whittle, J. (1988). Beyond optimization in open pit design. *Proceedings of the 28th International Symposium on the Application of Computers and Operations Research in the Mineral Industry (APCOM)*, 281-287.